A Proposal to Study High Mass Photoproduction

S.D. Holmes, B.C. Knapp *
Columbia University, New York, N.Y. 10027

D.A. Jensen, M.N. Kreisler, M.S.Z. Rabin, K. Raychaudhuri
University of Massachusetts, Amherst, Mass. 01003

J. Butler, J. Cumalat, I. Gaines, D. Harding
Fermilab, Batavia, Ill. 60510

* Spokesperson.

Submitted September 1979

Table of Contents

	Page
I. Introduction	1
II. Physics Program	
A. Detection of Signals in the Presence of Backgrounds	2
B. Why Photoproduction from Nuclear Target	3
C. Isolation of Interesting High Mass Phenomena	4
III. Photon Beam	
A. Energy and Intensity Requirements	10
B. Energy Spectrum of Proposed Photon Beam	11
C. Hadron Contamination	12
IV. Detector	14
A. Detector Dimensions and Acceptance Considerations	15
B. Detector Layout	16
C. Drift Chambers	18
D. Photon Detector	19
E. Charged Particle Identification	21
F. Hardware Processor	24
V. Experiment: Interaction and Data Rates	27
A. Coherent Production	28
B. Rare Processes with Clear Signatures	30
C. Event Trigger	31
D. Comparison to Tagged Beam and e^+e^- Annihilation	34
E. Future Plans	35
VI. Construction: Costs and Time Estimates	37
VII. Summary	39
References	40
Table Captions and Tables	41
Figure Captions and Figures	48

I. Introduction

We propose an experiment in the Fermilab broad band neutral beam to study photoproduction of massive states from nuclear targets. The major physics goals of the proposed program fall into three overlapping categories:

1) the detailed study of diffractively produced states with masses up to ~ 8 GeV/c^2,

2) the study of photoproduced leptons pairs with masses up to ~ 10 GeV, along with any accompanying hadrons,

3) the study of massive (4-12 GeV) final states with distinct signatures such as two fully reconstructed decays of massive particles with well defined masses. Included are associated production of the quantum numbers C or B and the cascade decay of a heavy particle to states containing one or more charmed particles.

To accomplish these goals requires the two essential features of the proposal, namely:

The Fermilab Broad Band Neutral Beam

As we discuss below, the high energy and intensity available in the broad band beam make it possible to extend the mass range probed by photoproduction and to study quite rare processes.

An Innovative Spectrometer

To observe the phenomena listed above requires a spectrometer with very high efficiency for complete and accurate reconstruction of complicated reactions at high interaction rates. While the proposed spectrometer has unusually high efficiency for reconstruction of complex multiparticle states, its most novel feature is complete on-line event reconstruction that permits the most flexible and efficient possible selection of events and also reduces off-line computation and storage requirements.

Despite the innovative aspects of the spectrometer design (or, in fact, because of them), the spectrometer is modest in cost and could be operational (i.e. taking data) within 18 months.

II. Physics Program

As stated in the Introduction, our primary objective is the spectroscopy of heavier hadrons, particularly hadrons associated with the quantum numbers charm and bottom. We propose to achieve immediately the greatest practical detail and sensitivity by studying high energy photoproduction from nuclear targets, using a multiparticle spectrometer with unusually high reconstruction efficiency for complex states at information rates much higher than ever previously attempted. In this section, we discuss in more detail just what we wish to do and why.

A. Detection of Signals in the Presence of Backgrounds

Our ability to observe phenomena of such general physics interest as associated production of charm is limited more by relative background levels than possible production rates. Fermilab normally produces a factor of roughly 10^{10} more charm particles per hour than all existing e^+e^- colliding beam facilities, and yet the almost vanishingly low rates of the colliding beam facilities have provided almost all of our present knowledge of charm particle physics, because their background levels are so much lower than in external beam experiments.

We distinguish two types of backgrounds:

i) Backgrounds intrinsically indistinguishable from signal. If the fullest possible analysis fails to distinguish on an event-by-event basis between background and signal, one attempts at the very least to detect statistically significant departures from extrapolated backgrounds. We attempt to reduce such backgrounds by finding specific reactions or kinematic regions where signal-to-noise is maximum.

ii) Backgrounds which saturate the experimental detector at unpleasantly low signal rates. Here one encounters either the intrinsic rate limitation of the detector, such as loss

of measurement capability at detectable event rates above 10^7/sec, or the rate limitation imposed by the maximum rate at which data from the detector can be digested. Counter experiments have studied specific processes with simple signatures that permit fast rejection of unwanted backgrounds by factors of 10^2 to 10^9. Such experiments can have signal rates determined by the intrinsic rate limitation of the detector or even by the available beam intensity.

In multiparticle experiments of the type we propose, the distinction between signal and background may be quite unambiguous on an event-by-event basis but nevertheless too complicated for a traditional fast trigger decision. In Experiment 87A, for instance, we were unable to isolate candidates for charm production from much of the total cross section. We were therefore forced to keep the interaction rate low while writing 200 complex events per pulse onto tape for later off-line analysis. We believe, however, that we can now <u>completely eliminate</u> this limitation, by supplying sufficiently complete on-line reconstruction at the maximum rates we can envision in the broad band beam.

We describe the on-line reconstruction in more detail in Section IV. For the moment, we shall consider the technical difficulties of event selection, recording and later analysis to be adequately resolved and turn our attention to overcoming intrinsically indistinguishable backgrounds. We attempt to improve the signal-to-noise ratio at high signal rate by maximizing first the relative yield of desired reactions and second the amount of information measured for each reaction. By fully reconstructing associated production or diffractive dissociation, we both increase signal and decrease background.

B. <u>Why Photoproduction from Nuclear Target</u>

We choose photons because the photon appears to interact with less bias against new phenomena than do ordinary hadrons. Theoretically, this is because the photon couples directly to

new quarks through their electric charge.[1] Experimentally, charm particle production appears to be an order of magnitude larger fraction of the total hadronic cross section for photoproduction than for hadron beams.[2] Thus, although the absolute production cross section for charm particles is larger in hadron beams, the relative backgrounds are lower in photon-induced reactions.

We prefer a nuclear target, beryllium in particular, for much the same reason. While the total cross section per nucleon decreases slightly with increasing nuclear size, the yield per nucleon of massive states increases.[3] In addition, coherent diffractive production from the entire nucleus has a particularly clean experimental signature. Increasing the nuclear size much beyond beryllium is strongly inhibited by the rapid increase in the Bethe-Heitler pair production cross section.

C. Isolation of Interesting High Mass Phenomena

Even in photoproduction, the mere observation of high mass is not necessarily interesting. Consider the reaction

$$\gamma + p \rightarrow p + X \quad .$$

Clearly, if we see all outgoing particles we see a system whose invariant mass is just the total available center-of-mass energy. If we miss a few of the outgoing particles, we see somewhat lower mass. If we consider the invariant mass, M_X, of all outgoing particles except the proton, we expect that nearly 20% of the total cross section is diffractive dissociation of the photon, with a mass spectrum falling rapidly with increasing mass above 1 GeV. The rest of the cross section is slowly varying with M_X out to the kinematic limit. Although the majority of reactions with large M_X can be readily identified as production of two relatively low mass systems, one containing the target nucleon, it appears to us that isolation of intrinsically interesting high mass phenomena is not so simple.

Attempts to observe inclusive production of specific massive states and their subsequent decays to multihadron states suffer from large combinatorial backgrounds. Even among the final particles from a genuine charm particle pair production reaction, we would expect to find many plausible but wrong combinations of particles with invariant mass in the vicinity of a possible parent charm particle.

Thus, although in Experiment 87A we were in fact able to see single inclusive charm particle production with a small fraction of 1% of the sensitivity of the proposed experiment, we feel that our greatest sensitivity to the physics of new hadrons will lie in more highly constrained measurements, particularly fully reconstructed associated production of charm or bottom. For the production of charm and related hadrons, we expect the cleanest probe to be fully reconstructed diffractive dissociation. As we attempt to show in the remainder of the proposal, we believe that we can study the spectroscopy of these hadrons - their existence, quantum numbers, production and decay modes - with greater sensitivity and detail than any other proposed program, including e^+e^- annihilation.

1. Diffractive Photoproduction

By diffractive photoproduction we mean reactions

$$\gamma + A \rightarrow A + X$$

in which the nucleus remains intact and for which the resulting coherence between scattering amplitudes produces a characteristic forward peaking of the production cross section,

$$\frac{d\sigma}{dP_t^2} \propto e^{-bP_t^2} ,$$

where b is proportional to the square of the transverse dimensions of the nucleus. For a beryllium nucleus, the transverse momentum distribution is characterized by a slope $b \sim 50\ (\mathrm{GeV}/c)^{-2}$. Thus roughly two-thirds of the

diffractive production from beryllium has transverse momentum less than 140 MeV/c. Isolation of diffractive dissociation is experimentally simple: Reject events with typically noisy nuclear breakup and require small transverse momentum.

Such a photoproduced state has the following useful properties:

i) It is produced forward with the full energy of the parent photon, thereby maximizing its detection efficiency in a forward spectrometer.

ii) It carries most of the quantum numbers of the parent photon, particularly strangeness, baryon number and helicity. We thus learn the identity, as well as the energy, of the parent beam particle.

iii) The rapidly decreasing yield of diffractively produced states with increasing mass implies small backgrounds for specific reactions.

To illustrate these features, we show in Fig. 1 the observed P_t^2 distribution for exclusively produced charged pion pairs in Experiment 87A. In Fig. 2, we show the observed mass distribution for those events with $P_t^2 < 0.05$ $(\mathrm{GeV/c})^2$. We see quite clearly the coherent photoproduction of ρ and $\rho'(1600)$, but lose statistical significance above 2 GeV, for which we expect a thousand-fold increase in the proposed experiment. To demonstrate the utility of diffractive production, we show in Fig. 3 the inclusive pion pair mass distribution observed in the same experiment. Despite an average of almost one rho per event, the rho meson is almost invisible in inclusive multipion production, and observation of heavier states is quite hopeless.

Diffractive production can be just as useful for isolation of states other than vector mesons. Consider Fig. 4, in which we show the invariant mass distribution for the lowest mass $\pi^+\pi^-\pi^o$ combination within coherently produced $\pi^+\pi^+\pi^-\pi^-\pi^o$ states. A clearly visible $\eta \rightarrow \pi^+\pi^-\pi^o$ is present with little background,

despite the fact that the decay is completely invisible in inclusive production.

Because we expect a large fraction of the yield of a massive particle to appear in diffractive production, suppression of the high mass multiparticle combinatorial backgrounds should be even more impressive for production of charm particles and their relatives. Consider, for example, our previous ψ photoproduction from beryllium or carbon nuclei. The readily identifiable $\mu^+\mu^-$ decay permits identification of high energy ψ's regardless of accompanying secondary particles. About half of the detected ψ's are diffractively produced coherently from the entire nucleus. Attempts to detect hadronic decay modes would succeed readily in diffractive production, but inclusive production would be buried in background. Large fractions of accepted charm particle pairs, η_c and χ states, should appear in diffractive channels such as broad resonances in the 4 to 6 GeV region.

2. Associated Production of Charm and Bottom

We expect to see large signals with very little background in the complete reconstruction of associated production of charm or bottom. While the relaxation of the diffractive requirement may be useful for charm production, it is essential for bottom production. As we explain in Section III, we lack sufficiently energetic photons to produce 10 or 12 GeV states coherently from the entire nucleus. But even if we divide the theoretical predictions of Ref. 1 by three, we expect roughly 10^5 events with an associated pair of bottom particles. Although we do not know which decay modes, if any, will be favored, we are sensitive to all decays except those including a neutrino, neutron or K_L.

We can see that associated production provides a strong rejection of backgrounds if we note that after choosing possible

decay products for one heavy particle, we have considerably fewer combinations available for the second.

3. Special Decay Modes of Bottom Particles

We should be able to select events containing bottom production, even if not quite fully reconstructed, by simply recording all events with a visible sum of individual particle transverse momentum magnitudes exceeding some moderately large value, perhaps 6 GeV/c. We could afford to record almost 10^{-3} of the total cross section in this manner. If we produce one or more particles whose masses add up to 10 GeV or more, we would expect reasonably isotropic and relativistic decays to yield an average of at least 7 GeV for the sum of the transverse momentum magnitudes for the final decay products. This follows immediately from the observation that the average value of the sine of the polar angle is:

$$\langle \sin \theta^* \rangle = 0.785 \quad .$$

After recording most events containing bottom production, we can then search for events with only one fully reconstructed bottom particle, the other presumably missing one or more neutrals. As we discuss in Section V, we are quite sensitive to decay fractions as low as 1% to states including a ψ or one or two charm particles, even though we can readily identify only a fraction of the subsequent decays of these particles.

Note that we are expecting a signal on the order of 100 events for any reconstructable decay mode with 0.1% branching fraction. Thus we might worry more about the backgrounds than simply detectable signals. We have no reliable method for estimating backgrounds. If we consider, for example, $B \rightarrow \psi K\pi$, where we detect the ψ through its clear dilepton decay, we expect a mass resolution of less than 40 MeV full width. In Experiment 87A, we observed a possible continuum of 1/5 of an event per 40 MeV. If we were to scale these

events up by the same factor of 150 that we expect for genuine B decays, we would then predict 30 background events under the B signal. Whatever the purely inclusive background turns out to be, it should be further suppressed by requiring some evidence for a second bottom particle in the form of more visible transverse momentum.

4. Direct or Cascade Decays to Lepton Pairs

The observation of lepton pairs, e^+e^- or $\mu^+\mu^-$, provides a clean experimental signature for electromagnetic coupling through a virtual photon. The most obvious example of this is the decay of heavy vector mesons. We can detect the dilepton decays of ψ or Υ, regardless of any accompanying particles. Both triggering efficiency and detection efficiency are nearly unity for energetic massive pairs. Backgrounds are negligible.

III. Photon Beam

In this section, we argue that the relevant energy scale for photoproduction of a massive state varies roughly as the square of the mass being produced. We then show that the Fermilab broadband beam is by far the most intense source of high energy photons available anywhere within the next few years. We point out that for the program we propose, the hadron contamination in the beam provides negligible background and possibly some useful physics.

A. Energy and Intensity Requirements

For photoproduction of a state of mass M, the first and most obvious energy requirement is that the photon energy be above the threshold energy for photoproduction from a single nucleon target:

$$E_{th} = M + M^2/2M_N \quad .$$

This is our first indication that the energy required to photoproduce a massive state varies as the square of photoproduced mass, but as we shall see this is a severe underestimate of the energies required for practical photoproduction. We consider separately the energy dependence of inclusive production of some interesting states and the energies required for coherent production from a beryllium nucleus.

1. Photoproduction of $C\bar{C}$, $B\bar{B}$ and Massive Vector Mesons

In the article by Fritzsch and Streng,[1] the inclusive cross sections for $C\bar{C}$ and $B\bar{B}$ are predicted to behave as $(1-E_{th}/E_\gamma)$ and the exclusive cross sections for photoproduction of ψ and Υ from a single nucleon are predicted to behave as $(1-E_{th}/E_\gamma)^2$ with an unphysical extrapolation to $t = 0$. For the vector meson photoproduction, we have chosen to provide our own fit to the experimental data for ψ photoproduction, obtaining the result shown in Fig. 5:

$$\left.\frac{d\sigma}{dt}\right|_{\theta=0} = 66\ (1-E_{th}/E_\gamma)^{3.1}\ \mathrm{nb/GeV}^2 \quad .$$

This form adequately describes the data and yields an energy dependence that scales approximately as mass squared, reaching half the asymptotic cross section at five times threshold energy.

2. Coherent Diffraction from Beryllium: t_{min} Effect

For coherent photoproduction from a nucleus, the minimum longitudinal momentum transfer to the nucleus is

$$q_{min} = M^2/2E_\gamma \quad .$$

If the product of q_{min} times the smaller of a coherence length or nuclear dimension becomes comparable to unity, the production is suppressed by destructive interference. Although this effect is not normally isolated experimentally from other dependence on photon energy and target recoil properties, one customarily considers coherent production to be suppressed by a factor $e^{bt_{min}}$, where $t_{min} = -q^2_{min}$ and b is the slope observed in transverse momentum distributions. For beryllium, a value of q_{min} = 140 MeV will suppress coherent production by a factor of three, yielding an effective threshold for coherent diffractive production:

$$E_{min} = \frac{M^2}{2}\sqrt{b}$$

$$= \frac{M^2}{2(140\ \text{MeV})} \quad .$$

In Table I, we list for various masses both the threshold energy for photoproduction from a single nucleon, E_{th}, and the effective threshold for diffractive dissociation from beryllium, E_{min} .

B. Energy Spectrum of Proposed Photon Beams

We now compare the two photon beams available at Fermilab and the BEG beam proposed for CERN. For both Fermilab beams we assume an incident proton intensity of 6 x 10^{12} at 400 GeV. We assume the usual 105 ft of liquid deuterium and the largest

presently available aperture for the broad band beam. To achieve highest intensity, the Fermilab tagged beam is assumed to be operated in untagged mode with a thick (20%) radiator. The CERN beam is described for 400 GeV protons and a 30% radiator. In Fig. 6, we show the photon intensity as a function of energy for these beams. For the Fermilab tagged beam we show separately the intensity for 100, 150, and 200 GeV electrons, showing the tradeoff required between energy and overall intensity. In Fig. 7 , we show the number of photons above fixed energy:

$$N_\gamma(E_\gamma) = \int_{E_\gamma}^{E_{max}} \frac{dN_\gamma}{dE}\, dE \quad .$$

For energies greater than 100 GeV, the yield of photons per incident proton is a factor of ten higher for the broad band beam than for the tagged beam run in untagged mode with the relative intensities diverging rapidly with increasing energy.

The broad band beam is by far the most intense available source of photons with energies greater than 100 GeV, and with sufficient intensities between 50 and 150 GeV to require a forward spectrometer capable of very high interaction rates.

C. Hadron Contamination

In addition to high energy photons, the broad band beam contains a small number of K_L and neutrons. Because the total cross section for hadronic interactions in the target is hundreds of times larger for K_L and neutrons than for photons, this hadron component is not negligible. We have measured the hadron contribution to the total interaction rate by simply removing the photon component with six radiation lengths of lead. We observe roughly equal contributions to the total interaction rate for energies between 50 and 150 GeV, with the hadron contribution increased to 80% of reactions between 250 and 300 GeV.

At worst, this hadron contamination of the beam might increase backgrounds by factors of two to five depending on total energy. Our emphasis on highly constrained signals should reject hadron-induced backgrounds at least as well as photon-induced backgrounds. For diffractive production, we can achieve event-by-event identification of parent particles. For more inclusive measurements such as associated bottom production, we can separate contributions to observed signals by running with and without photons in the beam. We expect hadron-induced backgrounds to be considerably reduced from the E-87A inclusive charm search, where the strange particle signature of a charm particle decay emphasized the K_L induced reactions so that 80% of the charm particle candidates were hadron induced.

IV. The Detector

The physics program outlined above requires a very special detector. In particular, we require:

i. A detector with very high efficiency for complete reconstruction of complex states.

ii. A detector which performs the traditional fast trigger function - selection of desired events - when the desired signature is very complicated.

iii. A detector whose performance does not deteriorate in the presence of tens of millions of detectable particles per second.

iv. A detector capable of supplying, in useful form, considerably more information than normally available for off-line study.

We will describe below a detector which meets all of these requirements. Its design has been guided in large part by our experience with the E-87A detector, whose principles of operation, strengths and weaknesses are well understood.

The new detector must have greater geometrical acceptance, more efficient particle identification and photon detection, and the ability to operate at higher interaction rates. Although the improvement in each separate item will turn out to be a modest factor, the overall increase in the product of acceptance times interaction rate will be more than a factor of 100 for those states accessible to E-87A. The largest single improvement must therefore be in the information handling, for both event selection and event recording. Although the overall improvement is a startling innovation, no new physical principles are introduced. In particular, none of the apparently sophisticated electronics involves marginal or state-of-the-art components. Even the hardware processor is built with digital circuitry (ECL 10k) which we have used for years on a comparable scale.

The modifications planned for the detector are summarized immediately below and later described in greater detail:

1. Spectrometer: We increase the solid angle acceptance by a factor of 6 over E-87A. We increase the redundancy of the wire chamber system in a manner that simplifies and improves the pattern recognition.

2. Particle identification: We greatly enhance efficiency for complete event reconstruction by increasing the segmentation and solid angle acceptance of the Cerenkov counters and photon detector, and by adding a lower threshold momentum Cerenkov counter.

3. Information handling: A preliminary design has been completed for a processor that will allow almost 100,000 events per second to be fully reconstructed on-line, with only about 10% deadtime. This will allow efficient and flexible event selection at high interaction rates. Recording the processing results will tremendously reduce off-line computation requirements.

A. Detector Dimensions and Acceptance Considerations

To understand the relevant dimensions of the detector, we need to consider momentarily the properties of Lorentz transformations and the spectrum of masses and energies we intend to measure. Consider a system of invariant mass M_X with laboratory energy $E = \gamma M_X$ and velocity $\beta \approx 1$. In the M_X rest frame, a particle of mass m and momentum p* is produced at an angle θ^* away from the axis of the Lorentz transformation to the lab frame. This particle appears in the lab with an angle

$$\tan \theta_L = (1/\gamma) \frac{\sin \theta^*}{\cos \theta^* + \sqrt{1+(m/p^*)^2}} .$$

This relation is plotted in Fig. 8 for $m/p^* = 0, 0.5, 1$. For massive particles, the laboratory angle has a maximum of $(p^*/m)(1/\gamma)$. For highly relativistic center-of-mass-system particles such as photons, 80% of the center-of-mass solid angle lies within $2/\gamma$ in the lab, 94% within $4/\gamma$. By

increasing the lab solid angle a factor of 4 in going from $2/\gamma$ to $4/\gamma$, we pick up only 14% more center-of-mass solid angle. All K mesons with p^* less than 1 GeV appear in the lab at angles less than $2/\gamma$.

For photon detection we have an additional inefficiency introduced by the hole required in the photon detector for the photon beam. Here we miss a fraction of the center-of-mass solid angle $(\gamma\theta_H)^2$. For our present design, $\theta_H = 5$ mr, and we lose 6% at $\gamma = 50$. Since more than half of the center-of-mass solid angle appears at laboratory angles less than 20 mr at $\gamma = 50$, the finite resolving power of the charged particle identification and the photon detector become increasingly serious problems at higher energies.

The detector described below has an inner detector that covers lab angles up to 120 mr with a highly segmented multiparticle spectrometer, and an outer detector that covers lab angles up to 250 mr with a less segmented detector designed for lower momentum particles. These angles correspond to $2/\gamma$ and $4/\gamma$ for $\gamma = 16$. We believe the detector is well designed to cover the range $16 \leqslant \gamma \leqslant 50$ with very high efficiency for accurate reconstruction of the multiparticle states which we propose to measure.

B. Detector Layout

The proposed detector layout is shown in Fig. 9 . The arrangement is very similar to that used in Experiments 87A and 401: two bending magnets with five stations of wire chambers, Cerenkov counters and photon/lepton/hadron detection and separation.

The target (T) is inside the first bending magnet (M1) and surrounded by a simple recoil detector (R). The narrow wire spacing drift chambers are designed to cover $\pm$ 250 mr (P0, P1, P2) and $\pm$ 120 mr (P3, P4) in both bending and nonbending views. Each chamber contains four planes, labelled x, y, u and v, measuring the nonbending view, the bending view and $\pm 11^\circ$ away from the bending view. The individual chamber parameters are listed in Table II.

The bending magnet M2 must be a new magnet, with an aperture of 40 in. x 40 in. and a length of 60 in. The maximum desired field integral is 450 MeV corresponding to a field of 10 kG. The two magnets would normally be run with opposite polarity, with field ratios chosen to provide no net deflection 20 in. downstream of P4, permitting electrons produced in the target to pass harmlessly through the hole in the photon calorimeter. Running with opposite polarity also increases the number of desired particles transported safely through the entire spectrometer and reduces the range of angles to be covered by each mirror in the downstream Cerenkov counter. The spectrometer resolution is conservatively estimated at $\pm$ 0.1 mr, with $\Delta p/p^2 = \pm 0.0002$ in M2 and $\Delta p/p^2 = \pm 0.0010$ in M1. This is identical to the resolution obtained in E-87A, because we have used the improvement in spatial resolution to shorten lever arms and increase solid angle. If we succeed in achieving 100 micron rms position resolution in the drift chambers, which appears practical but unproven, our resolution will improve another factor of two.

The entire spectrometer acceptance is covered by photon calorimeter with the exception of a 4 in. x 4 in. hole for beam particles and electron pairs from the target. The region 5-120 mr is covered by a Pb/MWPC calorimeter behind the last drift chamber. This detector should have photon energy rms resolution of about $20\%/\sqrt{E}$ and will be as finely segmented as practical, 3000 channels. The region 120-250 mr will see many fewer and lower energy particles, requiring less segmentation but better energy resolution. This region would be covered by a relatively thin Pb/MWPC and a Pb glass array, immediately in front of M2.

The Cerenkov counters C0, C1, and C2 are segmented atmospheric pressure gas counters with pion threshold momenta of 3, 6, and 12 GeV respectively. With over 200 phototubes, the segmentation and momentum range of these counters permit efficient particle identification for the range of energies,

multiplicities and masses we hope to measure.

Scintillation counter hodoscopes S1 and S2 are used in trigger formation. At the rear of the detector are a hadron calorimeter and muon identifier.

C. Drift Chambers

The charged particle spectrometer is designed to provide high resolution and high efficiency for measurements of multiparticle states in the presence of 30 million e^+e^- pairs per pulse and 3 million muons per square meter per pulse. With 3 mm gaps between anode and cathode planes, the three upstream chambers have maximum memory times of 60 ns, and maximum drift times of 20 to 40 ns for 2 mm to 4 mm anode wire spacing. A new amplifier/discriminator recently developed at Nevis is nearly deadtimeless and has greater sensitivity than our ten year old design used in E-87A. Operating the chambers at lower gas gain and with shorter gaps than our present chambers will result in much lower stored energy and total ionization.

The drift chamber configuration is not very traditional, but is a slight variation of our present arrangement. The four planes per module include no staggered pair of parallel wires. Instead, once the track is reasonably well determined, almost any two planes form a staggered pair, so that the left/right ambiguity is resolved even when one time measurement is missing or in error. With our narrow wire spacing and wide range of track angles, the initial improvement in time and position for which wide spacing drift chambers require staggered pairs is neither necessary nor possible.

Our present experience indicates that we can reconstruct more than a dozen tracks from a single interaction in the presence of one or two unrelated photon conversions and several out-of-time hits and still have very close to 100%

reconstruction efficiency. The reconstruction algorithm was developed for Experiment 87A. We first ignore the time information and find all single view tracks which have no missing hits. Different views are then paired: two views fully determine the track, which is then fit to all planes with an iterative least square fit to five independent track parameters using the drift times and realistic magnetic field. Missing hits are thus tolerated in at most two views. With single plane inefficiencies of well under 1%, in-time tracks very seldom miss three hits.

We would use a time digitizer developed in the later stages of E-87A. It is purely digital, providing 32 time bins of width 2.5 ns, with a maximum of a single hit per wire. We have achieved finer than 200 micron resolution with the E-87A chambers which were not originally designed for time measurement. We hope to achieve 100 micron resolution, but for the purposes of this proposal we restrict our expectations to 200 microns. The individual wire plane digitizations can be read out in parallel at 10 MHz, and so an event with 10 hits per plane requires about 1 μs for complete readout.

D. Photon Detector

To obtain high efficiency for full reconstruction of multiparticle states requires very high efficiency for reconstruction of a single particle in the presence of other nearby particles. We wish to build a photon detector immediately behind the last drift chamber module. This detector must be 8 ft x 8 ft with a 4 in. square beam hole. The detector must tolerate more than a million electron pairs per second produced by beam interactions in material between the two magnets. It should have sufficient segmentation and resolving power to allow separate measurement of several photons in the presence of several hadrons, with

sufficient energy and position resolution to allow identification of intermediate particles such as neutral pions and to insure accurate reconstruction of the entire event.

Since most photons result from neutral pion decay, identifying other sources of photons becomes easier if neutral pions are reliably reconstructed. Our ability to see interesting signals involving photons from other sources depends on our ability to reduce backgrounds. Identifying the two photon decay of a fairly stable particle, for instance, requires good mass resolution, but one would readily trade a factor of three in mass resolution for improved detection efficiency and a ten-fold reduction in background.

We have just completed tests of a prototype Pb/MWPC photon calorimeter which has rms energy resolution of $24\%/\sqrt{E}$. This is perhaps four times worse than we might be able to achieve with Pb glass counters, but is amply compensated by rms position resolution finer than 2 mm and the ability to separately resolve two showers separated by more than 4 cm.

The sampling size is set by several considerations. The spatial resolution is optimum and relatively insensitive to confusion if the shower leaves big signals in more than one element. The energy measurement is similarly insensitive to confusion if the sampling size is somewhat smaller than the shower size. The optimum would probably be a two dimensional array of 1 cm^2 elements, but we see no practical way to achieve this. We plan instead to segment the detector first into quadrants, with further segmentation into 1 cm vertical and horizontal strips. The basic sample is 6 mm of atmospheric pressure isobutane with 25% argon and a trace of methylal, with electrons liberated by charged particles and then collected and multiplied by 30 micron diameter anode wires spaced 3 mm apart. Each plane of anode wires is

centered in the 6 mm gas gap between two cathode planes, one segmented into horizontal strips and the other into vertical strips. Each gas gap is preceded by a lead radiator, typically 0.5 radiation lengths, for a total of 22 radiation lengths. Corresponding strips from a sequence of gas gaps are then tied together so that their current is collected and amplified by a high gain current amplifier. The counter tested was 1 ft x 4 ft with 24 gaps, the first preceded by 1.5 radiation lengths, the next 15 preceded by 0.5 radiation lengths each and the last 8 preceded by 1 radiation length each.

The Pb/MWPC calorimeter has an output pulse width of less than 100 ns. With provision to flag out-of-time pulses, high efficiency at full resolution is possible at rates above a megacycle. We have developed a very high quality ADC compatible with the high interaction rate and high event reconstruction rate, but quite inexpensive ($25/channel). The ADC is 12 bits, with nonlinear dynamic baseline shift. Digitization can be accomplished within 10 to 20 μs, at the end of which time a list of pulse heights above digital pedestal is present in a separate buffer for each 256 channels. After the fast gate, the integrating capacitor can be reset within 100 ns at any time, transferred to an analog buffer within 1 μs, or held until the output buffer is available. We have recently built 6000 such ADC's at Nevis for other experiments, but without the analog buffer and with more cumbersome readout. We require 4000 channels for this experiment.

E. Charged Particle Identification

Distinguishing among the charged stable hadrons (π, K, p) in multiparticle states is probably the most difficult challenge we presently face. The problem has received considerable attention, and possible solutions for Tevatron energies have been proposed. [4] We continue to rely, at least temporarily, on segmented threshold Cerenkov counters.

The disadvantages of such systems are the limited momentum range over which identification is possible and the confusion arising from finite segmentation, but they have the distinct advantage of falling within our present capabilities. We propose to improve the segmentation slightly over E-87A and to extend the momentum range to lower momenta. We postpone any serious attempt to raise the high momentum limit or achieve fully efficient segmentation.

In E-87A we used two threshold counters with pion thresholds of 6 and 12 GeV. This permitted full separation between roughly 20 and 45 GeV, with pion identification down to about 6 GeV and high energy proton identification up to about 90 GeV. We would now add a third counter with pion threshold 3 GeV, which would permit full separation down to 10 GeV and pion identification down to nearly 3 GeV.

The segmentation problem is two-fold. To eliminate confusion, not only must the number of phototubes be considerably larger than the number of particles, but the mapping of Cerenkov light onto phototubes must permit separation. If we map light from several particles uniformly over the same region, segmentation is no help. In both high threshold counters, light from a single particle illuminates a 5 in. diameter disc at the back of the counter. Viewed from the target, this is 12 mr for the downstream counter. Since the density of high energy forward particles is proportional to γ^2, with the entire forward hemisphere appearing at lab angles of less than $1/\gamma$, separation of individual particles becomes increasingly difficult at high energies.

We describe the three Cerenkov counters in Table III. We are proposing slight improvement in both the segmentation and imaging within the original solid angle acceptance of the counters C1 and C2, with much less segmentation at larger angles. In E-87A, C1 and C2 had 12 and 16 phototubes, but they covered less than 10% of the proposed solid angle acceptance and resulted in some confusion in 30% of the

accepted four-body final states.

We use rectangular arrays of spherical mirrors to reflect Cerenkov light onto phototubes. For C0 and C1, we require aluminized mylar plane mirrors to deflect the light to spherical mirrors outside the active aperture of the spectrometer. For particles from the target region with momentum above pion threshold, all Cerenkov light reaching an outer mirror is imaged directly onto the good photocathode region of a 5 in. phototube. Reflecting cones to increase the light collection of these tubes would only increase the number of undesirable photons from other sources. Each inner mirror focuses Cerenkov light onto a rectangular mirror baffle which further segments the light with at most one grazing reflection onto small (1.6 in.)phototubes.

If the segmentation were fine enough, and in the focal plane of each spherical mirror, we could measure the Cerenkov angle. With considerably coarser segmentation than would be required for a true imaging counter, we instead attempt to minimize the spread of light from a single particle compared to particle separations. We therefore focus on each baffle a sharp image of the center plane of the Cerenkov counter.

The total number of phototubes is modest: twenty-four 5 in. tubes and one-hundred and eighty 1.6 in. tubes. The small tubes are only ten stage and require fast amplifiers with small dynamic range but rapid recovery from overload. These small tubes are expected to cope with the light from the 30 million electron pairs per pulse. Our experience has also shown that the tubes must cope with modest rates of charged particles passing through their glass envelopes, producing quite large signals.

F. Hardware Processor

The experimental program outlined in this proposal requires fairly complete on-line event reconstruction within tens of microseconds. Since the Fermilab Cyber 175 system takes a thousand times longer to perform the same computation, this might at first glance appear to be a difficult and dangerous requirement. We believe, however, that such information processing power has been possible for the past few years, using simple, reliable and inexpensive processors assembled for specific problems.

We first develop a general approach to such processing by identifying small simple hardware elements and simple rules for their interconnection that permit any digital computation to be performed with optimum efficiency, measured in operations/second/dollar. Such a general approach not only permits general application, but is probably necessary for practical solution to a specific complex problem which probably spans most of the general features of digital computation by itself.

Our understanding of the general principles continues to evolve. Had we built the proposed processor a year ago, it would have worked exactly as expected. Today we can build a smaller version that would be twice as fast. After building and using such a device, we could undoubtedly do even better, but the original device would remain functional and compatible with any expansion of the problem.

The general principles are quite simple. Data are transferred from register to register under control of a central clock. The clock period, presently 25 ns, is determined by the time required for register to register transmission through an intermediate arithmetic operation, memory reference or intermodule transmission line. Central control is exerted only by the clock, and by a control/communication bus which is idle during normal processing, but can be used to access any register in the system from the outside, allowing diagnostic exercises and the loading

of tables.

In general, we have neither central memory nor stored program. Memory is an integral part of the processor, providing tables of precomputations, lists of variable data, and maps. Three essential control functions appear in the computation data paths:

i. V, here is a new data element (from source).
ii. C, sequence of data elements is complete (from source).
iii. H, unable to accept transmission (from receiver).

A computation requiring n sequential steps can be performed in a pipeline of n distinct hardware elements so that the delay through the pipeline is n cycles, but a new computation can begin each cycle. Many such pipelines can operate simultaneously and independently. Such a structure is called a pipelined parallel processor.

The parallel pipeline structure appears at more than one level. On a macroscopic scale we expect an event to have analog signals digitized in parallel with track reconstruction, while at the same time the previously accepted event is undergoing kinematic reconstruction. Such a pipeline may eventually be several events deep. All information that might eventually be used must be stored until the final disposition decision.

Additional, possibly unforeseen, computations can always be added, either in parallel at some stage of the pipeline, or in series as a new pipeline stage. Such new computations should not affect the rate of event reconstruction.

The incredible cost effectiveness of computation in this structure results from the possibility of using simple special purpose devices for their specific purposes at full speed with few idle periods. The pipeline structure almost guarantees this capability. Operations which must be performed very many times can be unfolded into a large fast pipeline, while infrequently performed operations can be folded in several ways to maintain the same operations/second/dollar.

The processor can be simulated exactly in Fortran on a normal computer so that one can study the processor performance before actually building it. We construct software modules that simulate corresponding hardware modules exactly, and then specify their interconnections, including the control/communication bus. Given the input data for the computation, we can predict the status of every element in the processor, cycle by cycle. We thus determine how long the computation would require and what the result would be. We thus isolate bottlenecks and underutilized hardware. Both the hardware and the software version can analyze raw data from tape. In addition to the necessary diagnostic and developmental studies, this permits use of the processor for Monte Carlo studies.

We have preliminary designs for a data analysis, selection and histogram structure which would permit studies of very high rate processes without recording individual events on tape. We do not anticipate such rates for reactions of general physics interest in the proposed experiment, nor do we see clearly how to make use of such rates yet, but such a feature will allow on-line diagnostic and calibration studies continuously without interfering with the selection and recording of events of more general physics interest.

The size, physical complexity, and cost of the processor are all small compared to the hardware supplying the input data. The design and construction of actual hardware should always be quick and simple. The time and complexity appear at the software level.

V. The Experiment: Interaction and Data Rates

We anticipate running with 3-6 x 10^{12} 400 GeV protons per pulse incident on the existing beryllium target. The neutral beam collimators would be set at the present maximum aperture with the 32 m of liquid deuterium in place. The experimental target would be a piece of beryllium 1.75 cm thick (5% radiation length), in which about 4% of photons and 5% of hadrons interact. On the average, secondary particles have about 2.5% probability of interacting, and so about 10% of the four-body final states suffer secondary interactions within the target.

We have designed a detector which should perform well at the very high rates accompanying 6 x 10^{12} protons per pulse and the largest beam size. Such high intensity may not always be available or desirable, but will be assumed for consideration of the instantaneous rates and the challenge they present. Total integrated rates are based on an exposure of about 10^{18} protons, which would be 500 hours at 6 x 10^{12} or 1000 hours at 3 x 10^{12}, assuming 400 pulses per hour. For such a run, the integrated luminosity is 3.7 x 10^4/nb for photons above 50 GeV, and 1.4 x 10^4/nb for photons above 100 GeV. The integrated luminosity in E-87A for energies above 50 GeV was 1.0 x 10^3/nb.

At 6 x 10^{12} incident protons and the largest collimator setting, the neutral beam at the photon target provides about 10^8 photons with energy above 50 GeV within a spot size 7 cm x 7 cm. Extrapolating from Experiment 87A, the total rate of e^+e^- pair production in the target will then be 3 x 10^7 pairs/pulse, and the peak muon flux in the area will be less than 3 x 10^6/meter^2/pulse or about 15 million muons per pulse incident on the entire detector. The total rate of hadron production by photons with energy above 50 GeV is more than 2 x 10^4 per pulse, with a similar number produced by energetic hadrons in the beam and about twice as many produced by lower energy photons. We summarize these running conditions in Table IV.

We summarize below the acceptance and expected rates for selected states based on extrapolations from rates observed in E-87A or on current theoretical predictions. States are divided into two overlapping categories: those that we expect to observe in coherent diffraction from the entire nucleus and those representing interesting rare events with sufficiently clean signatures that we would not require coherent production to isolate the signal from backgrounds.

We expect an increase in observed signal over E-87A that depends on the state in question, but ranges dramatically upward from a factor of more than 200. There are several factors responsible for this increase. The total luminosity is a factor of 37 higher. In general, the geometrical acceptance has increased by at least a factor of 4, and the triggering efficiency by at least a factor of 2. The probability of unambiguous identification of a typical charged hadron has increased from less than 0.7 to more than 0.9, and the possibility of efficient detection of photons in multi-particle final states becomes at last possible. This enormous increase in the efficiency of identification of charged particles and the detection of photons permits not only a large increase in signal but also a large reduction of backgrounds.

A. Coherent Production

In Table V , we list acceptance and expected rate for a representative sample of coherently produced final states. We have not included odd pion final states, or in fact any final states containing photons, because of the difficulty of extrapolating from E-87A. We plan to study such states and expect a majority of states with more than two charged particles to contain photons. Many interesting states for which our detection efficiency is high have no reliable estimates for production cross sections, but should be readily visible. Such states include high mass vector mesons and diffractively produced continuum which decay into charm-anticharm pairs or states containing η_c's or χ's.

We see from Table V that not only do we expect large numbers of events at high masses, but we have extremely large samples at masses below 3 GeV. We now consider the listed states:

1.,2.) The coherent $\pi^+\pi^-$ mass distribution from E-87A has already been shown in Fig. 2 . The figure shows ρ and ρ' along with some possible structure near 2.1 GeV. This distribution should become more interesting with the increase in statistics by a factor of 1000 which we anticipate for masses above the ρ.

3.) The large number of events expected in the four charged pion channel will allow a thorough study of the still puzzling decays of the $\rho'(1600)$. Comparable statistics can be expected for the $\pi^+\pi^-\pi^o\pi^o$ state. Any higher mass structures should be observable up to masses of about 8 GeV, and should become easier to understand when widths are small compared to the difference from threshold mass.

4.,5.) $K^+K^+K^-K^-$ or $K^+K^-\pi^+\pi^-$: As in the four pion state, information will be available out to about 8 GeV with very high statistics at lower masses. One intriguing possibility is the existence of $\phi\phi$ resonances. The three $\phi\phi$ events observed in E-87A all lie within 50 MeV of 2.4 GeV. Our sensitivity to this state is about 30 events/pb. Our ability to see Primakoff production of η_c will depend on the branching fraction of η_c into the specific channels such as $\phi\phi$ and the partial width into $\gamma\gamma$. According to Quigg and Rosner,[5] the Primakoff cross section at 200 GeV is,

$$\sigma(\gamma+\mathrm{Be} \rightarrow \eta_c+\mathrm{Be}) = (10\ \mathrm{pb/nucleon})\ \frac{\Gamma(\eta_c\rightarrow\gamma\gamma)}{1\ \mathrm{keV}} \ .$$

Irrespective of whether we see Primakoff production of η_c we do expect to see η_c in coherent production with additional hadrons, just as we see copious production of $\eta\pi^+\pi^-$.

B. Rare Processes with Clear Signatures

In Table VI , we list acceptance and predicted event rates for specific rare processes. We leave out examples of conventional particle production that could be selected, such as $\Lambda\bar{\Lambda}$ and Ω^-. We now discuss some of these processes in detail:

2) In E-87A we observed 90 events containing a ψ plus hadron, of which 30 events contained at least one identified K meson. Extrapolating from this we would expect to see 250 times as many ψ accompanied by hadrons, and provide more complete measurement of the hadrons. This implies 13,000 such events with 4,000 containing an identified K meson. These events are interesting for several reasons other than simply studying properties of inclusive ψ production. Observation of the accompanying particles should provide information about the dynamics of charm production, including illumination of OZI predictions. Other possibilities include the observation of heavier states which decay to ψ plus other particles, whether by weak, electromagnetic or strong interaction.

3) As shown in the table, we expect more than a million events with a fully reconstructed D meson. Inclusive D meson production in itself is probably not best done in this experiment, but triggering on a visible D candidate would allow us to look for associated production of other charm particles or decays from a higher mass narrow state. Specific known decay modes of the Λ_c are equally easy to select. Cross sections for production of other states in association with observable known decays are not known, but production of F mesons and the remaining baryons will be observable unless suppressed by two orders of magnitude relative to $D\bar{D}$.

4) Bottom production: The model of $B\bar{B}$ production discussed in Ref. 1 predicts an asymptotic cross section for $B\bar{B}$ production of 27 nb, with an energy dependence similar to

that given in Fig. 5 . The model is quite simple and predicts cross sections for photoproduction of heavy quarks which scale to lowest order as $\sigma \propto (e_q/m_q)^2$. The model predicts an asymptotic charm cross section of about 1.0 μb and a ψ cross section of 50 nb. In E-87A we measured

$$\sigma(\gamma+C \rightarrow D^0+X) \approx 500 \text{ nb/nucleon}$$

$$\sigma(\gamma+C \rightarrow \psi+X) \approx 30 \text{ nb/nucleon} .$$

Integrating the predicted energy dependent cross section over the photon spectrum, we obtain a total of 325K $B\bar{B}$ events, most of which should be fully within our acceptance. The fraction of these decays which can be reconstructed is unknown, of course. We cannot reconstruct states with a neutrino, a neutron or a K_L. Even with a wide range of detectable decay modes, we should be able to see $B\bar{B}$ production by requiring fully reconstructed associated production. Specific cascade decays to ψ and charm particles may permit observation of single B inclusive production.

5) Our estimated upsilon production is based on a related prediction for the cross section, which becomes 270 pb at high energies. Using the energy dependence which we obtained for the ψ, and assuming a leptonic branching ratio of 4 %, we predict 30 detected $\Upsilon \rightarrow \ell^+\ell^-$.

C. Event Trigger

We propose to record any event falling into one of the following three categories:

1) Any coherently produced state, except low mass pion pairs, with energy above 50 GeV. Experimentally, coherent means total observed charge zero, low P_t^2 and nothing detected in a recoil detector sensitive to fairly low energy photons. Since coherent diffractive photoproduction represents about 5% of the total cross section, with the ρ excluded, this would be well over a thousand events per pulse, including hadron induced events. Because we have no desire to fill a

magnetic tape every 5 minutes, the majority of these events would be recorded in very compact form, averaging about twenty 16-bit words per event. Rare and unusually interesting events would be recorded in greater detail, including raw drift chamber data and/or raw ADC data (no pedestals). If unnecessarily large numbers of low mass events would be recorded this way, we could always choose to record a fixed fraction of the low mass and low multiplicity events.

2) Any state containing a lepton pair, except low mass Bethe-Heitler. Even including low mass Drell-Yan and vector meson decays, this amounts to less than 10^{-3} of the total cross section.

3) Candidates for clear signature production of C or B. This would include candidates for specific charm particle decays with enough visible mass to be candidates for reconstructed associated production or cascade from a heavier state. The charm particle decay must be to fully identified hadrons and have a mass within experimental resolution ($\leqslant$ 5 MeV) of the correct mass. To also include most $B\bar{B}$ production but keep the number of candidates below 10^{-3} of the total cross section, we would record events with at least 6 GeV for the sum of the individual particles' transverse momentum (magnitude).

We hope to write less than half as many words per pulse onto tape as in E-87A, or at most 32 K 16-bit words per pulse, composed roughly equally of 500-800 low mass simple topologies recorded in compact form and 50-80 fully recorded complex or rare events. In 500 hours of 400 pulses each, for a total of 2×10^5 pulses, this translates to more than 10 million rare events and 100 million simple topologies, carefully selected with full off-line precision from 4×10^9 high energy photoproduction reactions and a comparable number of neutron and K_L induced reactions.

We envision a triggering scheme similar at the primitive level to the one used in E-87A. We first form a fast trigger (Master Gate) which is used to gate ADC's, TDC's and coincidence registers. The decision to accept the event for the next stage of processing, that is track reconstruction and charge digitization, is formed by a slow trigger (DC logic) which performs nonrecursive digital operations based on the status of drift chamber TDC latches and of coincidence registers which record scintillation counter coincidences and low precision (1 to 4 bits) analog-to-digital conversion. The gate widths, the DC logic time and the time required to reset the ADC's are each nearly 100 ns. The Master Gate deadtime is therefore about 250 ns and so the Master Gate rate must be kept below 400 kc to keep its contribution to total system deadtime below 10%. This is considerably less than the 30 million electron pairs produced in the target or the 15 million random muons at the back of the detector, but ten times the number of energetic hadronic final states produced in the target each pulse.

The Master Gate is therefore to be the sum of two unrelated triggers: the first attempting to pick up all target interactions except muon pairs and low mass Bethe-Heitler electron pairs by requiring a minimum of perhaps 5 GeV in calorimeters that fill the aperture except for the beam hole and that portion of the photon calorimeter accessible to low mass electron pairs produced by beam interactions with material between the two magnets. The second trigger attempts to pick out muon pairs coming from the target region by using scintillation counter hodoscopes in the nonbending view. This suppresses the few million random coincidences per pulse between muons illuminating the largest areas of the detector without passing near the target region. We anticipate no difficulty in keeping the Master Gate well below 400 kc.

The slow trigger must then reduce the trigger rate to the level of 50 kc. This can be done with a sum of simple triggers requiring something more impressive in the calorimeters or using the drift chambers as fine grained hodoscopes to guarantee charged particles from the target vicinity other than low mass electron pairs.

Upon a slow trigger decision to analyze further, about a microsecond is then required to transfer all the analog and digital information to processing buffers before the detector is ready to accept another event. We can therefore operate with a total deadtime of 250 ns times the Master Gate rate plus about 1 μs times the slow trigger rate for a total of 10% to 20% deadtime, even though we require 10 to 20 μs to analyze each of more than 50 K events per second.

D. Comparison to Tagged Beam and e^+e^- Annihilation

We regard the program set forward in this proposal as complementary to the program planned in the tagged photon laboratory. Although there will inevitably be some overlap in the physics produced we intend to concentrate our efforts on those areas which are dependent upon the high energy and high intensity of the broad band beam. In our view, there are two such areas:

1. Photoproduction of very high mass states. We have argued that the production of states with masses in the range 5-12 GeV/c^2 is best accomplished in the broad band beam owing to its relatively high intensity at high energy.

2. Photoproduction of rare events with complicated topologies. We have argued that the observation of rare events with complicated but well defined signatures is possible only if running is done at very high intensities with a detector capable of correctly identifying and measuring such events.

We would not expect to compete with the tagged beam in areas in which a knowledge of the photon energy or the

lack of hadron contamination in the beam is critical. (Such an area would be measurement of the energy dependence of inclusive charm production.) However we do expect to be able to study final states such as very high mass vector mesons, associated production of charm pairs with each particle decaying through an observable decay mode, and the inclusive production of B mesons which are beyond the reach of the tagged beam due to the two considerations listed above.

Most of the states accessible to photoproduction experiments can also be observed in e^+e^- interactions. However, there are major differences, the main one being that the entire mass range is covered simultaneously in photoproduction. In general, rates (measured in events/hour) for the production of specific vector mesons are higher in storage rings run at the appropriate energies, while rates for charmed particle production (and presumably B meson production also) are orders of magnitude higher in photoproduction. For example, in e^+e^- annihilation at the 3.77 GeV resonance, the $D^o\bar{D}^o$ cross section is $\sim$ 10 nb ($\sim$ 2 nb off resonance) while in photoproduction the cross section is $\sim$ 500 nb. The time averaged luminosity for the experiment proposed here is $2.1 \times 10^{31}/cm^2/sec$ (assuming 1 pulse every 9 sec) which is comparable to the luminosity obtainable in e^+e^- storage rings.

E. Future Plans

We hope eventually to extend the experimental program of this detector to hadron induced reactions and to the higher masses and energies which become accessible with TeV protons. The present broad band beam can readily become a high quality neutron or K_L beam. Both the detector and the present beam line are compatible with the efficient utilization of whatever proton beam is available during the possibly hectic transition to a superconducting main ring of energy up to 500 GeV.

Because the laboratory angles of secondary particles decrease with increasing energy, practical secondary beams can be built with considerably higher intensities, as well as higher energies. Several members of this collaboration

are presently involved in the design of a high energy e/γ/ hadron beam line which would be available after the Proton Lab is upgraded to Tevatron energies. Operated as a broad band photon beam, it would have high intensity of higher energy photons with no hadron contamination. Charged or neutral hadron beams would also be available.

We have designed the presently proposed detector so that the changes required for operation in the Tevatron beam would consist of additions to the proposed detector without replacement of any major elements. The longitudinal dimensions of the detector would increase, but not the transverse dimensions.

To take full advantage of the Tevatron beam would require two major advances in the detector operation, which we believe we could make after the program of the present proposal is well underway. The only real hardware challenge is the extension of charged hadron identification to higher energies. At the moment, we suspect that this could be accomplished by converting the inner segments of C2 to high precision imaging Cerenkov counter, using highly segmented phototubes with micro channel dynode structures. The other advance which we believe possible, but do not wish to explain or defend at this point, is the efficient utilization of the two or three orders of magnitude increase in information rate possible in hadron beams. Interaction rates of more than 10^6 high energy hadrons per second are possible and should be compared with more like 10^4 for high energy photons in this proposal.

VI. Construction: Costs and Time Estimates

We estimate construction costs for new equipment plus replacement cost of old equipment which we wish to use to be:

	Mechanical	New Electronics	Old Electronics	Total
Drift Chambers	$ 90 K	$110 K	$ 40 K	$240 K
Hardware Processor		100 K		100 K
Photon Calorimeter	100 K	160 K		260 K
Cerenkov Counters	100 K	40 K	40 K	180 K
Hadron Calorimeter	45 K	15 K		60 K
Muon Identifier	10 K	10 K	20 K	40 K
Trigger and Recoil System	10 K	10 K		20 K
	$355 K	$445 K	$100 K	$900 K

We request a major piece of new equipment from Fermilab: an analyzing magnet with one meter square useful aperture, providing a field integral of 15 kG meter with a pole length of at most 1.5 meters. We also request that the lab supply material for the muon identifier.

The $45 K mechanical assembly cost of the hadron calorimeter includes an estimate of the cost of replacing the existing 5 ft x 6½ ft iron plates with 9 ft x 9 ft iron plates. We could make use of much of the E-87A cabling, MWPC electronics, phototubes, and scintillator for a total of at least $100 K of the estimated $900 K of new equipment.

All electronics, the drift chambers, Cerenkov counters, hadron calorimeter and muon identifier could be installed within 12 months of approval and funding. Construction and installation of a new analyzing magnet and photon calorimeter

might require 18 months. With installation of the drift chamber system and track reconstruction hardware, we would wish to use muons accompanying targeting for the Tagged Photon Facility (TPF) for debugging and calibration. If approved in November 1979, we could be fully operational by mid-1981 without disturbing any other experimental program.

Predictions of long mid-year accelerator shutdown for construction, present uncertainties associated with transition to superconducting main-ring operation, and the prospect of proton lab "pause" for upgrading to Tevatron energies, all make predictions of running schedules difficult. We could be ready by mid-1981, installed in the present 87-A pit EE4. Operation of the present broad band beam with the detector in EE4 is compatible with construction of a new beam line. The present beam and detector location would not be compatible with TPF operation, but our proposed physics program requires sufficiently modest running time, about 10 calender weeks, that interference with the tagged beam program should be minimal. We would hope later to move the detector into a new proton beam line which would permit utilization of TeV protons simultaneously with TPF operation.

We believe that our off line computation requirements will be less than those of E-87A. We wish to retain the Fermilab PDP-11 presently used for data acquisition.

VII. Summary

We have discussed in this proposal a program to study the photoproduction of high mass hadronic states. We believe that the exciting physics contained in these states is best extracted through the wide band neutral beam used in conjunction with the proposed detector. The experiment as described can be mounted for a modest cost over a reasonable time period, and has been designed to have a natural extension to the Tevatron.

References

1 H. Fritzsch, K.H. Streng, Phys. Lett. 72B, 385 (1978).
B. Margolis, Phys. Rev. D17, 1310 (1978).
H. Fritzsch, K.H. Streng, Phys. Lett. 78B, 447 (1978).

2 M. Atiya et al, Phys. Rev. Lett. 43, 414 (1979).
K.W. Brown et al, Phys. Rev. Lett. 43, 410 (1979).

3 The study of dilepton and dihadron production at high mass and single (inclusive) hadron production at large P_T indicates that the A dependence of these processes is characterized by A^{α} where α is typically 1.1-1.2, while for the total hadron-hadron cross section α is typically 0.8. The A dependence of the total photoproduction cross section is given by $\alpha \approx 0.9$ while the high mass photoproduction is unmeasured. See,
J.W. Cronin et al, Phys. Rev. D11, 3105 (1975).
R.L. McCarthy et al, Phys. Rev. Lett. 40, 213 (1978).
D.M. Kaplan et al, Phys. Rev. Lett. 40, 435 (1978).
K.J. Anderson et al, Phys. Rev. Lett. 42, 944 (1979).
R.M. Egloff, Ph.D. Thesis, University of Toronto (1979).

4 W. Willis, Physics Today, October, 1978.

5 C. Quigg, J.L. Rosner, Phys. Rev. D16, 1491 (1978).

Table Captions

I. A compilation of E_{min} and E_{th} as a function of mass M. E_{min} is the photon energy needed to produce a t value of 0.02 GeV^2 while E_{th} is the production threshold energy.

II. Wire chamber sizes and wire spacings.

III. Cerenkov counter design parameters.

IV. A summary of the proposed running conditions.

V. Rates for selected coherent processes.

VI. Rates for selected rare processes.

Table I

M(GeV)	$E_{min} = M^2/2(0.14)$	$E_{th} = M + M^2/2M_N$
1	3.6	1.5
2	14.3	4.1
3	32.1	7.8
4	57.1	12.5
5	89.3	18.3
6	129.	25.2
7	175.	33.1
8	229.	42.1
9	289.	52.2
10	357.	63.3
12	514.	88.8

Table II

Chamber		Distance From Target	Dimension	Spacing	# of Wires
Pφ	X Y,U,V	30 in.	15" x 15"	2 mm	192 192 x 3
P1	X Y,U,V	55 "	30" x 30"	3 mm	256 256 x 3
P2	X Y,U,V	80 "	40" x 40"	4 mm	256 256 x 3
P3	X Y,U,V	226 "	53" x 68"	6 mm	224 288 x 3
P4	X Y,U,V	430 "	91" x 113"	6 mm	384 480 x 3
					5728 wires

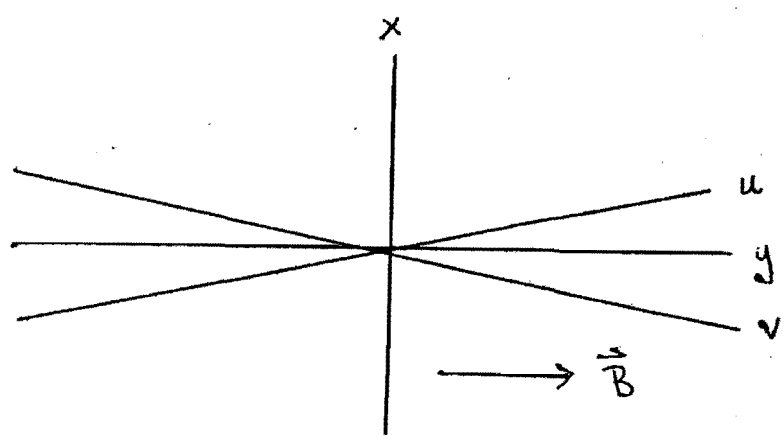

Table III

Cerenkov Counter

	C_0	C_1	C_2
Radiator	C_4H_{10}	N_2	N_2/He
$(n-1)x10^6$	1200	300	75
Pion Threshold	3	6	12
Length	20 in.	100 in.	180 in.
Downstream Size	40 " x 40"	48" x 48"	100" x 100"
Number of Spherical Mirrors	16	20	25
Size of Mirrors	12" x 12"	16" x 16"	20" x 20"
θ_c	50 mr	25 mr	12 mr
# of Photoelectrons	6	8	4

Segmentation

C_0

1	6	6	1
1	6	6	1
1	6	6	1
1	6	6	1

C_1

1	4	4	1
1	6	6	1
1	12	12	1
1	6	6	1
1	4	4	1

C_2

1	1	4	1	1
1	4	6	4	1
1	6	12	6	1
1	4	6	4	1
1	1	4	1	1

4 =

6 =

12 = 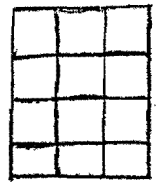

Note: Dotted lines correspond to E-87A acceptance.

Table IV

Conditions: 6×10^{12} ppp at 400 GeV, Large hole in CF408B
CF410B,
32 m of D_2.

Target: 5% r.l. of Be
e^+e^- rate = 30×10^6/pulse
μ's = $3 \times 10^6/m^2$/pulse
L = 18.5×10^{-2}/nb/pulse ($E_\gamma > 50$ GeV)
Hadronic Rate = 22,000/pulse $E_\gamma > 50$
8,400/pulse $E_\gamma > 100$

For 2×10^5 pulses (500 hours)
L = 3.7×10^4/nb $E_\gamma > 50$ GeV
1.4×10^4/nb $E_\gamma > 100$ GeV
5.1×10^3/nb $E_\gamma > 150$ GeV

Table V

(Coherent Processes)

State	E87(Obs)	Acc.87	Acc New	Expected
1. $\gamma \to \rho'(1600) \to \pi^+\pi^-$	800	0.04	1.00	720 K
2. $\gamma \to \pi^+\pi^-$ > 1 GeV	7500	0.04	1.00	6.7 M
> 2	400			360 K
> 3	50			45 K
3. $\gamma \to 4\pi$ > 1 GeV	60,000	0.15	0.98	14 M
> 2	11,000			2.6 M
> 3	1100			260 K
> 4	100			24 K
> 5	10			2.4 K
4. $\gamma \to K^+K^-K^+K^-$ > 2 GeV	50	0.05	0.40	14 K
> 3	8			2.3 K
> 4	1			300
$\phi\phi$	3			860
5. $\gamma \to KK\pi\pi$ > 1 GeV	7000	0.09	0.75	2.1 M
> 2	5000			1.5 M
> 3	500			150 K
> 4	70			21 K
> 5	10			3 K

Table VI

(Rare Processes)

State	E87 (Obs)	Acc 87A	Acc New	Expected
1. $\gamma \to \psi$				1.1 M
$\mu^+\mu^-$	350	0.15	0.97	80 K
e^+e^-	100	0.05		80 K
2. $\gamma \to \psi$+hadrons	90	0.20	0.80	13 K
ψ+K+hadrons	30	0.15	0.52 *	3.7K
$\psi' \to \psi\pi\pi$ $\hookrightarrow \mu^+\mu^-$	15	0.20	0.85	2.3K
3. $\gamma \to D^o(\bar{D}^o)$+any ($\sigma$=500nb)				18 M
$\hookrightarrow K^\pm\pi^\mp$	100	(0.005)	0.57 *	400K
$\hookrightarrow K^+\pi^-K^-\pi^+$	(1)	(0.005)	0.45 *	3.2K
$\hookrightarrow K^+\pi^-K^-\pi^+\pi^+\pi^-$	(4)	(0.01)	0.46 *	6.6K
4. $\gamma \to B(\bar{B})$+any ($\sigma=27(1-\frac{E_{th}}{E})$ nb)				325K
$\hookrightarrow \psi K^\pm\pi^\mp \to \ell^+\ell^- K^\pm\pi^\mp$			0.60 *	550 (1% BR)
$\hookrightarrow D^o\pi^\pm \to K^\pm\pi^\mp\pi^\pm$			0.50 *	85 (1% BR)
5. $\gamma \to \Upsilon$ ($\sigma=270(1-\frac{E_{th}}{E})^3$ pb)				800
$\mu^+\mu^-$			0.90	15
e^+e^-				15

* For final states involving K mesons the dominant inefficiency is from K/p separation below ~ 10 GeV/c

Figure Captions

1. The P_T^2 distribution for exclusively produced $\pi^+\pi^-$ in E-87A.
2. The mass distribution for coherently produced $\pi^+\pi^-$ in E-87A.
3. The inclusive $\pi^+\pi^-$ mass distribution from E-87A.
4. The mass distribution for the lowest mass $\pi^+\pi^-\pi^o$ combination within coherently produced $\pi^+\pi^-\pi^+\pi^-\pi^o$ events in E-87A.
5. The energy dependence of $d\sigma/dt$ at $\theta = 0$ for the photoproduction of ψ mesons. The fit curve is

$$\left.\frac{d\sigma}{dt}\right|_{\theta=0} = 66\ (1-E_{th}/E)^{3.1}\ \mathrm{nb/GeV}^2\ .$$

6. The photon energy spectra for various beams available at Fermilab:
   a) broad band beam with 6×10^{12} 400 GeV protons, large collimator hole, and 32 m of liquid D_2,
   b) tagged beam with 6×10^{12} 450 GeV protons, a 20% radiator (untagged mode) and 100 GeV electrons,
   c),d) same as b) with 150 GeV/200 GeV electrons.
7. The integrated photon spectra for the two Fermilab beams and the BEG beam at CERN. The CERN curve comes from the proposal SPSC/P 109.
8. The observed laboratory angle as a function of the center of mass angle for particles produced with $m/P^* =$ 0, 0.5, and 1.
9. The layout of the proposed detector shown in the non-bending view of the two magnets. The horizontal and vertical scales are the same.

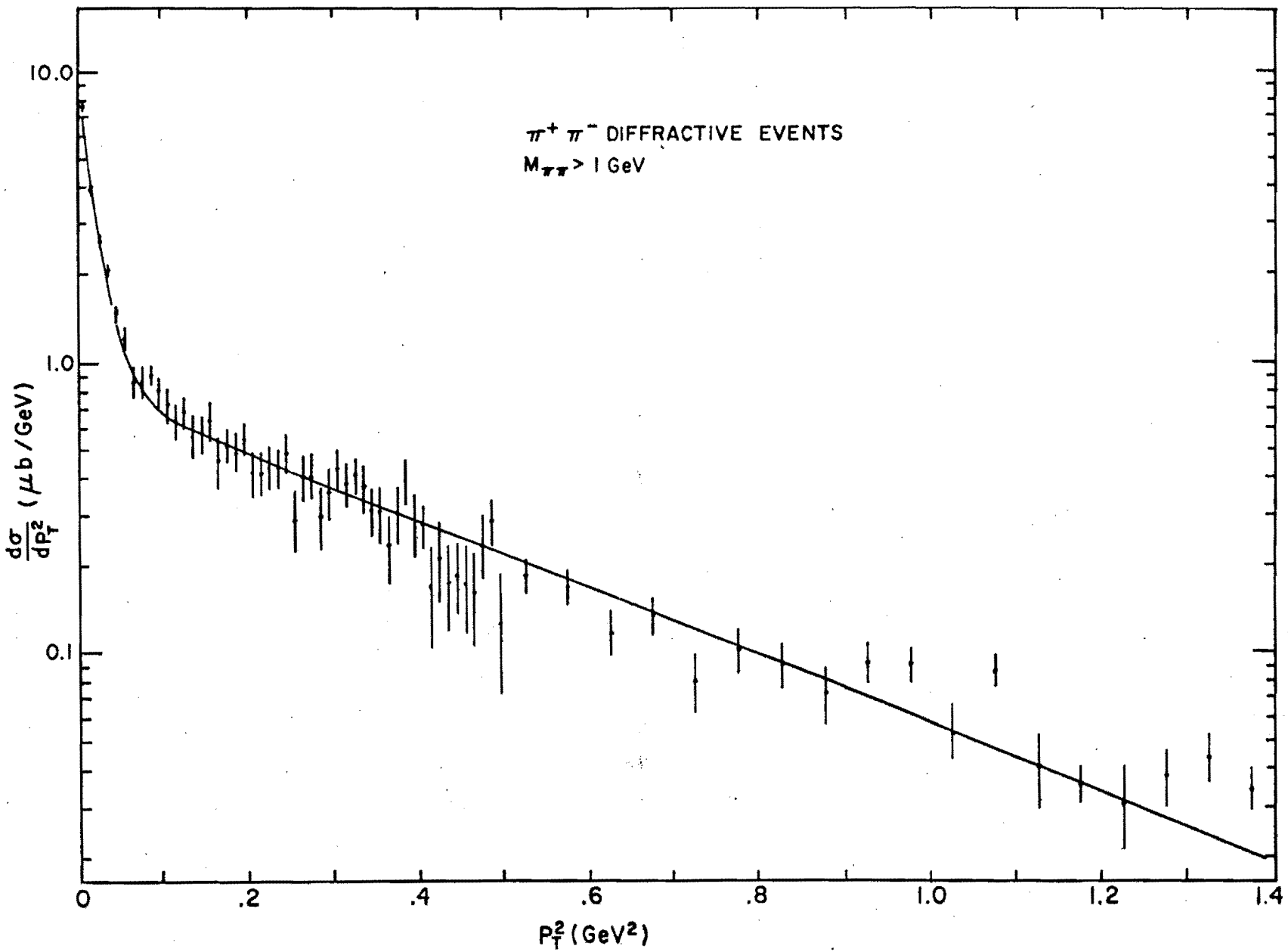
$\pi^+ \pi^-$ DIFFRACTIVE EVENTS
$M_{\pi\pi} > 1$ GeV
10.0
1.0
0.1
$\frac{d\sigma}{dP_T^2}$ (μb/GeV)
0
.2
.4
.6
.8
1.0
1.2
1.4
P_T^2 (GeV^2)

Fig. 1

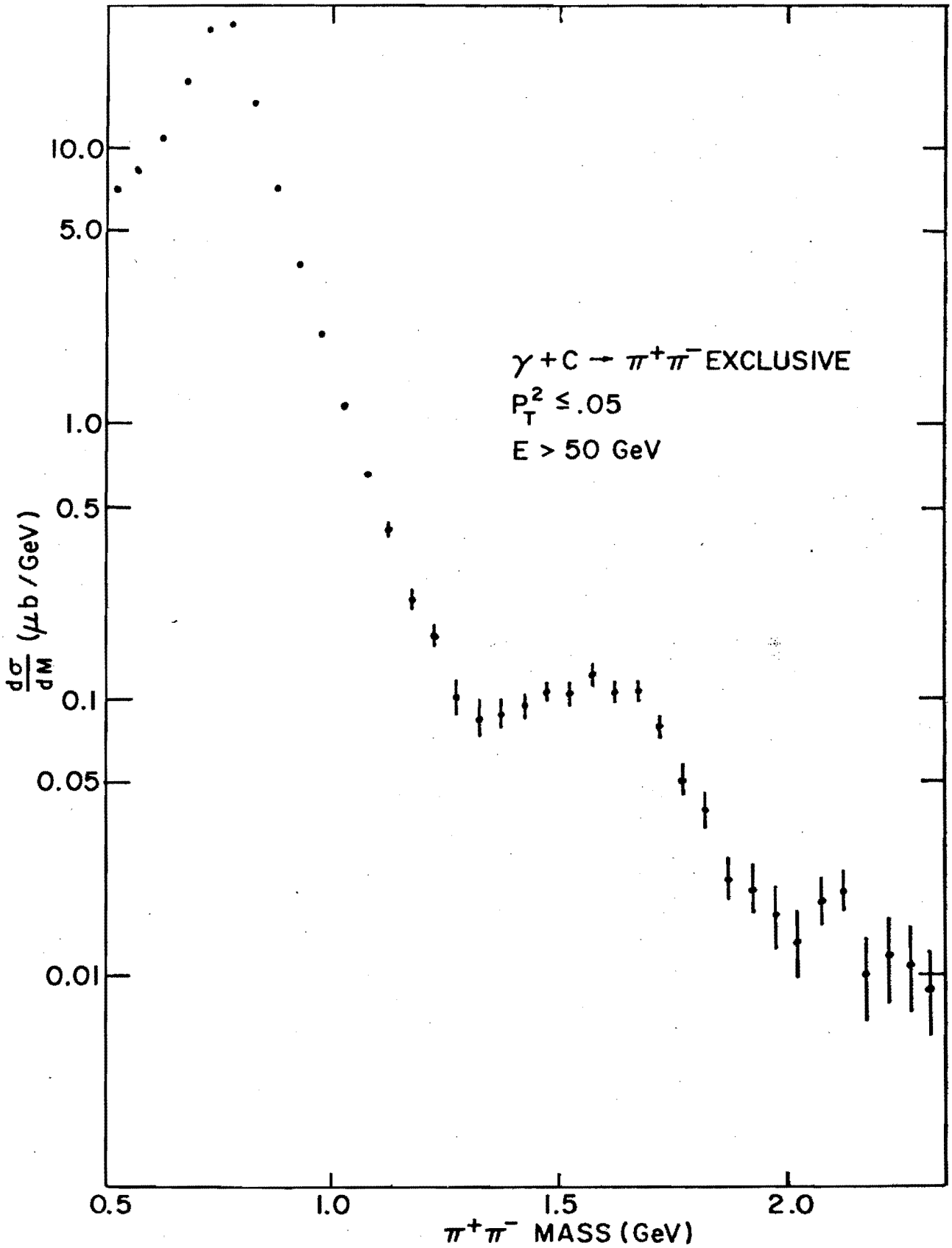
$\gamma + C \rightarrow \pi^+\pi^-$ EXCLUSIVE
$P_T^2 \leq .05$
E > 50 GeV
10.0
5.0
1.0
0.5
0.1
0.05
0.01
$\frac{d\sigma}{dM}$ (μb/GeV)
0.5
1.0
1.5
2.0
$\pi^+\pi^-$ MASS (GeV)

Fig. 2

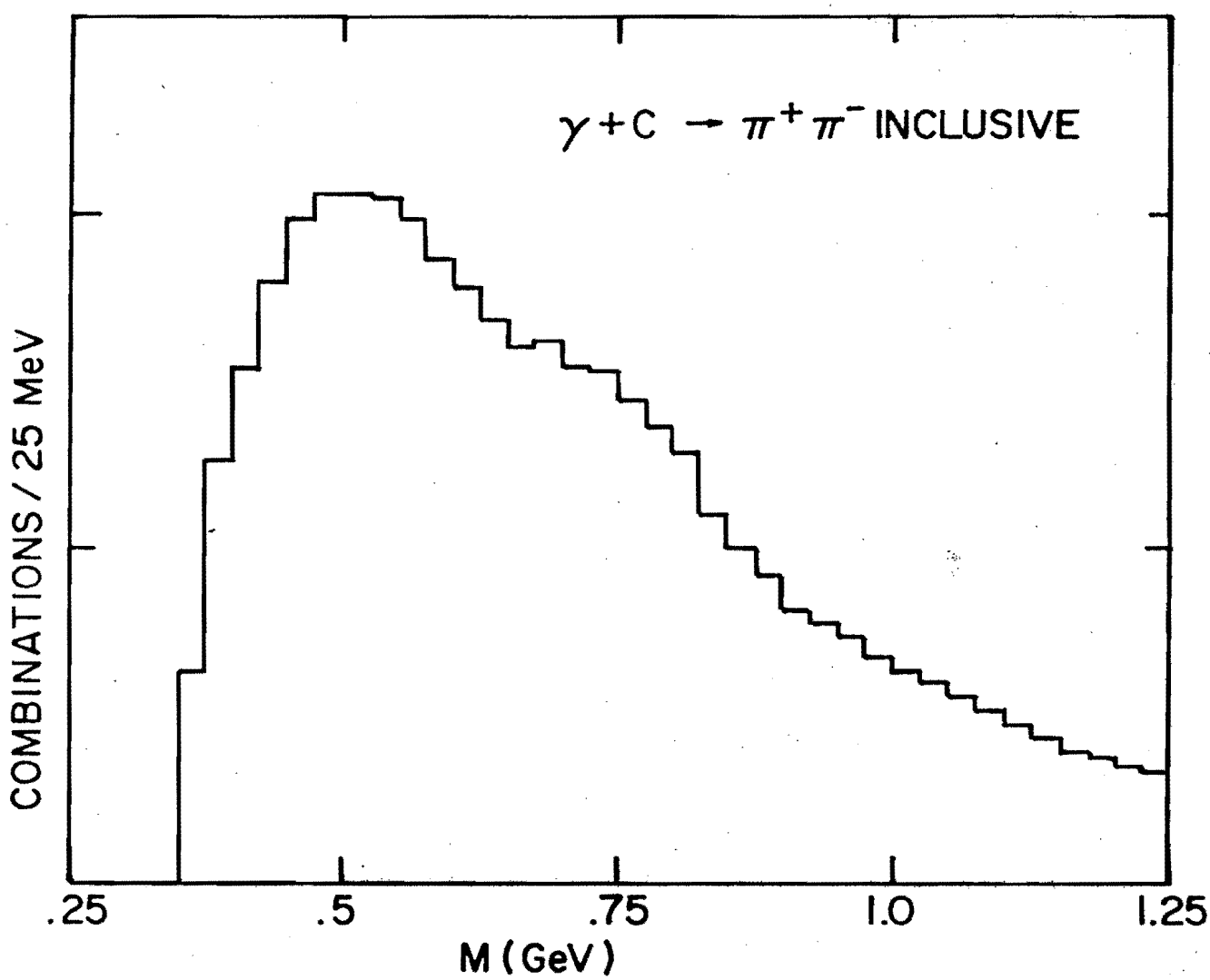
$\gamma + C \rightarrow \pi^+ \pi^-$ INCLUSIVE
COMBINATIONS / 25 MeV
.25
.5
.75
1.0
1.25
M (GeV)

Fig. 3

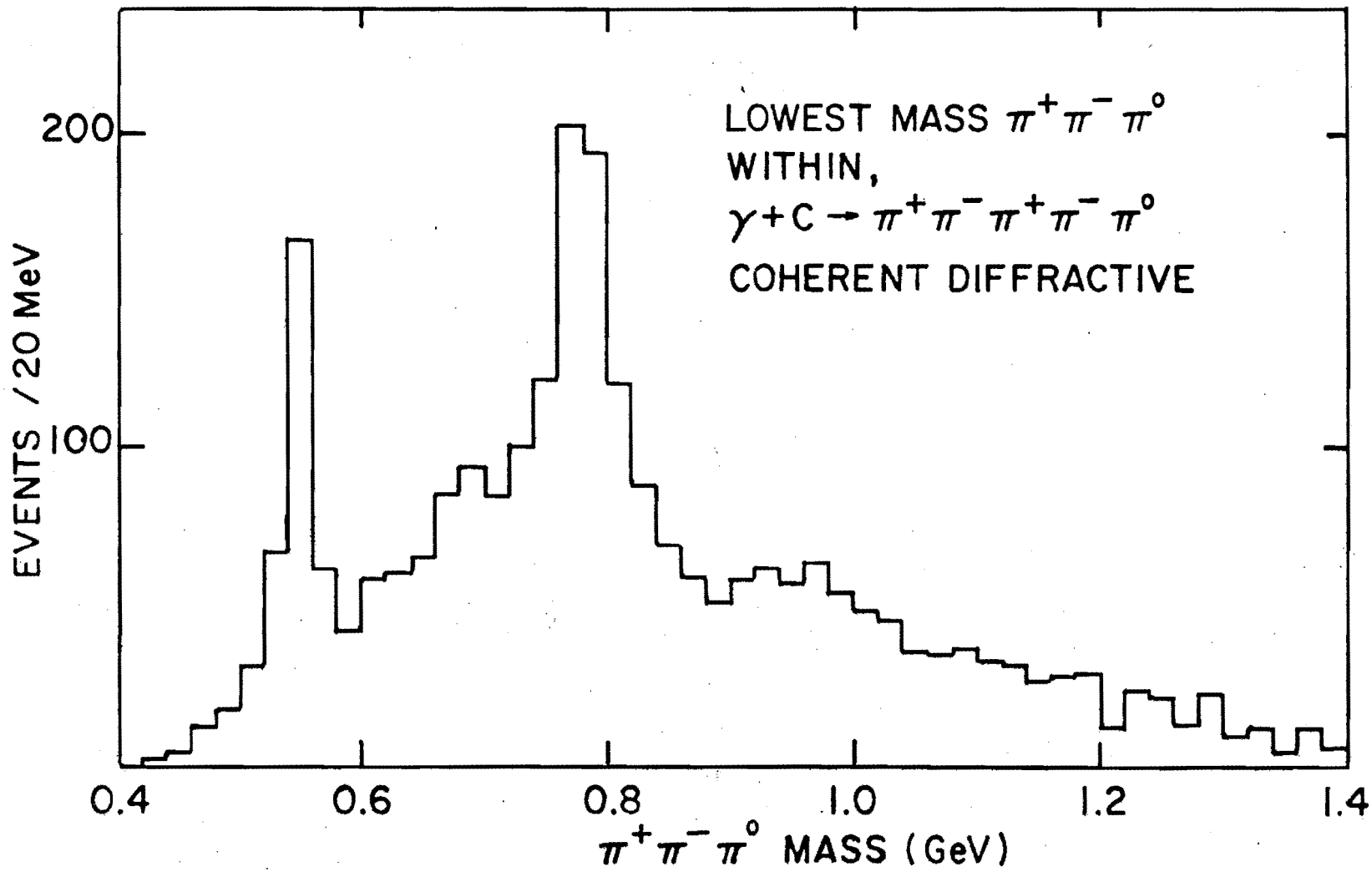
LOWEST MASS $\pi^+\pi^-\pi^0$
WITHIN,
$\gamma + C \rightarrow \pi^+\pi^-\pi^+\pi^-\pi^0$
COHERENT DIFFRACTIVE
EVENTS / 20 MeV
200
100
0.4
0.6
0.8
1.0
1.2
1.4
$\pi^+\pi^-\pi^0$ MASS (GeV)

Fig. 4

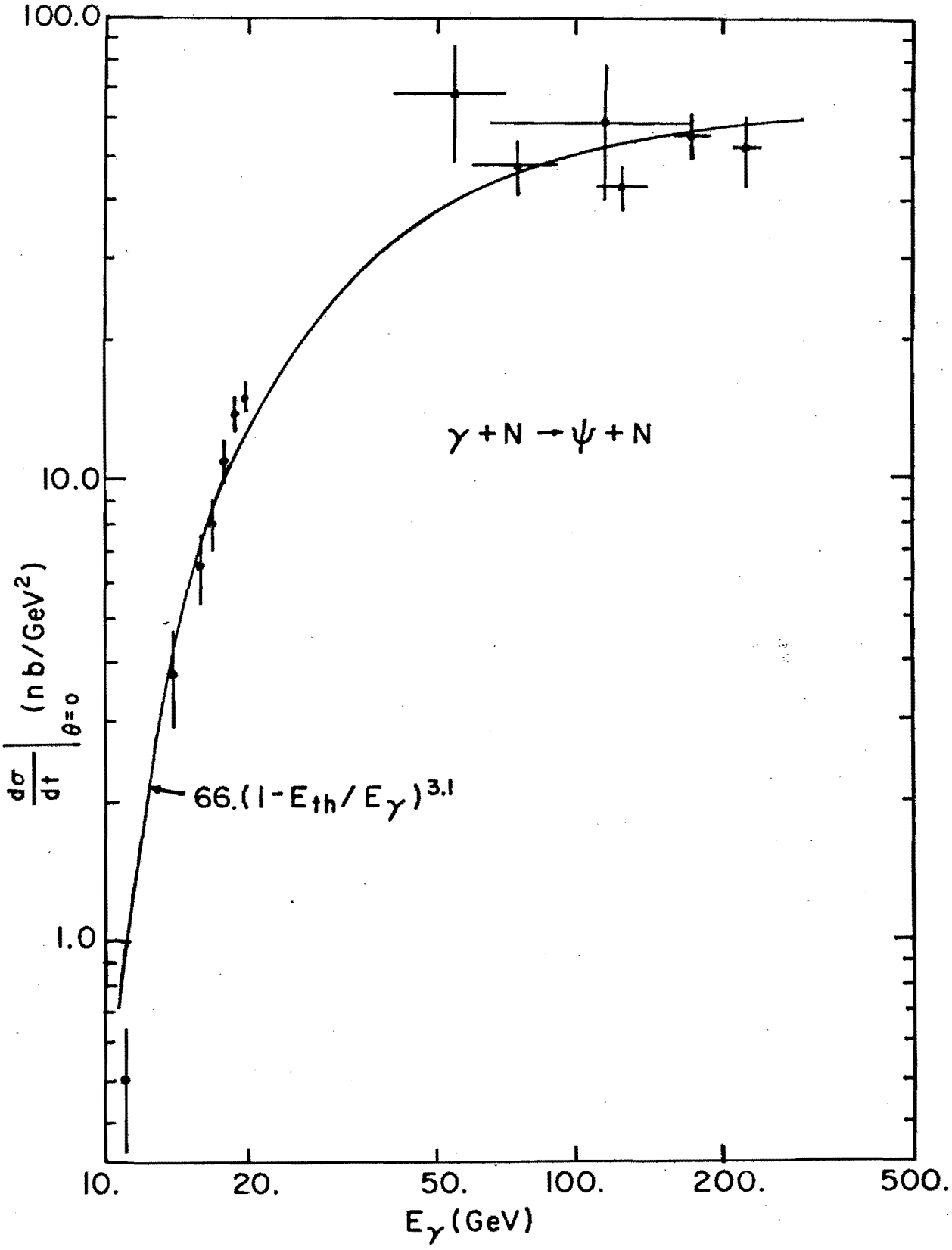
100.0
10.0
1.0
$\frac{d\sigma}{dt}\Big|_{\theta=0}$ (nb/GeV^2)
$\gamma + N \rightarrow \psi + N$
$66.(1-E_{th}/E_\gamma)^{3.1}$
10.
20.
50.
100.
200.
500.
E_γ (GeV)

Fig. 5

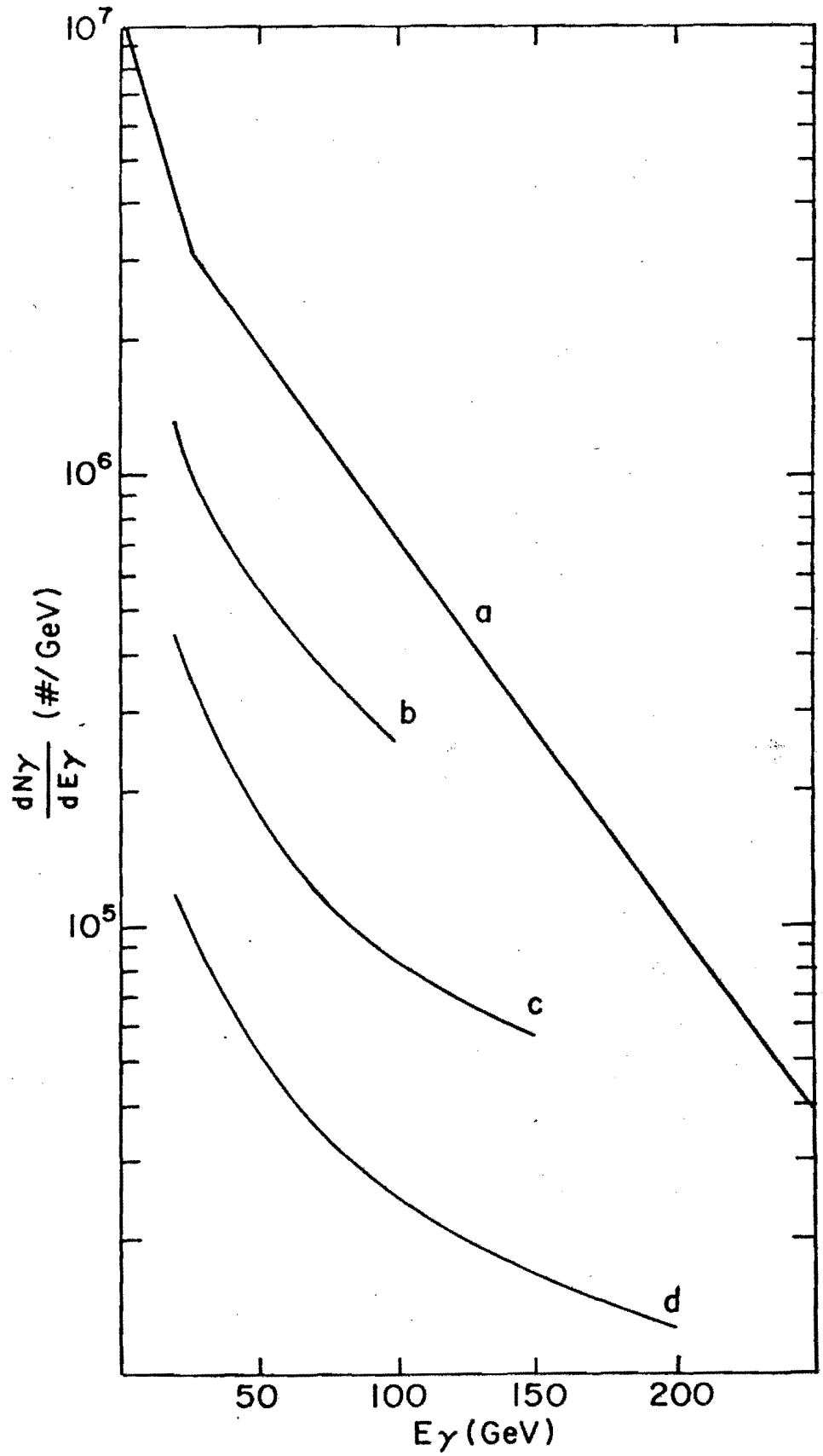
10^7
10^6
10^5
$\frac{dN\gamma}{dE\gamma}$ (#/GeV)
a
b
c
d
50
100
150
200
$E\gamma$ (GeV)

Fig. 6

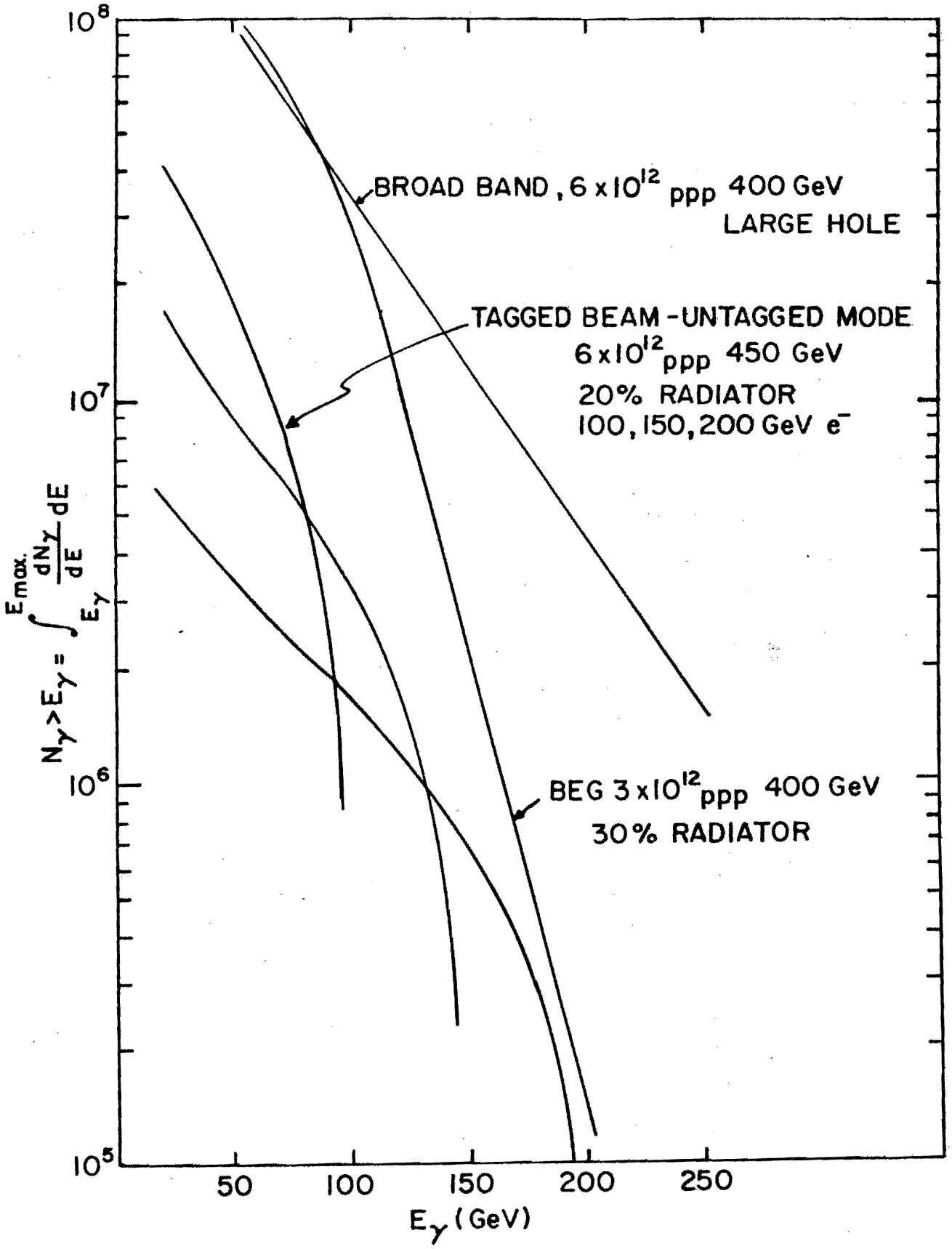
BROAD BAND, 6 x 10^12 ppp 400 GeV
LARGE HOLE
TAGGED BEAM - UNTAGGED MODE
6 x 10^12 ppp 450 GeV
20% RADIATOR
100, 150, 200 GeV e⁻
BEG 3 x 10^12 ppp 400 GeV
30% RADIATOR
10^8
10^7
10^6
10^5
50
100
150
200
250
E_γ (GeV)
N_γ > E_γ = ∫ (dN_γ/dE) dE

Fig. 7

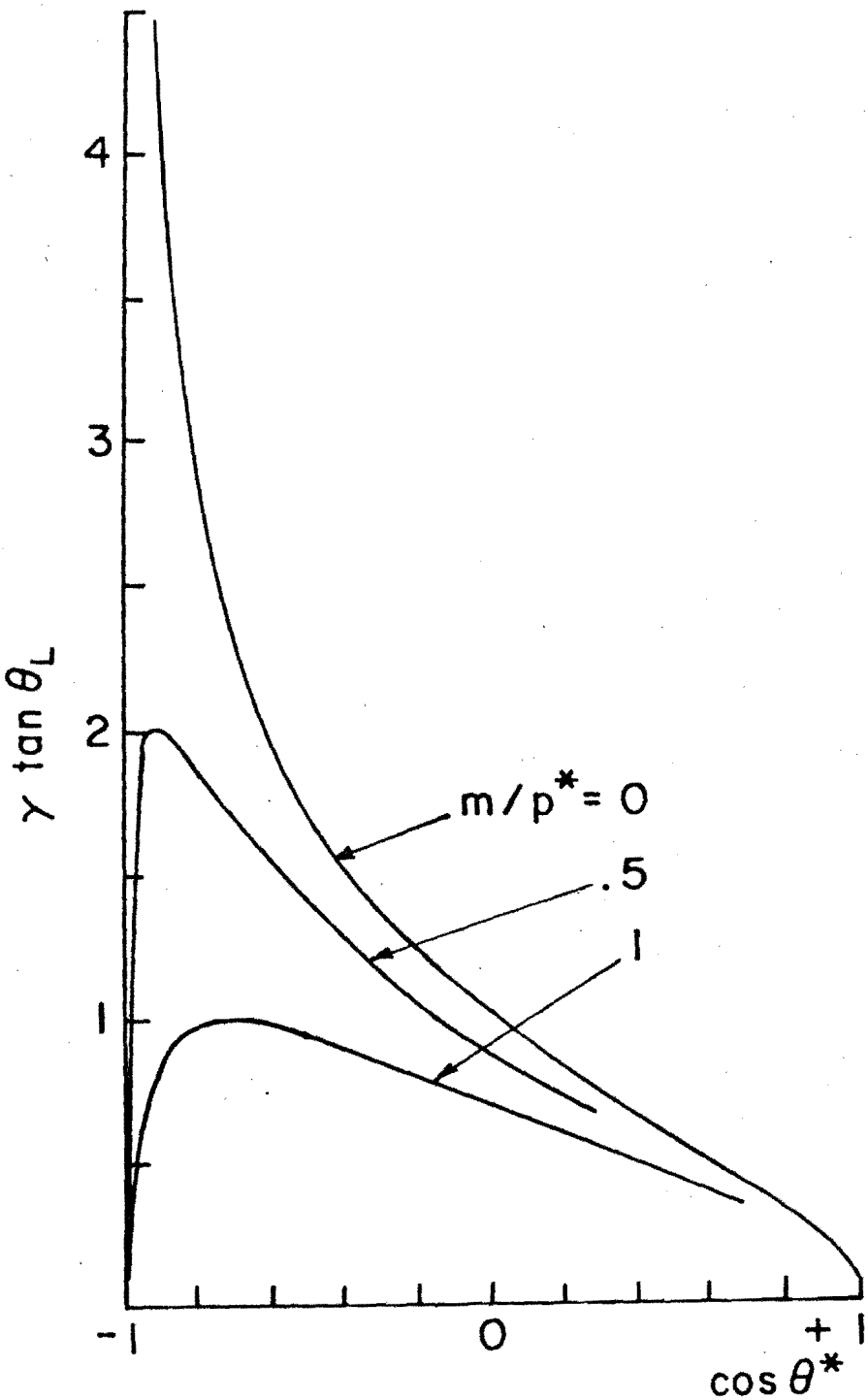

Fig. 8

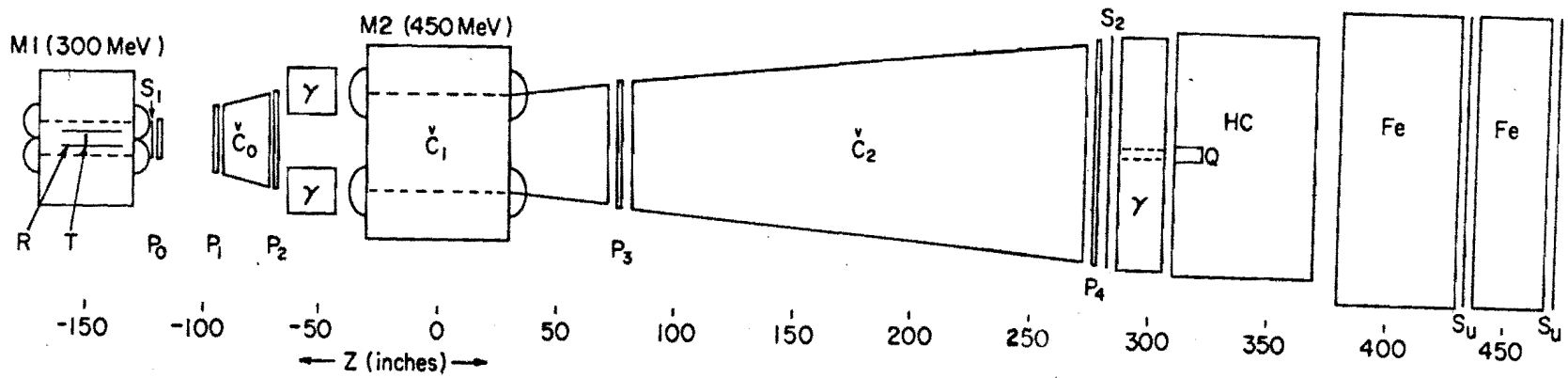
M1 (300 MeV)
M2 (450 MeV)
S1
R
T
P0
P1
P2
P3
P4
S2
Su
Su
γ
γ
γ
Č0
Č1
Č2
HC
Q
Fe
Fe
-150
-100
-50
0
50
100
150
200
250
300
350
400
450
Z (inches)

Fig. 9

Addendum to P 627: "A Proposal to Study High Mass Photoproduction"

S.D. Holmes, B.C. Knapp*, Columbia University

D.A. Jensen, M.N. Kreisler, M.S.Z. Rabin, K. Raychaudhuri, U of Massachusetts

J. Butler, J. Cumalat, I. Gaines, D. Harding, Fermilab

*Spokesperson

January 9, 1980

Contents | Page

Comparison between TPF and P 627 — 1

I. Comparison of Broad Band Neutral Beam with Bremsstrahlung Beams — 1

II. Comparison of the Forward Spectrometer — 8

Is the Broad Band Beam the Right Place for a New Detector? — 12

I. Hadron Contamination — 12

II. Muon Rates at Tevatron — 13

III. Conflict with TPF Operation — 14

IV. Tevatron Operation: Photon Yields and Event Rates — 15

Hardware Processor — 19

I. Motivation and General Design Goals — 19
Very Large Online Computation (Enormous operations/sec/$)
Flexibly Programmable by Manual Assembly
Simple Reliable Operation and Maintenance

II. General Principles of Present Design — 22
A. ECL 10 K Modular Construction
B. Synchronous Pipeline
C. Simple, Highly Decentralized Control
Central Clock, with H, C, V in Processing Path
D. Outside Access to Internal States for Initialization, Testing
E. Completely Well-Defined Sequence of States
1. Simple Exact Fortran Simulation
2. Simple Complete Diagnostics

III. Specific Example: Track Reconstruction — 28
A. Track Reconstruction Algorithm
B. Hardware Implementation
1. Single View Line Finder
2. View Matching
3. Track Fitter: 5 parameter least-squares fit to 20 drift times

C. Detailed Description and Schematic for Individual Modules
D. Construction Cost and Time Estimates

IV. Complete Data Acquisition and Processing System 63
A. Drift Chamber Measurements
B. Analog-to-Digital Conversion
C. Kinematic Reconstruction
D. Information Storage and Distribution
1. Transport System
2. Distributed Buffer
3. Online Histograms: Event Selection and Detector Calibration and Performance Checks

Budget and Schedule 72

Summary 75

COMPARISON BETWEEN TPF AND P 627

I. COMPARISON OF BROAD BAND NEUTRAL BEAM WITH BREMSSTRAHLUNG BEAMS

The greatest distinction between the tagged photon facility (TPF) and our proposal for the broad band beam lies in the enormous difference between the two photon beams. The broad band beam can provide typically two orders of magnitude more high energy photons per primary proton, with a harder photon spectrum. The 627 detector is therefore designed to handle higher instantaneous intensities and higher data acquisition rates than the E 516 detector could reasonably be expected to encounter. Particularly with the superconducting main ring, our detector would make full use of far more intensity of high energy photons than could be available from any Fermilab bremsstrahlung beam.

To illustrate the intensity issue, we present again Fig. 7 from our proposal, showing the number of photons above specified energy for the broad band beam, the Fermilab tagged beam and the BEG beam designed for CERN. For the broad band beam, we would obtain more than 10^8 photons with energies above 50 GeV for 6×10^{12} 400 GeV protons, representing no extrapolation of the yield per proton beyond present experience. The rates shown for the tagged beam are taken at face value from the TPF design report of May 1977 (TPFDR) and represent more than a tenfold extrapolation beyond present experience. The TPFDR rates are based on electron yields per proton about five times larger than any previously sustained yields, followed by conversion to photons in a thick 20% radiator.

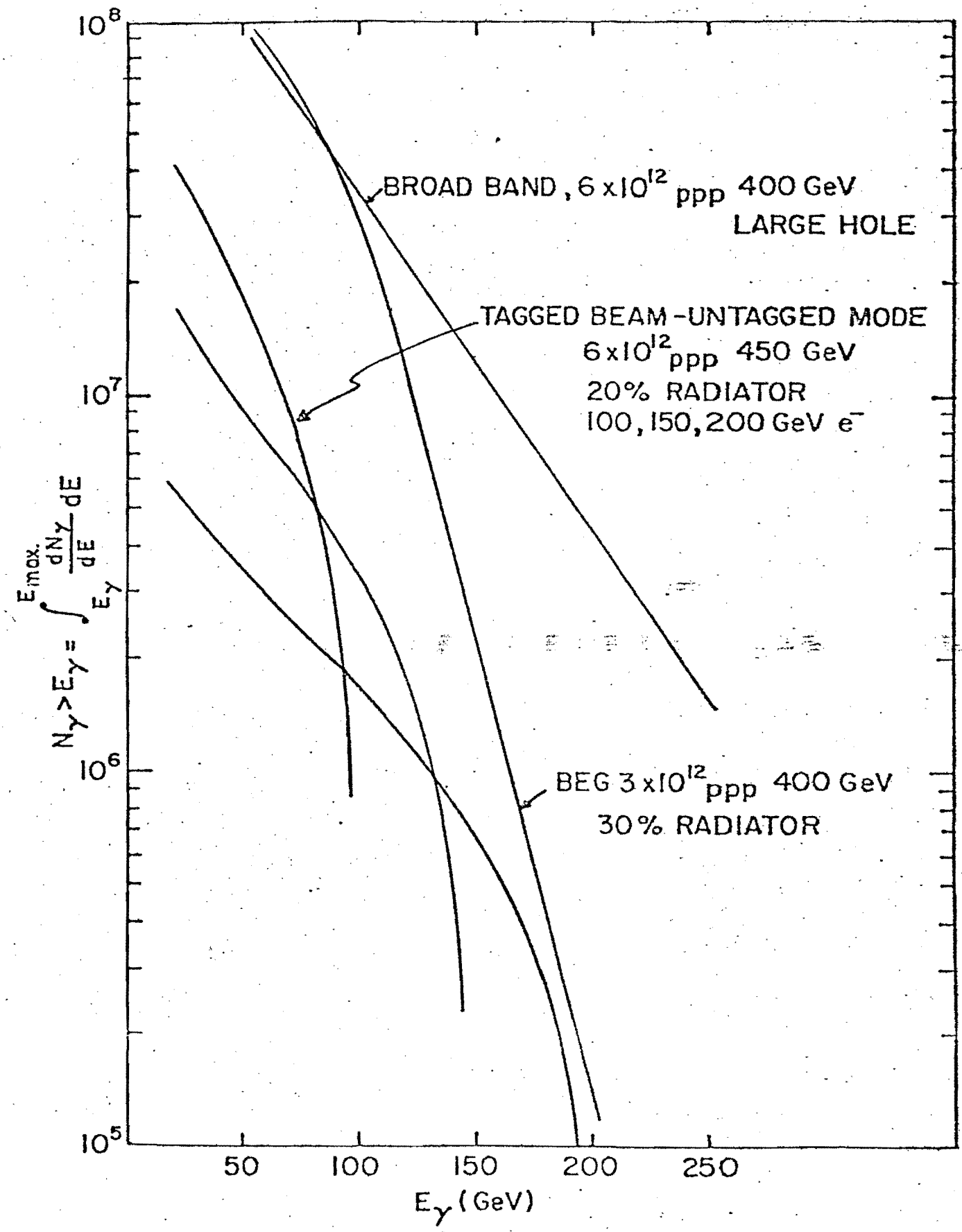
BROAD BAND, 6 x10^12 ppp 400 GeV
LARGE HOLE
TAGGED BEAM-UNTAGGED MODE
6x10^12 ppp 450 GeV
20% RADIATOR
100, 150, 200 GeV e⁻
BEG 3 x10^12 ppp 400 GeV
30% RADIATOR
10^8
10^7
10^6
10^5
50
100
150
200
250
E_γ (GeV)
N_γ > E_γ = ∫ dN_γ/dE dE

Fig. 7

The BEG beam and a similar beam designed at Fermilab would transport the maximum possible yield of electrons above a low momentum cutoff.

To maximize the yields of high energy photons in an untagged mode of operation, both TPF and BEG would use thick radiators in the electron beams, 20% to 30% radiation length. These radiators provide several low energy photons per beam electron, in a troublesome energy range below a few GeV. These low energy photons produce low energy electrons in the photon target and subsequent detector material. Electrons of less than a few hundred MeV will be reflected by the first analyzing magnet, enhancing the general level of activity in recoil detectors and any drift chambers within the magnetic field. The high intensity curves shown in Fig. 7 assumed 2×10^8 100 GeV electrons per pulse for TPF and 5×10^8 electrons per pulse for BEG, incident on a thick radiator before the photon target.

The fundamental difference in the dependence of photon yield upon photon energy in the different beams should be obvious. Both the broad band beam and the bremsstrahlung beams start with the same photons. The bremsstrahlung beams convert the photons to electrons and then convert back to photons, with considerable energy degradation at each conversion. The broad band beam simply transmits 3% of all photons within the maximum solid angle acceptance of 0.25 μsrad. We do see some enhancement of the spectrum at low

photon energies from electron pairs radiating in the deuterium before sufficient deflection by a magnetic field. A scintillation counter in the photon beam counts at twice the rate one would expect from extrapolation of the high energy photon spectrum.

The relative superiority of the broad band beam as an intense source of high energy photons increases rapidly with proton energy. The photon spectrum of the broad band beam is

$$\frac{dN_\gamma}{dX} = C\ N_p\ \Delta\Omega\ \left(E_p^{\ 2}\ x^2\ \frac{1}{\sigma}\ \frac{d\sigma}{dx dP_\perp^{\ 2}}\Big|_{P_\perp^{\ 2}=0}\right)$$

where $C \approx 0.03$ is the attenuation factor introduced by the deuterium ;

N_p is the number of interacting protons ;

$\Delta\Omega = 0.25 \times 10^{-6}$ is the solid angle acceptance of the beam; and

$x = E_\gamma / E_p$.

This has the simple form

$$\frac{dN_\gamma}{dx} = E_p^{\ 2} F(x) N_p$$

showing that the total number of photons above a fixed fraction of the primary proton energy increases as the square of the proton energy. This increased yield arises not from any increase in the forward production of photons by the primary protons, but rather from a rapidly increasing acceptance for the forward photons by the fixed solid angle of the neutral beam. Above energies sufficiently high that the angular spread of the forward production falls within the

acceptance, the increase in yield disappears. For a BEG beam, no such increase would occur. For TPF, which collects electrons from photons with initial production angles out to about 1 mrad vertically and 3 mrad horizontally, some increase in acceptance with energy is still possible, perhaps as much as the increase already assumed in Fig. 7.

To scale Fig. 7 to 1 TeV primary proton energy, simply scale electron and photon energies with proton energy and increase the broad band beam by a factor of 6.25. To estimate the actual number of photons per hour and the instantaneous intensities requires an estimate of the proton flux. Present rumors suggest that we might expect a 20 second spill every 60 seconds, with at best no increase in the number of protons per pulse over what has been available for about 1 second every 10. For a fixed number of protons per spill, the number of protons per hour would then fall by a factor of 6, but the instantaneous intensity of protons would obviously fall by a factor of 20. For the broad band beam, the total yield of photons per hour would remain essentially constant, with instantaneous electron pair rates falling by a factor of 0.3, but the hourly yield of photons above 100 GeV would increase by a factor of 4. In other words, if the primary proton energy increases from 400 GeV to 1 TeV, the yield per primary proton of photons above 100 GeV in the broad band beam will increase by a factor of 25, with 6.25 as many photons above 250 GeV per TeV proton as presently obtainable above 100 GeV per 400 GeV proton.

The broad band beam has in practice a much broader useful energy range than the TPF. The TPF can maximize total yield above a fixed photon energy by tuning the electron beam to a somewhat higher energy, providing no photons above that electron energy. If the 20% radiator proves practical, the TPF could produce at most 2% as many photons above 100 GeV per 1 TeV primary proton, simultaneously yielding no 200 GeV photons. The TPF could produce almost 1% as many photons above 200 GeV as the broad band beam, but accompanied by even smaller relative yields between 100 GeV and 200 GeV. We thus believe it correct to regard the broad band beam as two orders of magnitude more intense than the TPF bremsstrahlung beam, with a much harder photon energy spectrum.

To compensate for the low intensity of energetic photons, E 516 plans to use a very thick photon target: 2 m of liquid hydrogen or even deuterium. The difficulty with such thick targets is that a typical interesting reaction has six or more forward particles, and for a majority of such interactions, at least one secondary will interact on the way out of the target. In addition, more common lower mass forward systems often reinteract, forming an apparently more massive and complex forward system and therefore greater backgrounds, particularly at the trigger level. With full online reconstruction, we are in principle able to make better use of a thick target, but we are not convinced that one would wish to go beyond 5% interaction length.

In summary, the broad band neutral beam offers by far the highest intensity, highest energy photon beam which we have encountered. Furthermore, because the beam is not a bremsstrahlung beam, but instead contains photons from neutral pion decays in a distant primary target, we can safely permit our multiparticle spectrometer to view every single photon interaction in the photon target, at the highest possible photon intensities. One might also note at this point that the broad band beam can operate as a neutron source of approximately primary proton energy at intensities as high as we can use, and we could use very high intensity, probably about 10^8 neutrons per second producing a few million interactions/second with about 10^5/sec fully reconstructed. With six radiation lengths of Pb and a single cryostat in the beam, we would have a uniquely clean and intense K_L beam, with an energy spectrum and interaction rate similar to that of the photon beam.

II. COMPARISON OF THE FORWARD SPECTROMETERS

We claim that there exist reasonably fundamental differences between the two detectors which reflect the different purposes for which they are intended, which in turn reflect properties of the beams in which they would be located. Our detector, for instance, will reconstruct complex reactions more efficiently and operate at higher intensities, because we know nothing of the final state beyond what we reconstruct in the spectrometer, and because we intend to make use of the considerably higher photon intensities of the broad band beam.

To compare the possible future performance of the E 516 detector with our proposed detector, we consider the E 516 detector as it is presently taking shape, rather than as described in TPFDR, and also consider improvements which might overcome any limitations which become apparent. As stated in our proposal, we can readily see for E 516 a rewarding program of measurements involving known parent photon and recoil proton, with sufficient energy and intensity for detailed studies of charm particle production. The nearly assembled E 516 detector is quite impressive to see in person. After studying that detector, we conclude that it should eventually work more or less as intended, but would still be inappropriate for our purposes, despite its greater cost and complexity.

We have designed our magnetic spectrometer with emphasis on very high multiparticle reconstruction efficiency at very

high rates. The spectrometer requires sufficient redundancy to tolerate finite single wire inefficiencies and reasonably high rates of unrelated accidental coincidences. We must also maintain stable values for the electrostatic fields within the chambers. We have designed a new amplifier/discriminator with greater sensitivity and lower deadtime (~ none) than either our old design or the LeCroy circuits used by E 516. We can thus operate with lower wire gain, reducing space charge effects and total ionization. Our chamber design has maximum drift distances of 1 to 3 mm, with anode to cathode spacing ranging from 3 to 6 mm, so that drift times and memory times are as low as practical. Low peak fields at the cathode surfaces are achieved by having more cathode surface and appear in practice to help chamber stability. The larger cell sizes of the E 516 detector result in longer drift times, much longer clearing times for space charge, greater sensitivity to space charge effects and a need for greater stability and knowledge of the drift velocity.

Since one seldom finds two spectrometers with identical plane configurations, one must conclude that pattern recognition principles are not self-evident. Our own design represents a modest improvement over the E 87 geometry. We have no doubt whatsoever that the configuration leads to maximally reliable and efficient reconstruction. We have a track reconstruction algorithm which has proven reliable,

efficient and accurate. Our proposed drift chamber spectrometer would certainly be able to cope with higher instantaneous rates and more complicated events than the E 516 detector, but quantitative comparisons are difficult at this point. Certainly the E 516 magnetic spectrometer will cope with the intensities and multiplicities envisioned for E 516. Our reconstruction algorithm is sufficiently simple that its hardware implementation is also simple and inexpensive.

The greatest shortcoming of the E 516 detector is probably the marginal segmentation of the Cerenkov counters. On p. 48 of the TPFDR, we encounter the following sentence: "However, the identification of the strangeness of all the final state particles is difficult, and can be made only in some small fraction of the events." This is in fact just what we wish to do, however. The two TPF counters, C1 and C2, are essentially the same as the E 87 counters. The segmentation is indeed inadequate. The analysis presented on p. 40 of the TPFDR is quite misleading. The probability of confusion is obviously not a simple function of the number of secondary particles. The forward particle density also scales with the square of the ratio of the forward system energy divided by mass. The two counter system provides full hadron separation only between approximately 20 and 40 GeV. Considering the photon energies and the final state multiplicities expected, we suspect that the short counter with low pion threshold which we proposed to reduce the lower range of unambiguous separation

to 10 GeV would be even more useful for E 516.

The remaining detector components appear similar. The E 516 SLIC is less segmented and contains more interaction lengths of material than our proposed photon calorimeter, but it appears to have better energy resolution. The E 516 muon identification looks marginal at the moment, but the eventual addition of position measurement within the hadron calorimeter should cure any problems.

We turn next to comparison of the data acquisition system. With the exception of the sophisticated special electronics for the recoil detector, E 516 relies quite heavily on slow, expensive, and relatively unreliable LeCroy ADC's and TDC's. After digitization time of hundreds of microseconds, several hundred words per event are available at CAMAC transfer rates of a fraction of a megacycle. In our system, the storage elements of the receivers are freed within approximately 1 μsec, during which time the analog signals are transferred to buffer capacitors, and the digital information, such as drift chamber TDC contents, is transferred serially to digital buffers for reconstruction. We could reconstruct at least one typical event with full offline precision and detail every 10 μsec. While one could undoubtedly achieve similar capability with the E 516 detector by massive replacement of electronics, we do not see how the event rate in the TPF could fully justify such an effort. The E 516 plan to eventually incorporate simple information from the forward spectrometer into a trigger decision sounds necessary and sufficient.

IS THE BROAD BAND BEAM THE RIGHT PLACE FOR A NEW DETECTOR?

Rumored doubts about the long range prospects for the broad band beam have raised questions about the wisdom of committing the resources necessary to assemble the proposed detector in EE4, the present site of the E 87 detector. These doubts arise primarily from misinterpretation of previous experience with muons and hadron contamination, along with unrealistic extrapolation to Tevatron operation.

I. HADRON CONTAMINATION

Consider first the effect of the hadron component of the beam, which is essentially independent of proton energy, although the effectiveness of the deuterium filter does rise with hadron energy. From the most recent E 87 charm search, one might readily conclude that hadron contamination seriously compromises our ability to study photoproduction: fully 80% of the candidates for charm production were hadron induced, and we estimate that 40% to 50% of all reactions below 200 GeV were hadron induced. Although this is a considerable increase over the 15% which we observed in earlier 400 GeV operation, we assumed the larger value in the proposal as worst case operating conditions. The hadron component of the neutral beam consists of neutrons with a fairly flat energy distribution out to the primary proton energy, and K_L with an energy spectrum similar to that of the photons.

As a result of the inadequate angular acceptance of the E 87 analyzing magnet, out to a scant 40 mrad, the E 87 charm

search had negligible acceptance for charm particle pairs and could accept single charm particles only from very high energy photons. The mean visible energy for a recorded candidate was roughly 150 GeV, with considerable missing energy possible, particularly in neutral hadrons. The neutron contribution was therefore enormously enhanced. The signature required for analysis was one or two strange particles and possibly a baryon. The charm candidates therefore represented a considerably larger fraction of the total cross section for hadron interactions than for photoproduction reactions.

Even if the number of photoproduction and hadron interactions were comparable, we would not have large hadron-induced backgrounds for reactions which are more typical of photoproduction than of hadron interactions. Associated production of charm or bottom pairs, vector mesons and diffraction into nonstrange nonbaryon states are reactions which represent far larger fractions of the total cross section for photoproduction than for hadrons. These reactions will be unambiguously identifiable in the proposed experiment. Not only do we not expect significant hadron background for these photoproduction reactions, but we expect to eventually study in detail, charm, bottom and massive diffractive production by K_L and neutron, even though this should be considerably more difficult that for photoproduction simply because these processes represent smaller fractions of the total cross section.

One can undoubtedly think of measurements which require a priori knowledge of the identity and energy of the parent beam particle. For such measurements, one must rely on TPF and experiments in charged hadron beams. On the other hand, we could carry out the measurements which we propose at luminosities at least ten times higher than would appear possible in a bremsstrahlung beam or charged hadron beams, and still another factor of ten higher than TPF.

II. MUON RATES AT TEVATRON

The remaining primary objection to the broad band beam which we must face is the issue of muon flux at higher proton energies. The fear appears to be that we have already done the best we can to shield the detector from the three chief sources of muons: from meson decays in the proton dump, between the proton target and the dump, and in the beam halo upstream of the proton target, and that furthermore our present salvation is marginal and results from ranging out most of the muons below 30 GeV in material upstream of the detector, a feature which would disappear with an increase in the muon energy scale. That this fear is groundless should be readily apparent when one recognizes that although the yield of muons per proton increases linearly with proton energy, the instantaneous proton intensity will fall by at least a factor of 20 for a superconducting main ring. Even for 400 GeV protons, we rely quite heavily on magnetic deflection. The beam line is the product of the frontier days of Fermilab and can be

readily modified to obtain fewer muons per primary proton of 1 TeV than we presently obtain for 400 GeV. The target box must be modified in order to sweep higher energy protons out of the neutral beam into a magnetized dump. In addition, we would place a saturated iron magnet immediately after the target box, so that we maintain a fixed polarity horizontal magnetic field from the proton target through sweeping magnets, beam dump and at least three meters beyond the target box. We have always had sufficient magnetic field along the beam line to sufficiently deflect muons of primary proton energy, but have had difficulty keeping the deflections accumulating with a fixed sign. Iron toroids proved useless, and the return yokes of the cryostat magnets provide a muon transport system.

III. CONFLICT WITH TPF OPERATION

Another long range objection to the present beam may be the present incompatibility with TPF operation. A few days of rigging are now required to switch between broad band and electron beam operation. During TPF operation, radiation from an electron beam collimator on the west wall of EE4 makes the detector area inaccessible. An effort to establish simultaneous operation of the broad band beam and TPF may be justified by a scarcity of external beam time. A drastic option of building a new beam line and detector area has been proposed to eliminate this conflict and permit the option of a charged particle beam. A cheaper alternative would probably be to further separate the present beam lines at the target

box, which would require digging between EE1 and EE4, and to erect shielding between the electron beam and the detector area in EE4. In any case we would be very anxious to maintain the present broad band beam configuration: same deuterium absorber and no increase in the distance from proton target to photon target.

IV. TEVATRON OPERATION: PHOTON YIELDS AND EVENT RATES

As stated previously, the total yield of photons per proton scales as the square of the proton energy while the energy scale is proportional to the proton energy. The expected yield of photons for 6×10^{12} incident protons at 1 TeV is shown in the accompanying figure along with the yield for an equal number of 400 GeV protons.

Assuming 6×10^{12} TeV protons are delivered in one 20-second spill every minute, the total number of protons per hour is a factor of 6 lower than for present 400 GeV operation while the instantaneous proton rate is reduced by a factor of 20. However, the total number of photons produced per hour increases by a factor of 4 over 400 GeV operation for $E_\gamma > 100$ GeV, and by a factor of 10 for $E_\gamma > 200$ GeV. At the same time, the instantaneous e^+e^- rate drops a factor of 3 while the instantaneous μ rate drops a factor of 10. These results are summarized in the accompanying table.

Also included in the table are the expected hourly rates for massive final states in which the energy threshold dependence of the cross sections are expected to have a

significant effect on the production rates. We present a comparison of $D^{o}\bar{D}^{o}$, $B\bar{B}$, and Υ production for TeV and 400 GeV operation based on the same assumptions as in our proposal. In spite of a reduction of a factor of 6 in the number of incident protons per hour the expected hourly rate of charm pairs increases by 2, of bottom pairs by 4, and of Υ by 6. With the increased yield of high energy photons, we could carry out the proposed physics program in comparable time with 2 or 3 x 10^{12} protons per pulse. On the other hand, the reduction in instantaneous intensities would permit operation with more than 10^{13} protons per pulse, if they were available.

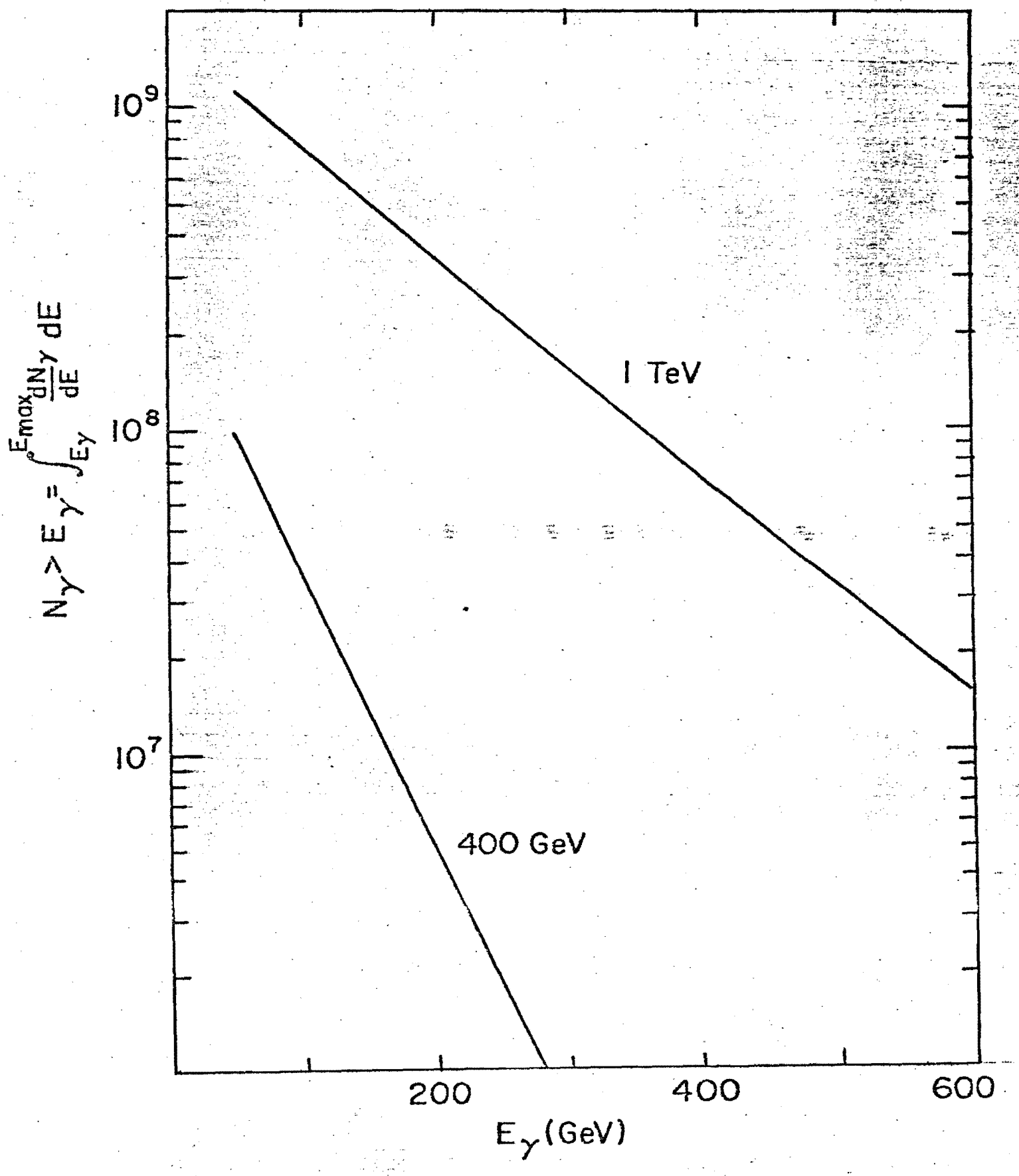
10^9
10^8
10^7
$N_\gamma > E_\gamma = \int_{E_\gamma}^{E_{max}} \frac{dN_\gamma}{dE} dE$
1 TeV
400 GeV
200
400
600
E_γ (GeV)

2101

Table I: Broad band beam hourly rates for present 400 GeV operation and projected Tevatron operation

Protons/pulse	400 GeV	1 TeV
Total seconds	3600	3600
Total spills	360	60
Total beam seconds	360	1200
Total beam protons	2.16×10^{15}	3.6×10^{14}
Total photons, $E_\gamma > 50$	3.6×10^{10}	6.7×10^{10}
Total photons, $E_\gamma > 100$	1.35×10^{10}	4.56×10^{10}
Total photons, $E_\gamma > 200$	1.87×10^{9}	2.07×10^{10}
* e^+e^- rate (5% radiator)	3×10^{7}/sec	9.4×10^{6}/sec
* μ rate	$3 \times 10^{6}/m^2$/sec	$3.8 \times 10^{5}/m^2$/sec
† $\gamma \to D^0\bar{D}^0$+any (σ=500 nb) •	32 K/hour	60 K/hour
$\to K^+\pi^-K^-\pi^+$	5.8/hour	10.7/hour
† $\gamma \to B(\bar{B})$+any ($\sigma=27(1-\frac{E_{th}}{E})$nb)	580/hour	2100/hour
$\to \psi K^\pm\pi^\mp \to \ell^+\ell^- K^\pm\pi^\mp$	1.0/hour	3.6/hour
† $\gamma \to \Upsilon(\sigma = 270(1-\frac{E_{th}}{E})^3$pb)	1.44/hour	8.5/hour
$\to \ell^+\ell^-$	0.054/hour	0.32/hour

† Same assumptions as Table VI of Proposal 627.

* Assumes e^+e^-/proton $\propto E_p^2$, μ/proton $\propto E_p$.

HARDWARE PROCESSOR

I. MOTIVATION AND GENERAL DESIGN GOALS

We have been designing for several years a general approach to data processing capable of complete reconstruction of complex multiparticle spectrometer events at rates in excess of 10^5/sec. The specific system we are now designing will be simple, reliable and inexpensive, providing far more computation power than any existing offline computation center. Such systems can in general provide high energy physics experiments with an enormous increase in the rate of readily available highly processed information.

A standard experiment has 10^3 to 10^5 measuring elements and can tolerate event rates well in excess of 10^6/sec. Typically, however, only a very primitive subset of the measuring elements is combined in some simple manner to form a crude trigger decision, selecting perhaps one hundred events for later analysis. Such event selection schemes place strong restrictions on the type of rare reactions which can be studied, often introduce large uncorrectable measurement distortions, and are not usually very efficient in that they tend to miss too many desired events and accept too many undesired events. Equally important for its impact on the final measurement, such information-starved schemes often result in a fundamental conflict between the need for direct measurement of interesting physics reactions and the need for constant monitoring and calibration of the detector. With high bandwidth online computation, we can relax the

crude trigger by a factor of a thousand or so and provide continuous online monitoring and calibration of the entire detector, including the reconstruction hardware.

We have attempted to be as general as possible in our approach to digital computation, both because we expect to apply the approach to other problems and because our specific application is complicated and likely to change with time. In fact, the general principles that we have been organizing would appear to have wider application than simply in computation hardware and have proven quite useful in the organization of the measuring elements (TDC's and ADC's) and in the organization of information transfer, or the general interface scheme which we refer to as the Transport Bus.

Ideally, we would like to design a small number of simple hardware modules with which one could construct the solution to any specific problem with the full generality of a standard Von Neumann machine. For our problem, we have indeed accomplished this, with a few simple modules sharing among themselves considerable common structure. In practice, a typical problem will probably have a hardware solution consisting primarily of modules chosen from a finite set of generally useful modules but quite possibly also requiring a few simple modules specially tailored to the specific problem.

Such a computer architecture may eventually be fully programmable and useful for general purpose central computation, but for the immediate future, we see practical

application only for special purpose construction of computation systems dedicated to specific problems which are at least awkward on normal stored program computers. Our structure is programmable in the sense that the computation algorithm consists of specific modules and their interconnections. Dynamic storage is used only for precomputed constants and intermediate results.

The computation power of this system will result strictly from the efficient matching of conventional hardware to the specific computation problem. The intrinsic speed or computation power of the hardware components will not be unusual. We intend to use standard industrial technology in a conservative manner. The necessity for matching the hardware to the computation results, in fact, in a small variety of quite dissimilar structures which appear to perform similar computations. A simple computation to be performed for each of a hundred unrelated inputs is not subject to the same optimization as a predetermined computation a hundred times larger for a single input, even though the two different problems might entail exactly the same computation. Similarly, an operation to be performed once cannot be performed in the same manner as an identical operation which must be performed one hundred times, if we are to maintain reasonably uniform efficiency of hardware utilization.

In the following pages, we attempt to provide a detailed description of the specific structure which we are designing. It is perhaps difficult to isolate the general priniciples of

the hardware computation from the specific details of the computation. The track reconstruction algorithm, for instance, has functioned successfully for years in offline Fortran programs, but it is obviously specific to our geometry. We will make limited reference to application in other geometries, in particular a solenoidal geometry.

II. GENERAL PRINCIPLES OF PRESENT DESIGN

A. ECL 10 K Modular Construction

The hardware modules use a limited set of ECL 10 K integrated circuits, of which the only examples of more than medium scale integration are memories, primarily a 4 bit by 256 word random access memory. Active processor information usually resides in registers which are either shift registers or counters. These registers are modified only on an edge of a central clock pulse, and any modification is determined by levels which are derived from the output levels of registers through directly coupled logical, arithmetic and memory reference operations within one full clock cycle, presently estimated to be 25 ns.

Communication between modules, for example, is accomplished in this manner, using flat multiconductor cable with crimp-on connectors. More than a dozen modules can usually be bussed together on one cable a few feet in length, although a single source with few receivers is common. Transmission from output register to input register requires a time equal to a few gate delays plus whatever transmission or settling time is required by the cable, which might well be 15 ns for

a cable loaded with more than a dozen modules. The transmission time must fit within the clock period, but otherwise we have no critical timing of intermodule communication.

A module contains few distinct elements: from one to four registers accompanied by a modest combination of logic, arithmetic and random access memory. Memory alone usually implies input and output data registers and input and output address registers. Much of the circuitry is common to many distinctly different modules.

B. Synchronous Pipeline

The resulting structure is a synchronous pipelined system in which all register modifications occur simultaneously, with synchronization achieved through a central clock, whose period is determined by the worst case register-to-register transmission time. The time delay through a sequence of operations may be considerably increased by synchronization through otherwise unnecessary registers, but this synchronization allows the absolute maximum rate of entry into the pipeline and enormously simplifies design and interconnection. Pipeline delay only affects the rate of computation when the delay is inserted in a loop, so that the result of one pipelined computation is required to begin another. Even in such a loop, pipeline delay will not affect computation rate if unrelated computations share the pipeline. The only practical example which we have encountered where pipeline delay slows the overall computation rate somewhat is in nested loops whose index sequence is affected by computations within the loop.

C. Simple Highly Decentralized Control Allows Efficient Parallel Computation

In addition to the central clock which is fanned out with equal time delay to every module, the only control information necessary accompanies the data in the processing paths. Quite primitive control information is all that is required for communication. Each unique data element must be identified, typically with a single bit labelled Valid. A block transmission is terminated by a single bit labelled Complete. If any receiving element in a register-to-register communication is unable to accept new information, a single bit communication labelled Hold is generated, indicating that the present communication must be postponed.

We thus face the prospect of a sequence of registers with register-to-register communication controlled by information travelling in at least two directions. Ordinarily, on each clock edge, we would expect register information to advance one register "forward", but, if we allow a Hold to propagate "backwards", we immediately encounter a situation in which a Hold signal must immediately propagate to the beginning of the sequence in a single clock period, not a particularly practical possibility. We do not attempt to lock up the entire pipeline whenever a Hold occurs, because this would be difficult to accomplish and would slow down computation excessively. A register which contains no valid data can be loaded on the next clock edge, regardless

of any downstream Hold, effectively blocking the Hold. Throughout a specific module, we provide the status of any downstream Hold generated within the module, along with the Valid status of intervening registers, allowing the Hold full propagation within and out of the module in a single clock period. We cannot readily envision such a look-ahead feature for intermodule communication and must therefore usually provide a redundant and normally invisible storage element at interfaces between modules. Thus when an input register of one module is unable to accept data, a Hold is generated on its input cable, preventing receivers on that cable from loading any valid data on the next clock edge, and forcing the sender to repeat any valid transmission. This Hold does not affect loading of the sending module's registers on the next clock edge, but rather is itself loaded into a single bit Hold register at the output, freezing a normally transparent latch inserted between the output register and the cable. This Hold register becomes an internal Hold for the sending module. The redundant storage element permits the Hold to propagate backwards, one module per clock period, blocked of course by an empty register in its path, just as Valid propagates forward, one register per clock period, blocked in turn by any Hold encountered.

Although probably not immediately obvious, this simple control scheme and its simple generalizations provide optimal

synchronization of possibly quite complicated structures with long diverging and converging pipelines with many mutually interfering inputs. Conflicts and therefore Holds may be generated at several depths in the pipeline on every cycle without overall interference ever exceeding worse case single element interference. A conflict often generates a not-Valid propagating forward and a Hold propagating backwards, but a not-Valid and a Hold annihilate on contact.

D. Outside Access to Internal States for Initialization and Testing

Because computation is not the only desired mode of operation, we do have an additional small control cable bussed to all modules. One line specifies Process mode, in which case the system functions as described above. For other modes of operation, this control bus provides read/write access to most internal storage elements so that pre-computed constants can be stored for subsequent computation or so that hardware performance checks can be performed. The bus is simple: three control bits specifying operating mode, eight address bits specifying module and storage element, and two data bits, one for input and one for output. If the element is an ordinary data register, it is also a shift register. The control bus can force parallel loading of its normal input levels or a serial shift in or out of the control bus data lines. If the element is a counter, it can similarly be loaded in parallel, incremented or decremented, but the

single bit of information available to the control bus depends on the specific counter and is typically a test for zero or equality with another register. Most other directly accessible elements are single bit flip-flops. Thus, with little additional hardware, we have managed to provide read/write access to internal storage in a manner which does not affect processing speed, but typically allows sixteen bit data transfer at rates above a megacycle for table loading and diagnostic checks.

E. Completely Well-Defined Sequence of States

1. Simple Exact Fortran Simulation

Because the system is synchronous, we know exactly what state to expect after a clock edge if we know the complete state of the system before the edge. We can thus simulate the entire processor offline with a simple Fortran program that describes the precise state of every storage element, clock period by clock period. Given the input information for the processor, we can thus predict the precise binary form and arrival time of the result. This Fortran program has the same modular form as the processor: a separate subroutine for each distinct module type. One need only supply a list of modules, specifying type of module and cable connections.

2. Simple Complete Diagnostics

With the aid of the control bus, the system can be almost arbitrarily subdivided. Small diagnostic computations can then be set up and executed by the subunit in Process

mode at full clock speed. Intermodule connections can be verified. Every single state and operation of a module can be checked. Sample computations, whether for the entire processor or subunits, can be simulated offline, fed to the processor and checked at predetermined clock periods.

Any hardware malfunction which interrupts processing, whether a permanent failure of a component or an intermittent which merely disturbed the operation sequence, can be quickly and automatically detected and identified. Intermittent failures which occur at too low a level to be detected by diagnostic exercises and fail to interrupt processing, will remain undetected, but could only introduce confusion and inefficiency at levels several orders of magnitude below the levels intrinsic to the measurements involved.

III. DETAILED EXAMPLE: TRACK RECONSTRUCTION

A. Track Reconstruction Algorithm

The magnetic spectrometer configuration is particularly simple: three drift chamber modules upstream of a dipole magnet and two drift chamber modules downstream. Most of the tracks originate in a target upstream of a dipole magnetic field immediately preceding the first drift chamber module, but this fact has no relevance to the primary reconstruction algorithm. Each of the five drift chamber modules contains four measurement planes, labelled X, Y, U, and V. The wire spacing within a plane varies from module to module, ranging from 2 mm in the first module to 6 mm in the last module, but corresponding views are parallel for all five modules.

One view, X, is the non-bending view. The other three views, Y, U, V, provide redundant narrow angle stereo in the bending view. There are no staggered pairs of parallel planes in a module. Instead, the planes are arranged within a module so that no more than two wires cross at any X, Y.

The primary track reconstruction algorithm consists of three distinct stages which can form three sequential pipeline levels. First, single view tracks are independently found in each of the three bending views. The particle trajectories follow a straight line in chambers 1, 2, 3 and then bend by a modest angle in the magnetic field before continuing in a straight line through chambers 4 and 5. The three parameter trajectory in a single view has two constraints with five measurements: the coordinate in plane 2 is a linear combination of the coordinates in planes 1 and 3, and the plane 4 coordinate is a linear combination of the coordinates of planes 1, 3, and 5. Our wire spacing is sufficiently fine that we do not require drift time information at this stage.

For each bending view, $\Delta\dot{Y}$, the change in Y slope in passing through the magnet, is simply a linear combination of the coordinates in planes 1, 3, and 5. After finding and listing all 5-plane single view tracks in each of the three bending views, we pair the lists and search for tracks in two views with similar values of $\Delta\dot{Y}$, generally two views of the same track. Any two views fully define the track in three dimensions with fair precision. We expect a small fraction of one percent to be the probability

that an in-time track passing near a wire will not result in a drift time measurement. The probability that the drift time is inappropriate is considerably larger, since the first and only measured time could be for another track, in-time or not, or even a delta ray from the correct track. The probability that at least one measurement is missing in more than one bending view is thus a small fraction of one percent. We thus find the correct track with very high detection efficiency, in fact, an average of about three times each, but with low precision. Some "tracks" found in this manner are fake.

We therefore next use the approximate track parameterization to predict the track coordinate in each of the twenty planes and perform an accurate least-square fit with five parameters, and up to twenty drift time measurements, accurately incorporating the actual magnetic field, fringe and all. We describe this in more detail below, but we use a simple iterative procedure which allows reassignment of measurement and drift ambiguity. A least square fit is performed first without drift time information, and subsequent interations start with a sufficiently well defined trajectory that the drift ambiguity exists only for drift distances less than an ever decreasing uncertainty.

To avoid multiple recording of the same track, we compare each new track with the complete list of previously recorded

tracks. If two tracks share an excessive number of measurements in the bending view, we keep the better track or the first track if the two are of comparable quality. To reduce the amount of needless fitting, each time we have a track of sufficient quality to insure that it is a correctly measured track, we flag the bending view measurements in modules 1, 3, and 5. For any initial pairing of single view trajectories to start a detailed fit, we then require that each view have at least one unflagged measurement among planes 1, 3, and 5.

After reconstruction of all five chamber tracks, a similar procedure yields the remaining straight line trajectories through chambers 1, 2, 3 which did not continue through chambers 4, 5. This completes the reconstruction of tracks originating upstream of the first chamber. A modest quite dissimilar effort is required to reconstruct V^o's decaying downstream of the first chamber and will not be discussed here.

B.1 Single View Line Finder

To find tracks in a single view requires a threefold nested loop: for every combination of first, third and fifth plane measurements, determine whether second and fourth plane measurements exist which satisfy constraint relations and, if so, record the indices of the plane 1, 3, 5 measurements along with the computed slope change $\Delta\dot{Y}$. The threefold loop readily decomposes into two binary loops. The first finds straight lines in planes 1, 2, 3 and the second continues the trajectory through planes 4, 5.

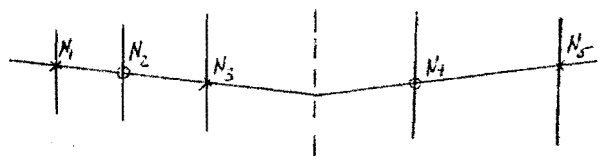

In one single view, the predicted number N_2' of the wire in plane 2, which lies on the line between wires N_1 and N_3 in planes 1 and 3 is

$$N_2' = AN_1 + BN_2 + C \quad .$$

The constants A, B, and C depend on the individual plane wire spacing, beam line coordinate and transverse displacement, and must therefore be changed each time a chamber is moved. The predicted N_2', generally not an integer, is computed to three binary places. The computation is performed by table reference and simple addition and the result compared with a bit map of measurement wire numbers in plane 2. The following diagram illustrates the logical partitioning into identifiable modules for the hardware search for such three point lines:

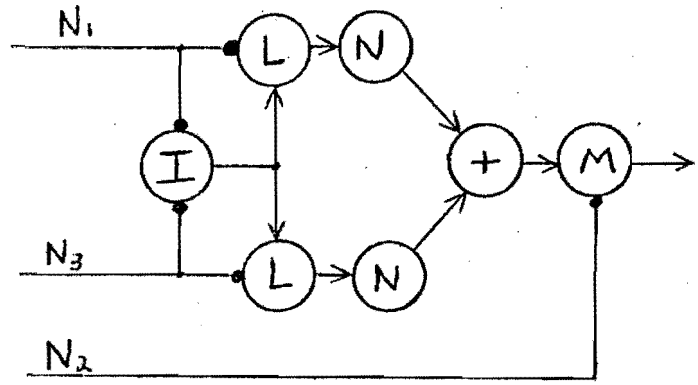

These symbols are defined in the following manner. A module is indicated by a circle containing an identifying symbol. Lines connecting these modules represent the inter-module cables. Input ports are of two types: a <u>read</u> input, indicated by an arrow, forms part of an active processing path through the output, but a <u>write</u> input, indicated by a solid blob, directly affects only internal storage within the module. The five distinct modules shown are

1) Binary index generator 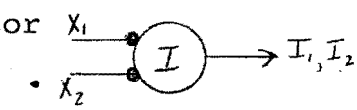

2) List 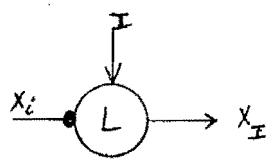

3) Normalizer

4) Adder 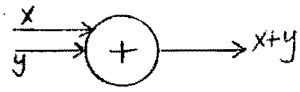

5) Map 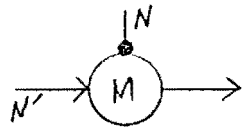

The binary index generator counts the number of valid transmissions at each input and generates all pairs of indices consistent with the accumulating counts. The list

stores sequentially in internal memory any data appearing at the write input port, and retrieves the data by index from the read input. The normalizer module generates a linear mapping of its input. The normalizer is a simpler equivalent of three physical modules: two lists and an adder. The adder is self-explanatory, except that it allows the additional options of subtraction or logical operations. The map determines whether a measurement N exists within a programmable road-width (up to $\pm$ 1.5 wire spacing in units of one-eighth wire spacing) of a prediction N'.

All modules can accept a new input each 25 ns clock period, but the list and map modules cannot simultaneously perform internal read and write, and so typically interrupt the read path to perform a write. If the number of measurements in each plane is n_i, the number of cycles required to store all data simultaneously is the largest of n_1, n_2, n_3. The number of cycles required to generate all combinations is $n_1 n_3$. In addition, n_2 cycles are required to reset the map. If we ignore propagation delay, we conclude that 120 cycles, or 3 μs, would be required for a perfect 10 track computation.

In practice, we want more than we have outlined so far. When the map test establishes that N_1 and N_3 determine a line through a measurement in plane 2, we want to retrieve the index pair I_1, I_3 for later use and also immediately retrieve N_1 and N_3 for computation of three new quantities. The first such number, $\tilde{N}_4$, will be added with linear transformations

of fifth plane measurements N_5 to form predictions for the fourth plane measurements N_4. The second additional computation linear in N_1 and N_3 is $\Delta\tilde{\dot{Y}}$, which will similarly be combined with a transformed N_5 to yield the slope change $\Delta\dot{Y}$. A quantity Y_T is used for three chamber track reconstruction.

We accomplish these additional computations with little additional hardware by re-using most of the same structure. We introduce another loop whose index we call <u>page</u>. This page index is sufficiently useful to become a three-bit addition to the control field of the cables. All input ports now have the option of recognizing only those cable communications with specific page bits, optionally modifying the page internally or using it internally for additional control or data. The normalizer, in particular, uses page to choose among tabulated linear functions. The full three-point line finder is thus

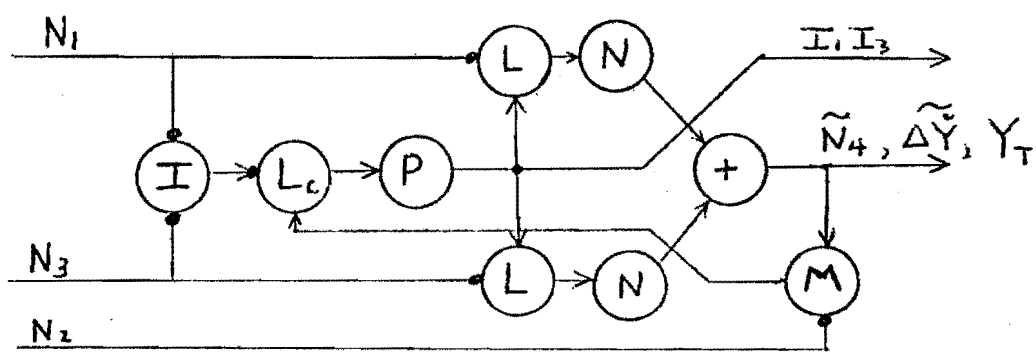

We have introduced two new modules:

6) Another list

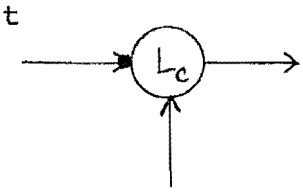

which is physically the same object as the previous list, except for options, one of which now makes the write input port also serve as a read port, transferring data from the write input register to the output register as well as into internal memory. Another independent option allows the read input to simply count distinct map transmissions, interrupting the write path to read from the memory with the accumulating count as index. The two read input ports produce output with differing page numbers.

7) A page counter $\longrightarrow$ (P) $\longrightarrow$ with one internal register, which simply passes input data to output and can be programmed to detect a specific page to begin a sequence of transmissions of the same data with incrementing page number.

Our hypothetical perfect 10 track event now requires an additional 30 cycles to generate the additional three computations per line, for a total of 3.75 μs. For real 10 track events, this time seldom exceeds 5 μs, despite extra measurements and accidental collinearity of unrelated points.

The individual 3-point lines found by the preceding structure form part of the input data for a similar binary loop which pairs these lines with plane 5 measurements N_5 and checks for the existence of plane 4 measurements N_4 within a programmed distance of the trajectory defined by N_1, N_3, and N_5. This structure appears as

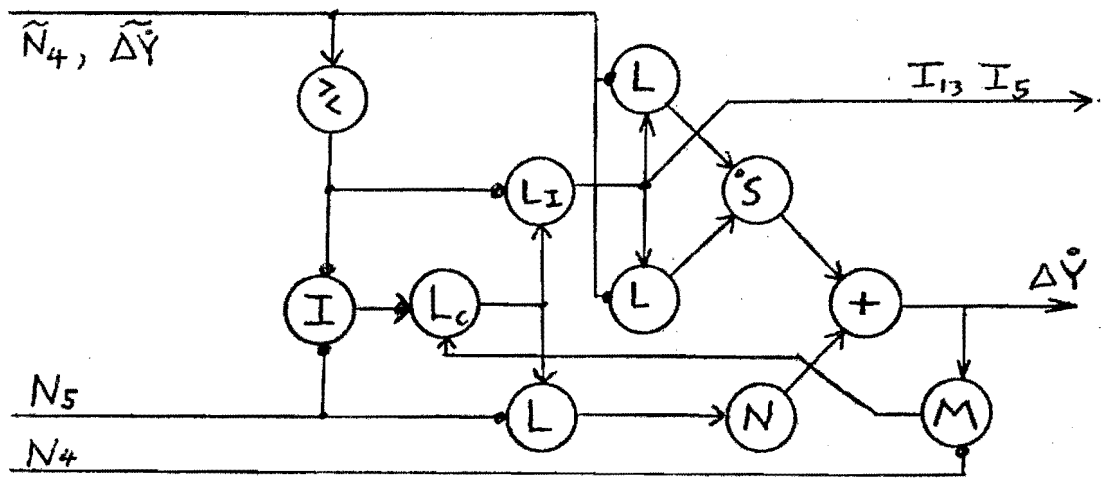

We have now introduced three new modules:

8) Comparator 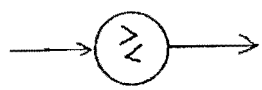

9) Index List 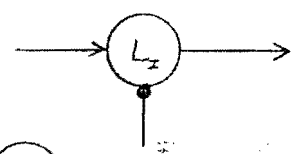

10) Switch 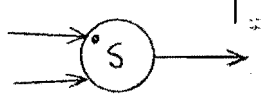

The comparator compares $\tilde{N}_4$ with predetermined limits to determine whether the 3-point line might have entered the magnet aperture and continued through chambers 4 and 5. If so, it is counted by the index generator and causes the index list module to store an accumulating count of comparisons. The switch module simply merges its two inputs sequentially onto the single output cable, with priority in case of simultaneous inputs indicated by the dot. When the index list module receives a read request, it maps an index of $\tilde{N}_4$ within limits into the index I_{13} of the corresponding 3 point line, passing along undisturbed the index I_5.

Data storage for the n_{13} total 3-point lines requires only n_{13} clock periods. Storage of the N_4, N_5 measurements and eventual reset of the map are as before. The number of cycles required to generate all N_4 predictions is just the number of plane 5 measurements times the number of $\tilde{N}_4$ which pass the comparator test. An additional cycle for each complete line is required to obtain $\Delta\dot{Y}$. The computation time required by this loop is similar to that of the 3-point line loop. The two loops operate simultaneously and independently, except that the second binary loop requires input from the first.

The complete line finder for the track processor consists of the above pair of binary loops operating independently in each of three momentum measuring views, or a total of six binary loops operating simultaneously for similar times, typically less than 5 μs for a real 10-track event.

B.2 View Matching

The only input to the view matching processor is the set of three single-view $\Delta\dot{Y}$ lists. Each of three pairs of views forms a binary loop identical to the UV pairing described below

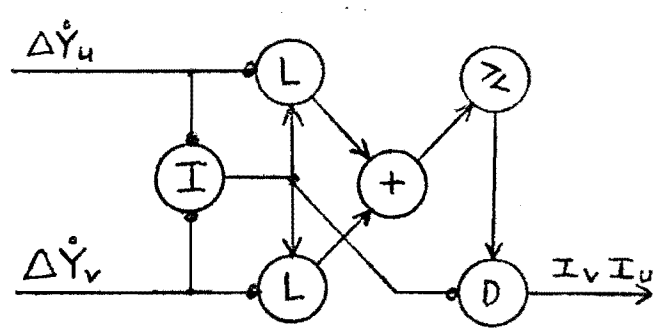

The slope changes measured for lines in each view are stored in lists, all pairs are passed to an adder module which performs a <u>subtraction</u>. If the difference between $\Delta\dot{Y}$ in two views is within comparator module limits, the delay module

passes on the index pair which will be used in track fitting to retrieve the two sets of three indices.

Although this is the simplest loop in the entire track processor, simulation studies show that it is the first to blow up in messy events. In principle, both the line finder and the view matching have computation times that grow as the square of the number of tracks. Roughly speaking, however, the fraction of the $n_1 n_3 n_5$ 3-plane combinations which accidentally satisfy the N_2, N_4 constraints increases for messy events. If our 10-track event generates ten correct and ten fake lines in each view, we have 400 line pairs in each view matching loop, or just over 10 μs for the view matching. Events with 20 measurements per plane typically require less than 20 μs but 100 per plane (more than one wire in four) will be insoluble even though a few hundred microseconds would suffice if the constraints held up. In simulation studies with E 87 raw data, we find that combining adjacent pairs of measurement for chambers 1, 3, 5 is necessary to reduce excessive repetition of lines for moderately complex cuts.

For the proposed photoproduction experiment, most reactions have fewer than six forward particles, so that even 100 μs for 10-track events would probably be acceptable.

If we later attempt to study high mass production by high energy neutrons, we would use some form of non-recursive trigger-logic to select candidates for reconstruction that undoubtedly would include a high rate of very complex reactions. By that time, we might add two more features to the line finder and view matcher.

The first addition tightens up as much as possible on the two constraints in the single view track projection. The maps produce a four-bit difference between prediction and the nearest measurement within the road if there is only one. By storing the first difference, N_2-N_2', and then combining it with N_4-N_4', we can interrogate a 256-word table to determine whether the track projection satisfies a more restrictive two-dimensional constraint.

The second addition increases the view matching constraints by requiring that, in the missing momentum-measuring view, at least two of the three planes 1, 3, 5 contain a measurement within a preset roadwidth of the value predicted from the two views. This would require an addition of three adders, six normalizers and nine maps.

B.3 Track Fitter

Although we have not completed the detailed logical design of the track fitter, we have fully simulated the arithmetic of the structure outlined below. We are now attempting to reduce the detailed logic to a minimal set of physical modules. We expect to complete design and simulation within one month, by early February 1980.

The input data for the track fitter consists of the full set of raw measurements along with results of the line finding and matching. The raw measurements consist of wire numbers and drift times, but the drift times are mapped immediately into a 4-bit fraction of maximum drift distance. (The mapping does not require knowledge of the track angle because the drift distances are short and because the tracks are almost normally incident.) The input from the preceding processor stages consists of lists of index pairs as well as the lists of wire numbers for chambers 1, 3 and 5 which were used to find lines and had adjacent pairs of wires combined into single entries.

The first step is to retrieve the original six wire numbers which define a matched pair of lines. The index pair telling us which two lines were matched is first used to retrieve the three indices I_1 I_3 I_5 defining each line. These indices are used to read one-bit lists which indicate whether the corresponding measurement has been assigned to a good track. Each of the two views is required to have at least one unused measurement in an effort to suppress fitting each track three times. Because the tagging of measurements occurs at the bottom of a long pipeline, several more candidates have entered the pipeline before a specific candidate can affect the one-bit lists. Candidates are therefore accepted preferentially from one view pairing, eg. UV.

Sets of six indices which pass the bit map test then retrieve the six wire numbers which define the two lines. The initial values of the five independent parameters of the particle trajectory are each linear in the six measurements

$$P_i^{\,o} = \sum_{n=1}^{6} A_{in}^{(p)} N_n + A_{i0}^{(p)} \quad .$$

The coefficients A_{in} are predetermined offline by a five parameter least square to the six measurements. The coefficients depend on which pair of planes we consider, indicated by the superscript p. The computation of the parameters is performed with a <u>sum-multiplier</u> structure which is the workhorse of the track fitter: for each pairing, the constants $A_{in}^{(p)}$ are stored in a 64-word table. In each table location, we store the sum of $A_{i0}^{(p)}$ and each of the constants $A_{in}^{(p)}$ for which the nth bit of the table address is 1. For computation, the 6 wire numbers N_n, along with a 2-bit page number identifying the desired set of constants, are all transmitted simultaneously but <u>bit-serially</u> on a single cable. The following diagram shows the logical structure of a sum-multiplier module:

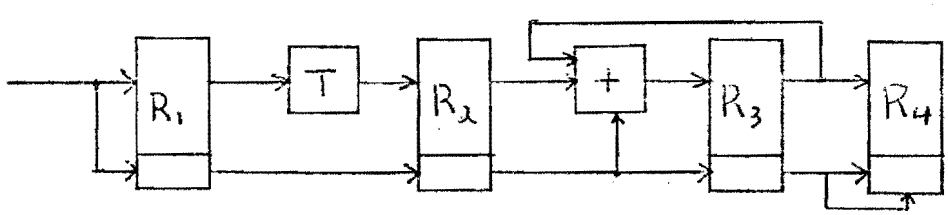

The six wire addresses are each transmitted together on one cable, one bit at a time, low order first. The six wire address bits and the 2-bit page form an 8-bit address for the 256-word table T. The input register R_1 is loaded from the cable every clock period. The contents of the addressed table location, T(R1), are loaded into R_2 the following cycle. An arithmetic logic unit (ALU) at the output of R_2 either adds the contents of R_2 to a second input or simply passes R_2 along. A control bit identifies the first transmission in a sequence, forcing the ALU to pass R_2 along to R_3. Otherwise the register R_3, connected to the other ALU input with a single bit shift, is effectively divided by two, added to R_2, and the result stored in R_3.

The wire numbers are 10-bit binary numbers. Therefore the tenth transmission is accompanied by a second control bit identifying the last transmission and loading R_4 with the contents of R_3 three cycles later. The input register R_1 is 10-bit, but the table, ALU and remaining registers have size determined by the computation. We require 12-bit precision for the initial parameterization, which in turn requires 16-bit arithmetic in this structure. The result is transferred from R_4 either bit-serially or in parallel.

A logic diagram of the track fitter would show the following sequence leading to the generation of the initial parameterization of a track candidate. First the paired indices of matched projections are stored in a separate buffer for each of the three pairings and retrieved serially with

a priority multiplexor which preferentially reads from the UV buffer but UY if no UV is available and VY if neither UY nor UV are available. The resulting index pairs, accompanied by page number identifying the pairing, read from lists of indices (I_{13}, I_5) and (I_1, I_3) generated by the line finder, forming the index set I_1 I_3 I_5 for each of the two views. These indices, in turn, access the one-bit tag lists. If each selected view has at least one of its three measurements not tagged as used by a very good track, these indices are next used to retrieve the actual wire numbers used by the line finder in planes 1, 3 and 5. All six wire numbers, accompanied by page, are shipped bit-serially to sum-multiplier modules with the aid of a bus controller whose primary function is to count to a preset number of cycles before turning on the last-bit indicator.

The five independent parameters are chosen to be the four parameters of a straight line before the analyzing magnet and the change in Y-slope after the magnetic deflection in the Y-direction. We wish instead to have two sets of 4 parameters describing the straight line trajectories before and after the magnet. The trajectory is described to a good approximation by a simple deflection at the magnet center plane. If we choose to parameterize the lines by slope and apparent intercept at this center plane, the second set of four parameters is just the first set with the Y-slope changed. The small corrections to this approximation are not

quite negligible, particularly for the otherwise unchanged X-slope. This requires table reference, 8-bit multiplication and 12-bit addition. The resulting parameterization, although accurate to only 12 bits, must be internally consistent to 16-bit accuracy.

This expanded 16-bit parameterization is next used to bit-serially generate simultaneously all 20 individual wire plane coordinates predicted by the approximate parameterization. If any of the planes are sufficiently inside magnetic fields, we must also compute the deviation of the actual trajectory from the straight line, multiplying tabulated field integrals by Y-slope change. The full prediction requires 15-bit accuracy: 9-bit integer wire number and 6-bit fraction.

We next simultaneously search the twenty lists for measurements within some preset distance of the prediction, keeping only the fractional predictions and for each wire within the road, simply the index and the difference between wire number and integer prediction. Along with the lists of measured drift distances, these fractional predictions and integer residuals are the only inputs to the least-square fit outlined below.

The least-square fit determines 6-bit corrections to the original parameterization which minimize the weighted sum of squares of differences between measurement and prediction for the twenty planes. The problem is now linearized. The change in coordinate ΔX_n for the nth plane is a linear combination of changes in the five parameters, ΔP_i:

$$\Delta X_n = \sum_{i=1}^{5} \alpha_{ni} \Delta P_i \quad .$$

If the residual error in plane n is δ_n, and the measurement is assigned a weight W_n, we wish to minimize with respect to ΔP_i

$$S = \sum_{n=1}^{20} W_n \left(\delta_n - \sum_{i=1}^{s} \alpha_{ni} \Delta P_i\right)^2 \quad .$$

The result is a matrix equation

$$M \overrightarrow{\Delta P} = \vec{\Delta}$$

where $M_{ij} = \sum_n W_n \alpha_{ni} \alpha_{nj}$

$$\Delta_i = \sum_n W_n \delta_n \alpha_{ni} \quad .$$

We first transform the equation by multiplication with the inverse of the usual value of the matrix:

$$M_{ij}^{o} = \sum_n \alpha_{ni} \alpha_{nj}$$

with the resulting equation

$$M' \overrightarrow{\Delta P} = \vec{\Delta}'$$

where $M_{ij}' = \sum_n W_n [(M^o)^{-1}_{ik} \alpha_{nk} \alpha_{nj}]$

$$\Delta_i' = \sum_n (W_n \delta_n) [(M^o)^{-1}_{ik} \alpha_{nk}] \quad .$$

The original M_{ij} has large positive diagonal elements ($M_{ij}^2 \leq M_{ii} M_{jj}$), but the new M_{ij}' is even better, quite close to the identity matrix. The weights W_n are usually 1, but are zero if no measurement has been assigned and otherwise inversely proportional to the mean square uncertainty in the measurement. The approximate solution is

$$\Delta P_i = \Delta_i' / M_{ii}'$$

which has the form

$$\Delta P_i = \left(\sum_{n=1}^{20} (W_n \delta_n) A_{ni}\right) / \left(\sum_{n=1}^{20} W_n \; B_{ni}\right) \quad .$$

The individual plane coordinate changes introduced by these ΔP_i are then calculated precisely. The α_{ni}, A_{ni} and B_{ni} are all predetermined constants, stored in appropriate sum-multipliers. We require one iteration ignoring drift time followed by three iterations incorporating the drift time. The sum multipliers all require 8-bit tables and arithmetic, but only four bit-serial transmissions are required per iteration. The iteration sequence is

1) map drift distances and residuals into W_n, $W_n \delta_n$;
2) generate 4-bit ΔP_i with 4-cycle bit-serial sum-multiply;
3) followed by 4-cycle divide;
4) generate 8-bit ΔX with 4-cycle bit-serial sum-multiply.

The iteration is a pipeline which can accept a new computation every four clock cycles, but has a total pipeline delay roughly four times larger. By buffering this pipeline to permit at least four tracks within the pipe, single tracks can pass through four iterations with a propagation delay of about 2 μs, but at a rate of one every 400 ns.

We next determine W_n, $W_n \delta_n^2$ for each plane and calculate ΣW_n, and $(\Sigma W_n \delta_n^2)/(\Sigma W_n)$. If the track satisfies a definition of very good, the indices for chamber 1,3,5 measurements are used to write into the tag lists described above. If the track passes a less restrictive cut, it is compared with all

previously accepted tracks for a plane-by-plane comparison of measurement indices. If two tracks share too many measurements, we keep the better track, or if comparable quality the first track.

The entire track fitting pipeline, which begins with the retrieval of six wire numbers to generate the initial parameterization, will probably accept a new candidate every 400 ns, and have a total pipeline delay of almost 4 μs. Real tracks will be submitted an average of about three times to the fitter unless suppressed by tagging roughly 10 candidates after initial submission, so that between 3 and 10 tracks we can expect little dependence on the number of tracks for total fitting time. The structure outlined above might require 10 μs for a typical 10 track event, but could be less than 5 μs for a comparable structure. The actual configuration will depend on the cost and complexity required for specified rate, as well as the rate requirements. If we are unable to reduce ADC time below 10 μs, we will have little incentive to push track fitting to much shorter time.

C. Detailed Description of Individual Modules

The following logic diagrams outline the internal logic of individual modules. We explain in detail the operation of the binary index generator. The internal storage elements are:

WC_i	write counter
RC_i	read counter
P_i	read pointer
A_i	data in list
C_i	write complete
B	inner loop pointer
G	first pair sent
V	Valid out
C	Complete out

All counters and flip-flops are reset to zero by an initialization condition generated either by the generation of Complete out or externally through the control bus. If we define the following logic levels

$$s = (RC_1 = P_1) + (RC_2 = P_2)$$

$$v = [(RC_1 \neq WC_1) + (RC_2 \neq WC_2)] \cdot (\overline{V \cdot H}) \cdot G$$

$$b = (RC_2 = WC_2) + \bar{B} \cdot (RC_1 \neq WC_1)$$

we can express the logical operation in a notation R = (X)(Y), which is meant to indicate that the contents of the register R will become X on the next clock edge if condition Y is true. The binary index generator operation is then fully defined by

$$RC_1 = (RC_1+1)(bsv+\bar{B}\bar{s}v)$$
$$(\ 0\ )\quad(\bar{b}sv)$$
$$RC_2 = (RC_2+1)(\bar{b}sv+B\bar{s}v)$$
$$(\ 0\ )\quad(bsv)$$
$$B = (b)\ (sv)$$
$$C = (C_1 \cdot C_2 \cdot (RC_1 = WC_1) \cdot (RC_2 = WC_2))(\bar{V})$$
$$V = (G \cdot (RC_1 \neq WC_1) + G \cdot (RC_2 \neq WC_2) + A_1 \cdot A_2 \cdot \bar{G})$$
$$G = (A_1 \cdot A_2)$$
$$WC_i = (WC_i+1)(\text{input cable } V \cdot \bar{H})$$
$$C_i = (1)(\text{input cable } C)$$
$$P_1 = (P_1+1)(S \cdot (RC_1 \neq P_1))$$
$$P_2 = (P_2+1)(S \cdot (RC_2 \neq P_2))$$

The binary index generator generates all possible pairs of indices less than or equal to the number of transmissions on each input. After at least one transmission on each input, the first index pair (0,0) is transmitted. The generator then functions as a nested loop, with the outer loop index a new value and the inner loop index ranging over all previously used indices for the other side. If possible, inner and outer loop designation is exchanged at the completion of each inner loop. This permits a binary loop to proceed even while two sets of data are being generated.

For index generation when tests within the loop could affect index sequence, the most common example of which is

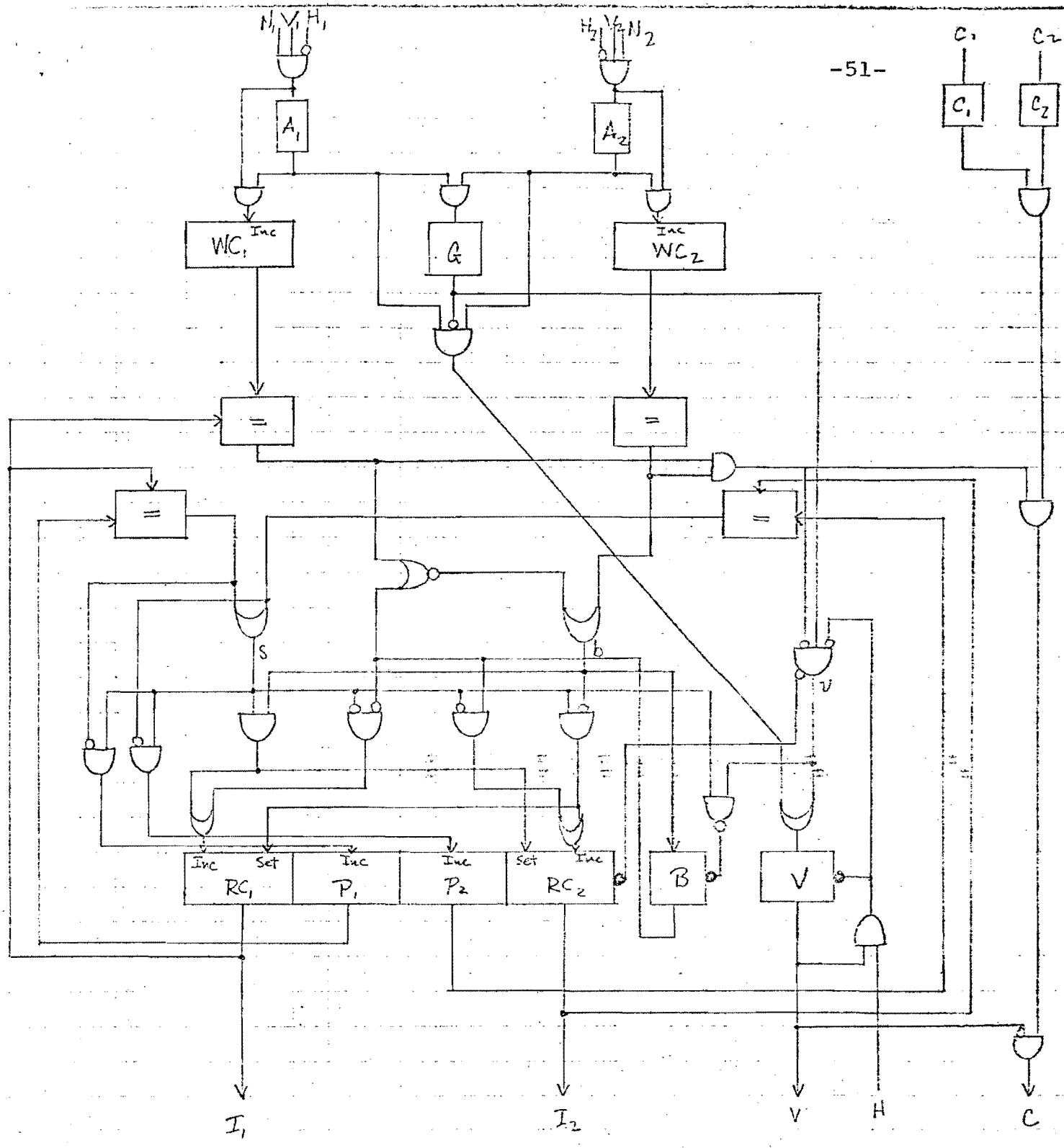

Binary Index Generator 1/80

1/60

Comparator

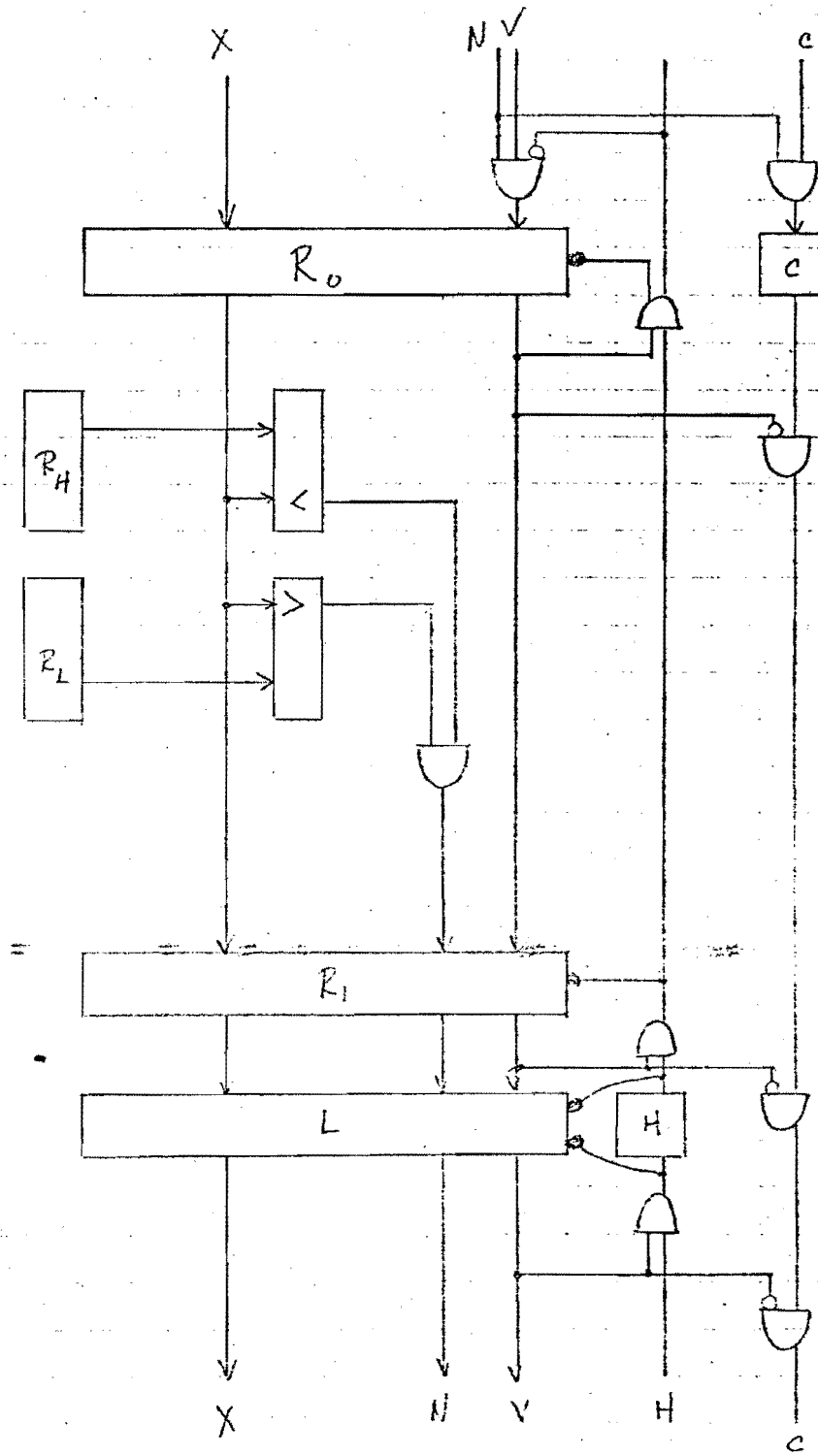

Index List

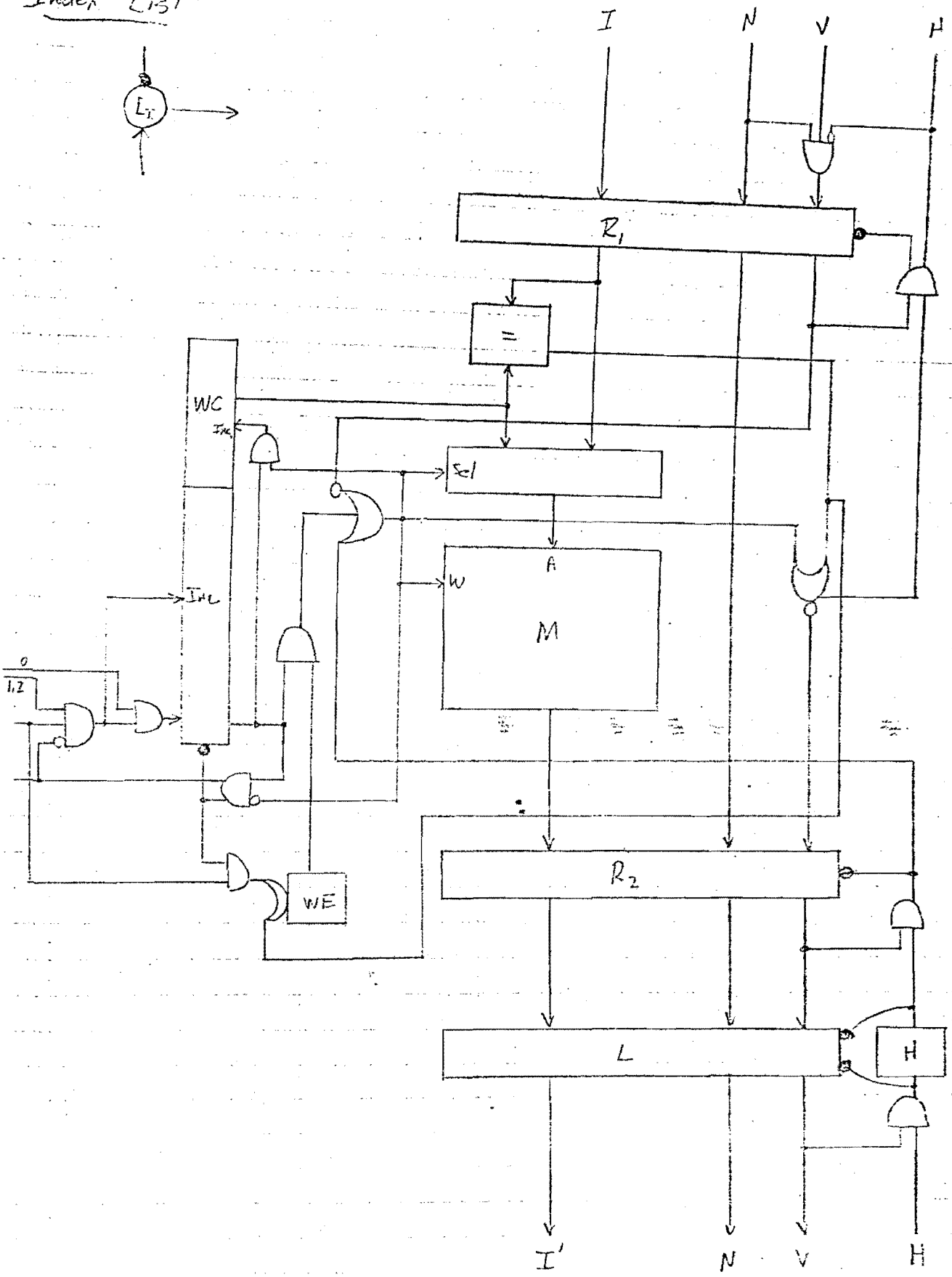

List (Read Priority)

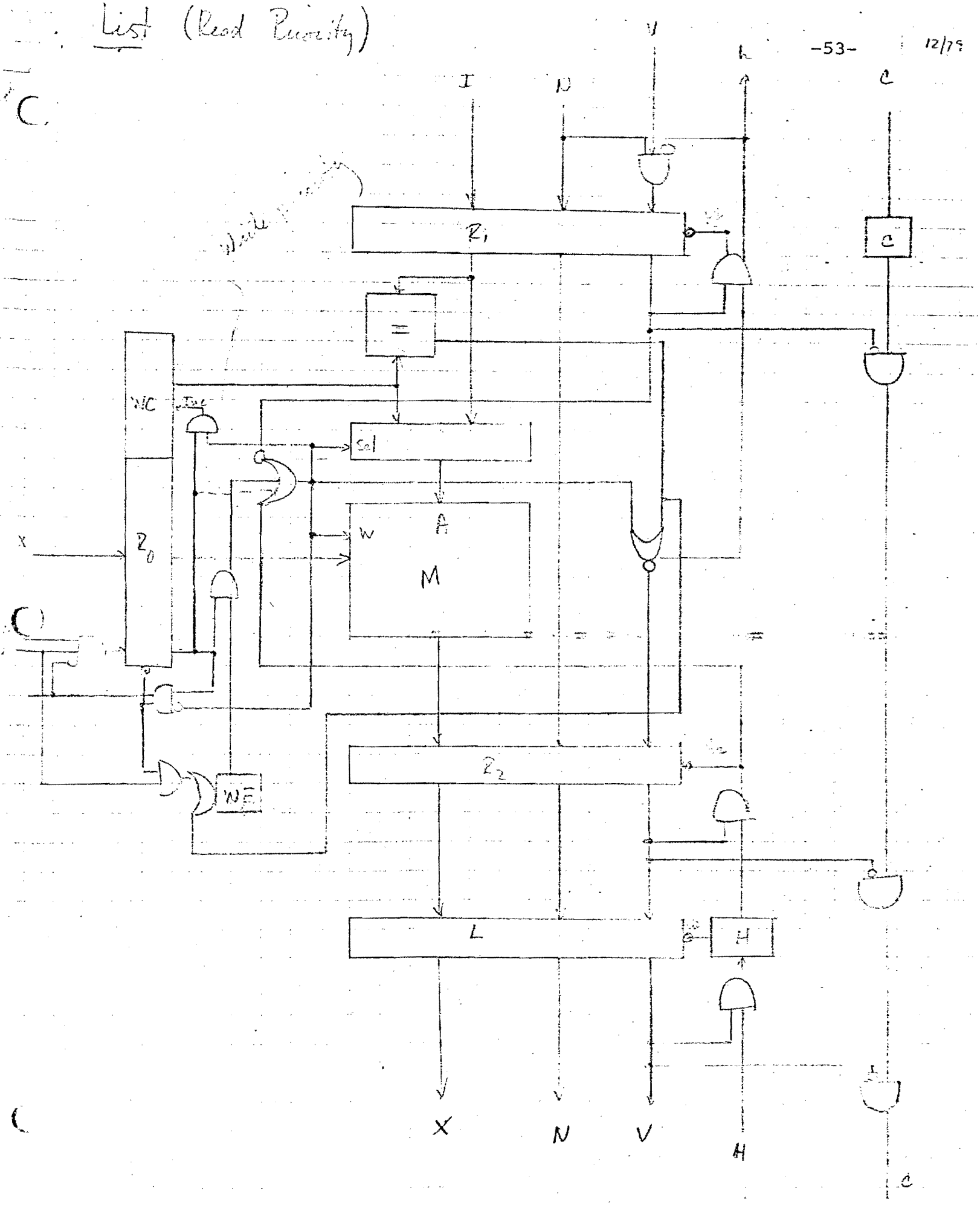

List. Counter

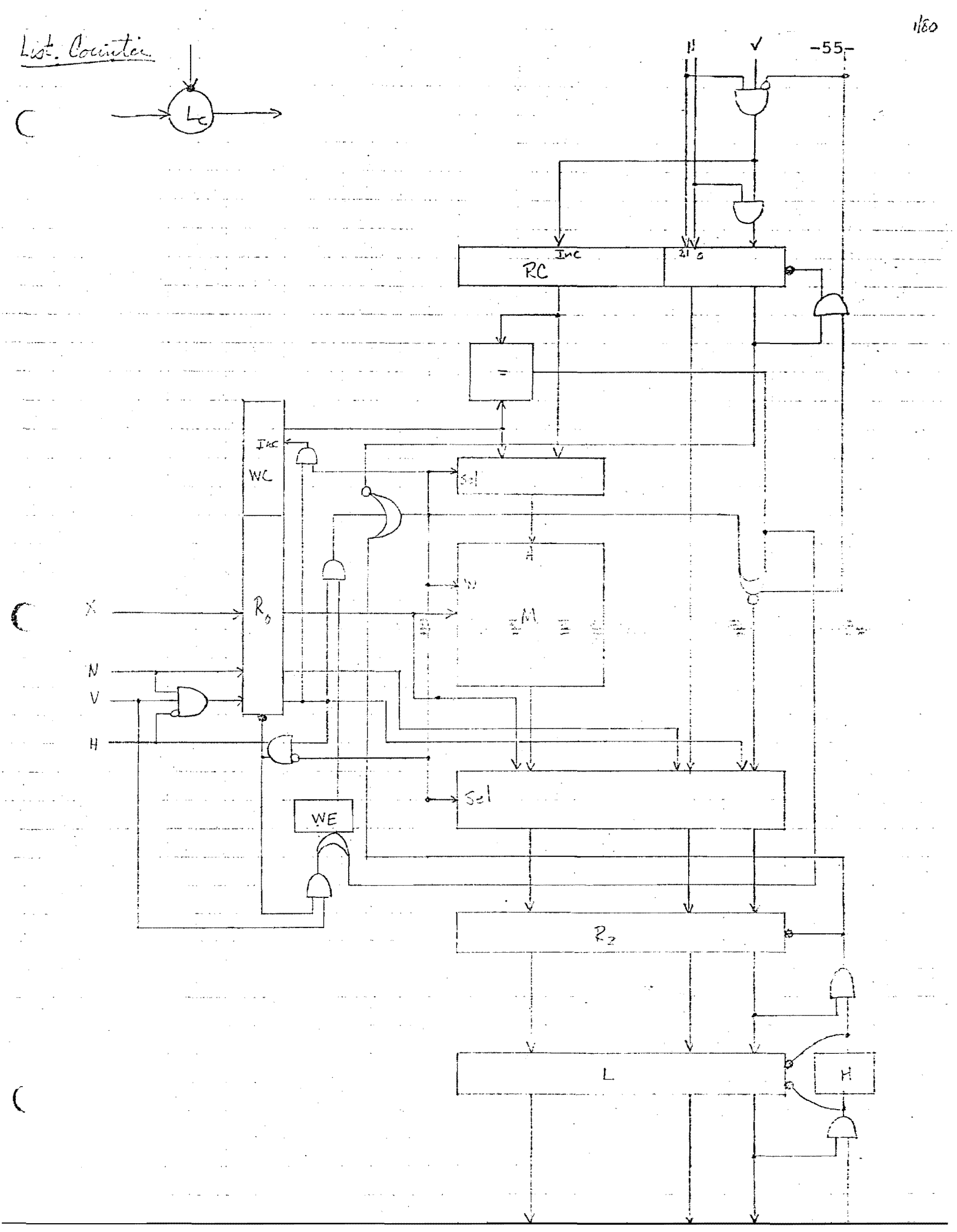

Page Generator

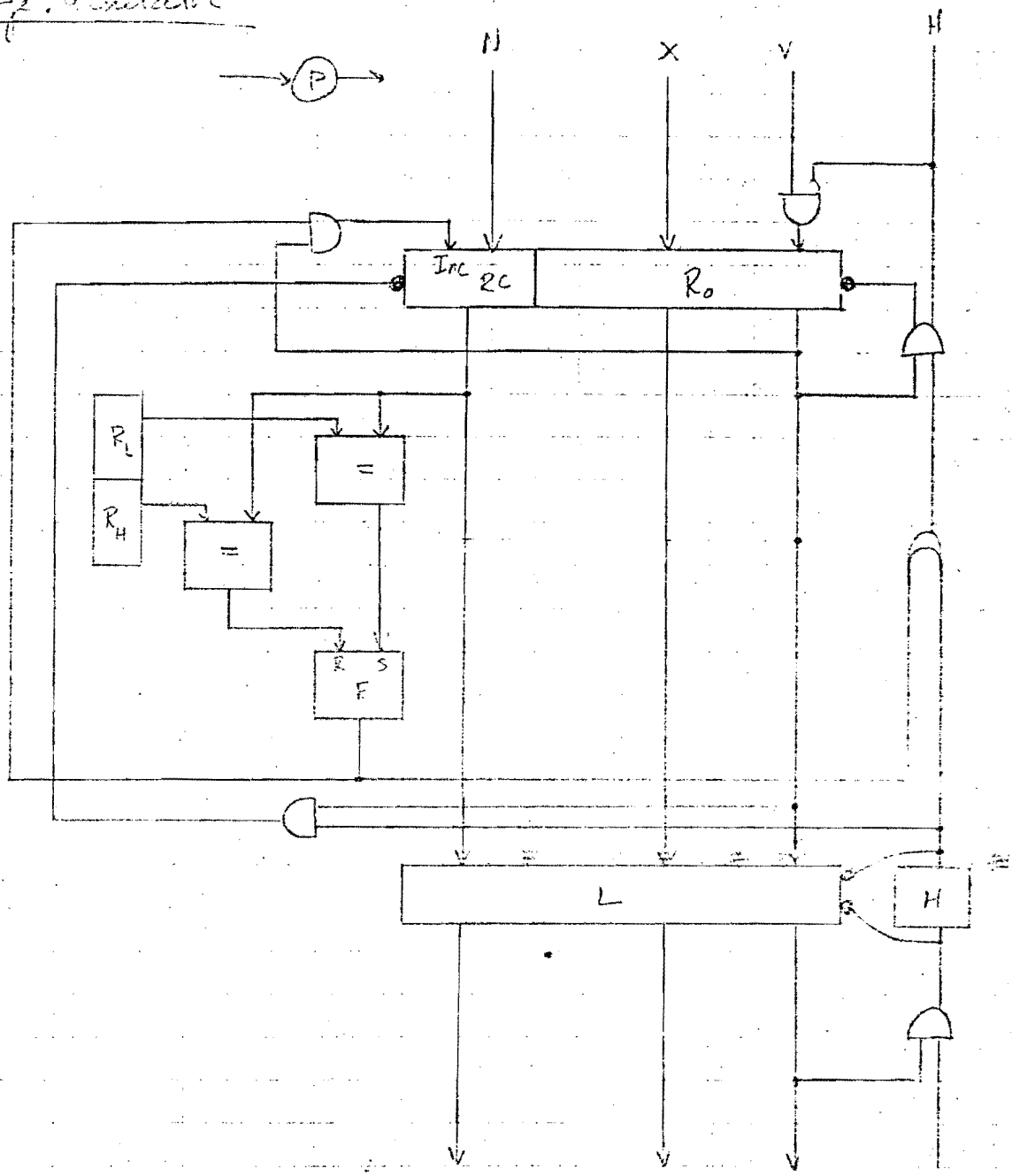

Normalizer

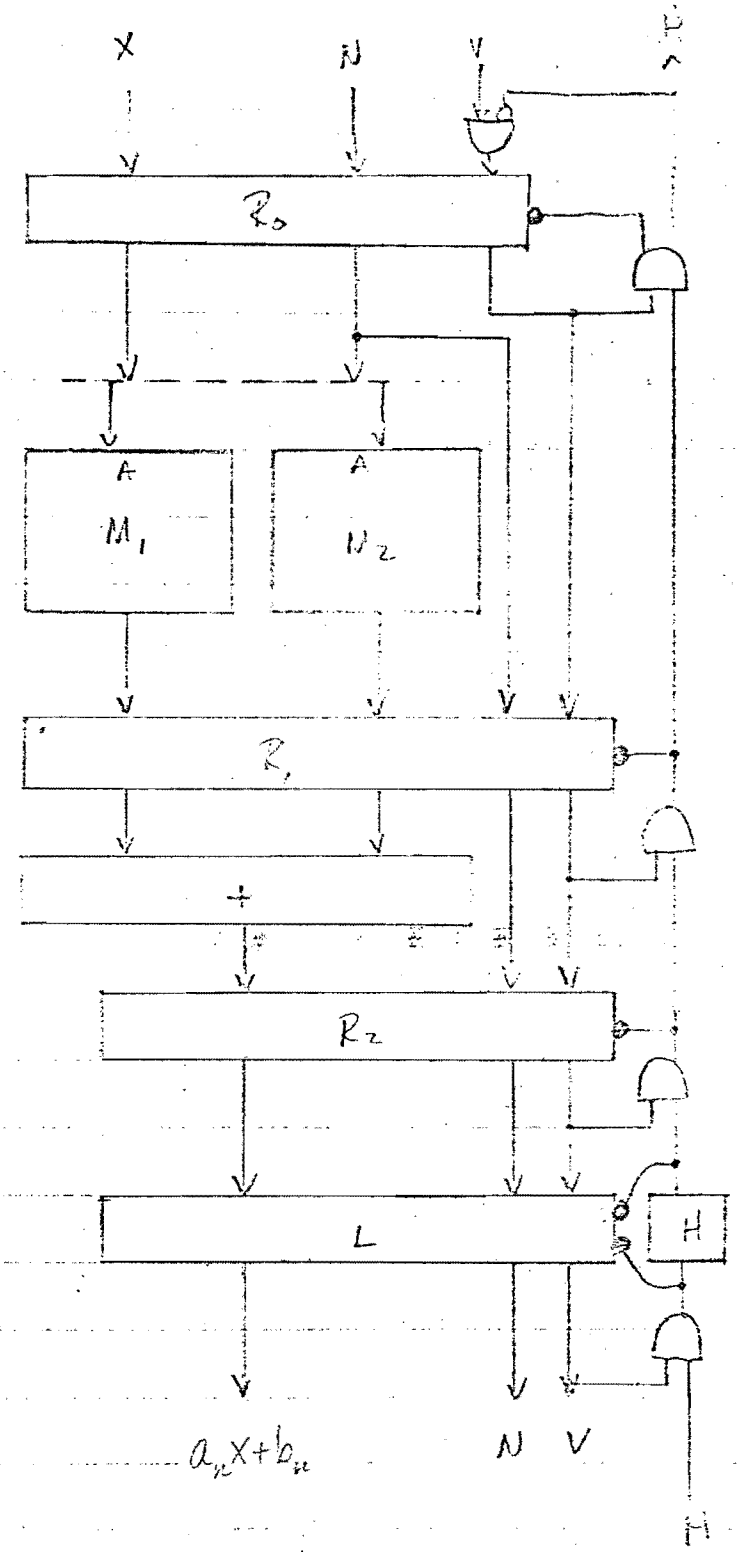

Multiplexer

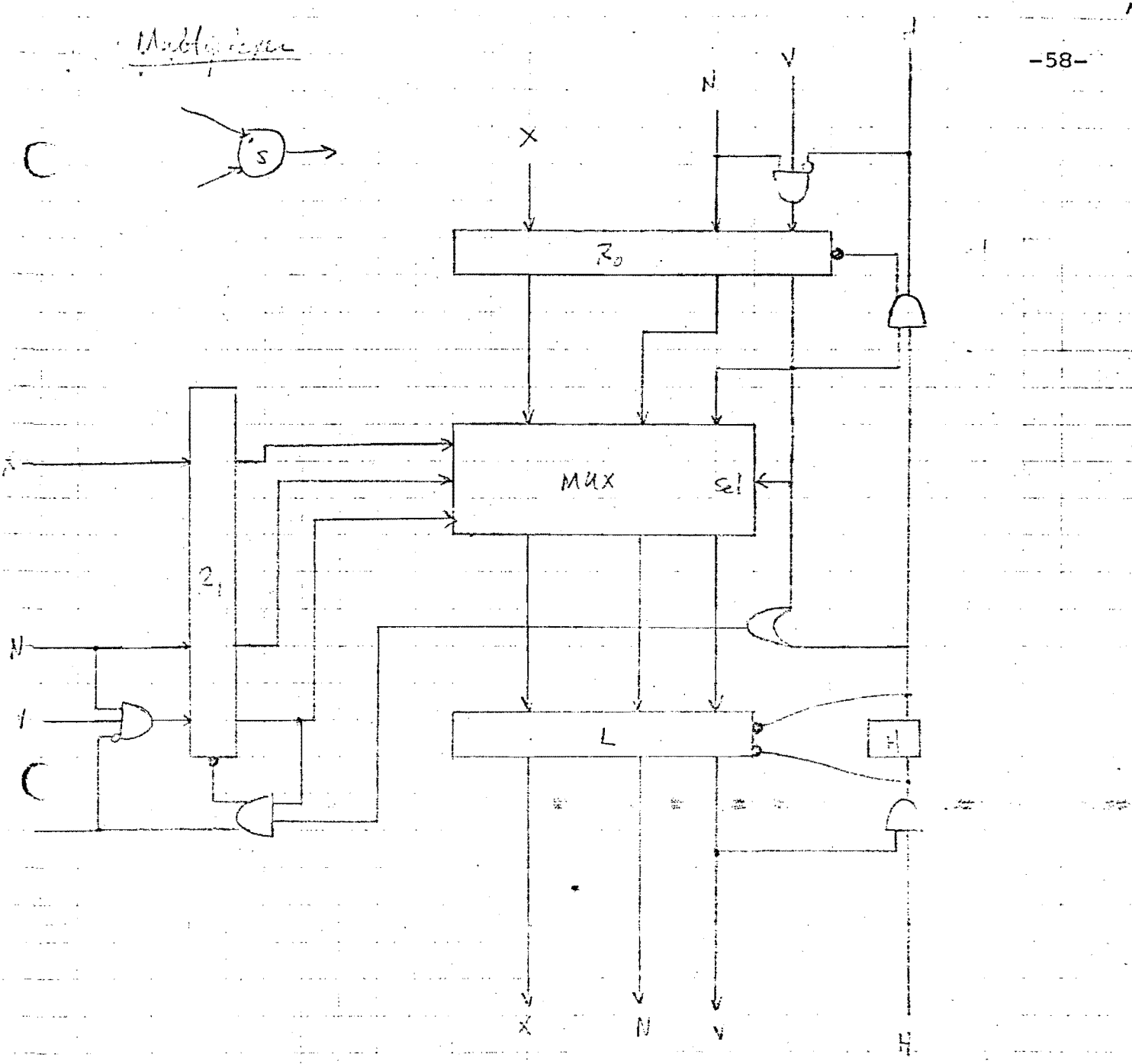

ADDER

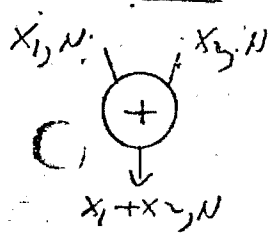

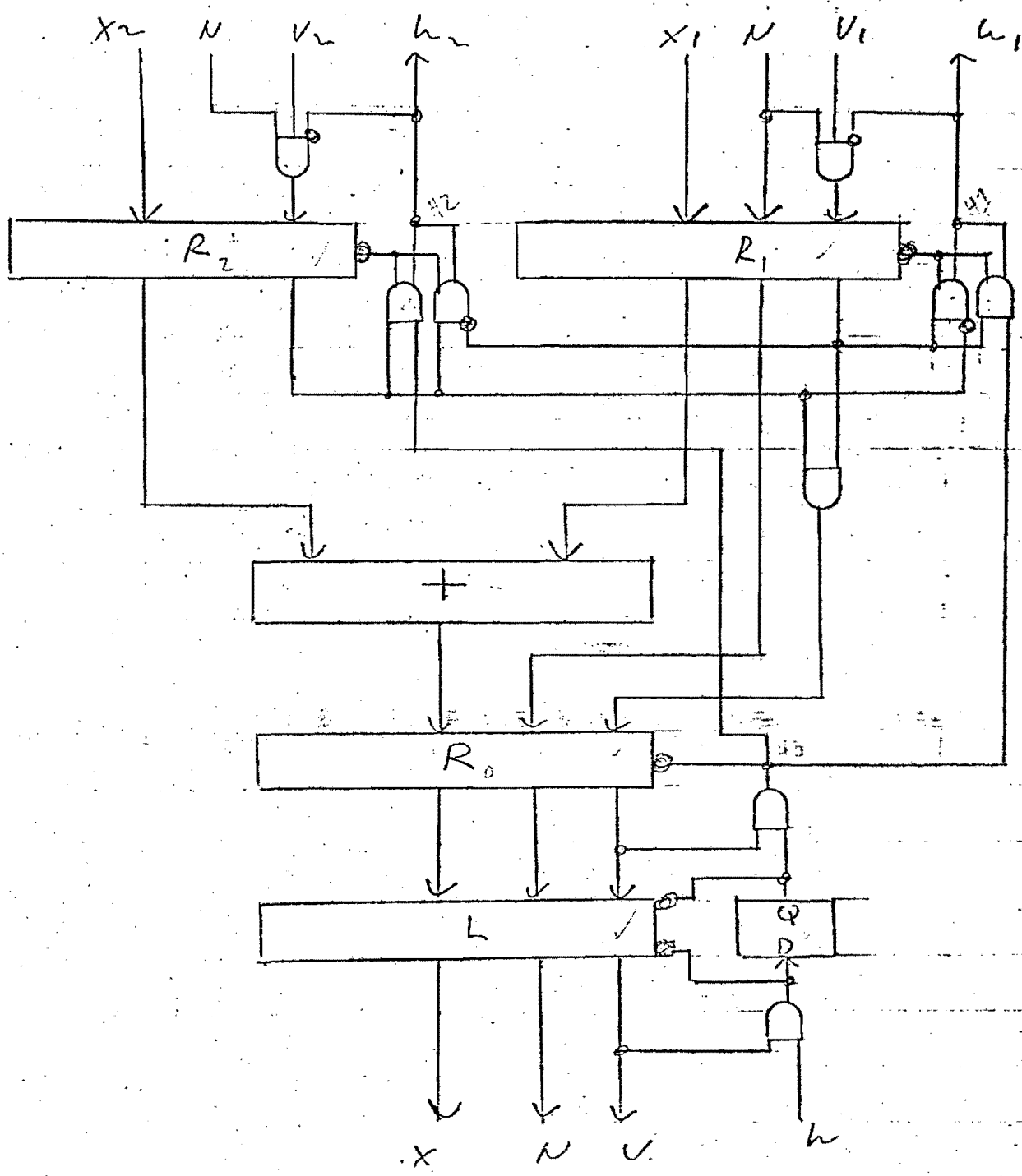

Map (Write Parity)

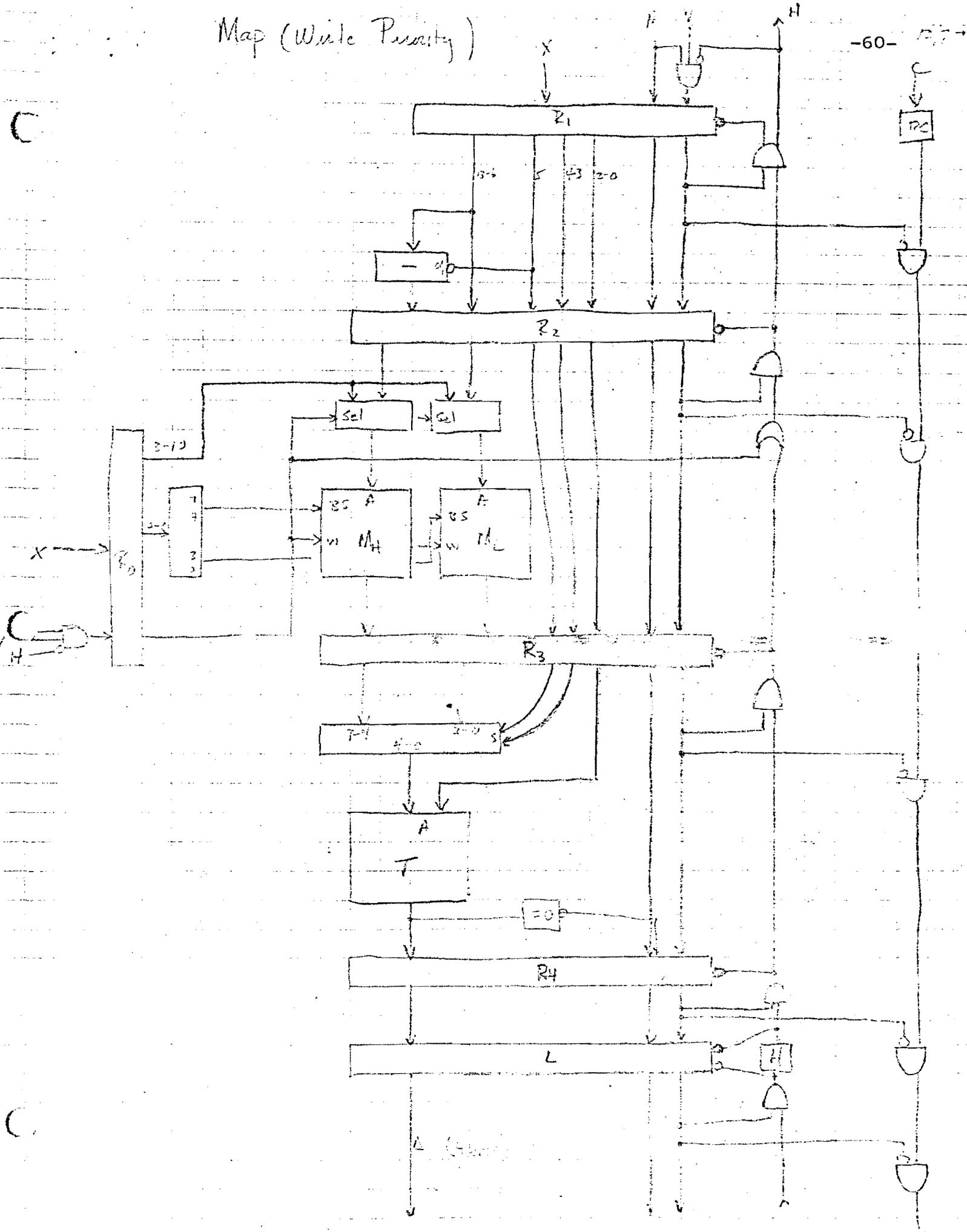

pairing of two lists of ordered data, this structure can postpone the need for a test decision, minimizing the effect of pipeline delay. If, for instance, the test result is that for subsequent indices RC_1, the index RC_2 should always be greater than the present value, RC_2+1 should be stored in a Lower Pointer, which replaces the zero loaded into RC_2 at the beginning of an inner loop.

D. Construction Costs and Time Estimates

Important general design decisions remain. Among these are packaging or physical construction. We have produced detailed layouts of the most complex modules, particularly the list, to verify the feasibility of single layer printed circuit boards and to determine the physical size. We will wait until logic design has been completed for more than just the track reconstruction before making a final decision. The considerations include ease of access and interconnection, packing density, cooling, reliability and cost. Complete design and prototypes should be available in the spring of 1980.

Our estimated $100 K for the entire processor, including track reconstruction, photon reconstruction, charged particle identification, kinematic reconstruction, distributed buffer, histograms and a central buffer, appears to be a reasonable upper limit. The system can be indefinitely expanded. Perhaps as we gain familiarity with the problem, we may attempt something more complicated than we could justify for a

first experiment. We are not including the cost of tape drives or online mini computer.

The processor will contain fewer components by far than either ADC or TDC system. Most modules would be commercially assembled. No unusual or difficult construction will be involved. We could have the entire system assembled within a year of approval.

IV. COMPLETE DATA ACQUISITION AND PROCESSING SYSTEM

In the following pages, we attempt to outline in some detail our proposed data acquisition system, beyond just event reconstruction hardware. The entire detector has been designed with the goal of accurately and reliably measuring reasonably complicated reactions at high rate: instantaneous rates on the order of 10^7/sec and event reconstruction rates in excess of 10^5/sec. The detector has more than 10^4 receiver elements, of which only a few percent provide positive information for a typical reaction. To make this information available to an event reconstruction system with a new event every few microseconds and a transfer time of less than a microsecond, we require receivers designed to do just that. The principles of operation of the front end permit reliable measurement in the presence of high instantaneous rates and a noisy environment.

A. Drift Chamber Measurements

An amplifier-discriminator has been developed at Nevis recently, the result of several years of intermittent study. The inexpensive, high speed, low-threshold and very nearly deadtimeless circuit has an externally referenced threshold and should permit reliable signal detection at the minimum levels possible within the constraints of noise and external feedback. The amplifier has low input impedance, $\sim 100\ \Omega$, and internal pulse shaping to maximize signal to noise. Push-pull output minimizes the disturbance of the nearby environment, reducing the difficulty of shielding the input from the output.

Actual operating thresholds depend on details of chamber construction, but will be lower than we have previously achieved.

The TDC system assumed in the proposal is a Nevis design which has been used for a few years in modest quantity. This TDC has a purely digital 5-bit time measurement with 2.4 ns time bins. Valid measurements are transmitted at 10 MHz. Built with ECL 10 K circuitry, the system is simple to use and very reliable. Some 800 channels of the 16-channel cards were constructed commercially in 1976 for $10/channel. Recent price quotations yield similar cost, because integrated circuit prices fell to compensate for increasing board costs. The cost is dominated by the multilayer printed circuit board.

We have recently reexamined this design, guided by our processor design effort, to see if we can do even better. Although we have not yet produced and tested a prototype, the design looks straightforward. We can produce a 32-channel card for about the price of the previous 16-channel card. The number of components per channel has been reduced by nearly a factor of two, and only double-sided single layer printed circuit boards are required. The TDC has a 4-bit time code, with the same 2.4 ns time bins, and 40 MHz readout of valid measurements. The time span can be increased in increments of two bits, with accompanying increase in board size and cost. A 2.4 ns time bin corresponds to 120 micron binning of drift distance, with 35 micron rms error introduced

by the binning in quadrature with larger measurement uncertainty. Sixteen such time bins are quite adequate for up to 3 mm wire spacing. For our largest wire spacing, 6 mm, we would double the size of a time bin, introducing 70 micron rms digitization error, which will be dominated by measurement error in the large drift chamber.

In addition to 32 input signals, the TDC has a fast gate and fast reset. During the gate, any input signal from a drift chamber discriminator sets a corresponding flip-flop and latches a 4-bit time code. Only the first signal is recorded for each channel. If a slower trigger decision rejects the event, a fast reset immediately clears all flip-flops.

If the event is to be recorded, a sparse-data readout procedure similar to the old TDC but with the addition of input and output registers on the communication bus, permits each plane to be read separately at 40 MHz. If we transfer at most 32 measurements per plane to the processor buffers, we can guarantee that the TDC system is always unloaded and ready for another event within 1 μs.

B. Analog to Digital Conversion

At Nevis, we have designed a 16-channel 12-bit ADC, of which 5,000 channels have been commercially constructed within the past year, for a total cost of less than $30/channel, including power and crate. The linear gate has dynamic baseline restoration which results in pedestal stability of a fraction of a bin, even in the presence of

low frequency noise, without the rate dependent pileup normally associated with AC coupling. The measurement was absolutely stable and linear to within 0.2%. A fast reset allows the integrating capacitor to be reset with a time constant of < 20 ns, for an effective reset time of ~ 100 ns.

The 16 channels are digitized one after another, with the results stored in memory on the card. The results are then shipped serially to a nearby card which subtracts tabulated digital pedestals, storing for later transfer only those measurements a preset value above pedestal. This design is not quite suitable for our purposes. Following a decision to digitize, more than 20 μs must elapse before the linear gate is again available.

The ADC may be the most challenging part of the processor. We require approximately 4,000 channels of ADC, whose total cost, even for $30/channel, will certainly exceed the total cost of the "hardware processor". For similar cost and complexity, a new ADC design incorporating minor changes from the previous design will introduce a 1 μs transfer of the analog signal from the integrating capacitors to buffer capacitors and increase the event rate by permitting data transfer from the card to proceed in parallel with digitization. We will reconsider the entire design, but most probably the event processing time will be determined by the ADC system, not the track reconstruction. To reduce the time per event below 10 μs may prove too difficult or expensive. For the moment,

we would be quite content with a 10 μs ADC, with a 1 μs buffer transfer.

C. Kinematic Reconstruction

Although kinematic reconstruction is deeper into the design pipeline than we have progressed, we attempt a brief look-ahead to establish the plausibility of online event selection based on precise reconstruction of possibly complicated expressions in a flexible manner. We perform such computations at the same event rate as the track reconstruction and charge digitization, first computing individual particle parameters, including charged particle identification, photons and identification of neutral pions, and then proceeding to multiparticle computations.

General features should include simple programmability, so that new computations can be introduced on short notice. The kinematic computations will probably be based on bit-serial transmission and arithmetic, with 16-bit fixed point numbers everywhere except within structures of the form $M = \sqrt{\Sigma X_i Y_i}$, which might have higher internal precision. Not that higher precision or floating point representation are impossible, but they introduce complexity and expense which should appear only where necessary. Bit serial arithmetic structures are incredibly simple and allow very simple data transmission. An isolated bit-serial adder, for instance, requires one 4-bit register and half of a dual one-bit adder:

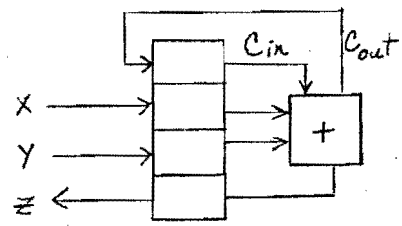

Simple structures using full word shift registers and ALU's can perform multiplication, division, and square root. With tables we can perform Taylor series expansions, etc.

Computations must be carefully set up to avoid unnecessarily large numbers of operations or high precision arithmetic. We try to avoid complicated operations within nested loops. Consider multiparticle invariant mass computations, for instance:

$$M^2 = (\Sigma\, E_i)^2 - (\Sigma\, \vec{P}_i)^2$$

$$= (\Sigma(E+P_z)_i)(\Sigma(E-P_z)_i) - P_\perp{}^2 \ .$$

We could compute $E-P_z$ by brute force, but we first note that

$$E-P_z = (m^2+P_\perp{}^2)/(E+P_z)$$

$$\approx (m^2+P_\perp{}^2)/2P_z \ .$$

The fractional error in the approximation is less than $(m^2+P_\perp{}^2)/(4P_z{}^2)$, less than 1% for a 5 GeV proton or a 200 mrad pion. The formula for invariant mass is then

$$M^2 + P_\perp{}^2 = (\Sigma\, E_i)\ \Sigma\ \left(\frac{m^2+P_\perp{}^2}{E}\right)_i \ .$$

Similarly for Lorentz transformations:

$$P_{||}^{*} = \gamma(P_{||}-\beta E)$$

$$E^{*} = \gamma(E-\beta P_{||}) \quad .$$

Both expressions have the form large number times difference between two large numbers equals small number, indicating a need for great numerical precision. On the other hand, 16-bit fixed point arithmetic is fine for

$$P_{||}^{*} = [\gamma(1-\beta)]E-\gamma(E-P_{||})$$

$$E^{*} = [\gamma(1-\beta)]P_{||}+\gamma(E-P_{||})$$

if we know $(E-P_{||})$ and $[\gamma(1-\beta)]$.

D. Information Storage and Distribution

1. Transport System

A data transport system has been designed at Nevis and supplied to existing experiments. Envisioned primarily as an interface between interfaces, the system consists of modules bussed together within a single crate, with the capability of limitless expansion to other crates, possibly quite distant. Sixteen-bit data words can be transferred between modules on the transport bus at rates up to 10 MHz. The communications use the same simple control functions described for the processor: Valid, Hold, Complete with now a larger Page or name field. Data transmissions may be identified with the name of the source module, permitting multiple destination modules to share a communication. Modules, eg. the link between crates, may contain random access memory, both for storage of data and to allow

programming of module operation. The equivalent of the control bus, described earlier for the processor, is just the same transport bus with a specific tag bit, permitting local access to modules for control and programming.

To establish communication between different objects, we need only interface each object to the transport bus. Subsequent communication can be readily established between any two or more devices. Several simultaneous (interleaved) unrelated conversations are possible, subject only to the 10 MHz limitation on total communication rate within a single crate, and somewhat slower communication between crates.

2. Distributed Buffer

We are still designing the distributed buffer required for a distributed pipelined processor. The initial raw data, and all intermediate computations which might be requested later, must be stored for each event, as they are generated, and retained for as many events as is necessary to decide what data to transfer out of the processor. We therefore are designing a buffer module which plugs directly onto a transport bus, and in addition, has a direct fast communication port. Blocks of data can then be stored by name, simultaneously in several buffers, and later retrieved or dismissed by name, usually through the transport bus.

3. Online Histograms

For event selection and detector calibration and performance checks, we are designing simple histogramming structures. The most complicated such structure, still quite simple, is patterned after the E 87 offline analysis program, and allows a family of histograms of related data so that we obtain histograms of selection criteria and the resulting effects of progressively more restrictive cuts. The related variables are bussed simultaneously but bit-serially to a block of identical modules which each contain sum-multipliers and histogram memories. Any linear combination of up to 8 variables, within an even larger set, can be histogrammed, and a trigger priority level can be established by comparison with preset limits. The histogram contents can be accessed through the bus, which is in fact a version of the transport bus, for either scope display or permanent storage.

BUDGET AND SCHEDULE

The cost of the proposed experiment can be divided into two components -- 1) the cost of constructing the spectrometer itself; and 2) the cost to the laboratory of its support. In both cases, we believe that the costs are relatively modest and that our estimate of the spectrometer costs are unusually accurate for the proposal stage of a large, complex experiment.

The cost of the spectrometer itself was estimated in the proposal to be ~ $900 K. Approximately half of the cost is in detector electronics (hardware processor, ADC's, TDC's, amplifier/discriminators, phototubes) and half in mechanical assembly costs (drift chambers, Cerenkov counters, gamma ray detector, hadron calorimeter). The electronics costs are well known since all the electronics are constructed using components with which we are very familiar, having used them for years. In constant dollars, the electronic costs are certainly overestimates, because we have provided upper limits when in doubt, and the component costs continue to decrease with time. These electronics costs are categorized below:

Hardware Processor	$100 K
ADC's 4000 x $35/channel	140 K
Analog Amp + Cable 3400 x $10	34 K
TDC's 7000 x $10/channel	70 K
Amp.Disc+ Cable 7000 x $15/channel	105 K
Phototubes 650 x $100/channel	65 K
Total	$514 K

The costs/channel include power and associated cabling necessary to transport signals from the pit to the counting room. Mechanical assembly costs are estimated in the proposal to be as follows:

Drift Chambers	$90 K	
Photon Calorimeter	100 K	(200 K)
Cerenkov Counters	100 K	
Hadron Calorimeter	45 K	
Muon Identifier	10 K	
Trigger and Recoil System	10 K	
Total	$355 K	(455 K)

Costs for the hadron calorimeter do not include the cost of the steel which would be supplied by Fermilab. We now believe that concrete will suffice for the muon detector. In addition, a closer examination of the cost of mechanical assembly of the photon calorimeter leads us to believe that $200 K is a more realistic estimate than our original $100 K. Again we emphasize that these estimates are based on our past experiences working with very similar detectors or prototypes. Detailed engineering studies of these components cannot be prepared until approval of the experiment has been granted. Additional miscellaneous items, both mechanical and electronic, are comparable to the uncertainty in the overall cost, leaving the overall estimate at ~ $1 M.

The major cost to Fermilab is connected with supplying an analyzing magnet. We desire a magnet with a 48 in. x 40 in. aperture, an effective field length of 60 in. and a 10 kG field (P_T = 450 MeV). Fermilab has estimated the total cost to Fermilab of such a magnet to be ~ $ 600 K including magnet construction, powering, cooling, and

installation. We believe this cost to be closer to $200K and are currently investigating the costs of building a new magnet with the desired parameters although we have not abandoned efforts to obtain an existing magnet from elsewhere.

Another potential cost to Fermilab is that arising from discussions of the desirability of constructing a new beam line. As we have indicated earlier, we have a very strong desire to remain in the broad band beam because of its high intensity/high energy qualities. We feel that a much more attractive possibility than construction of a new beam would be the undertaking of the previously discussed modifications to make the broad band and tagged beams compatible.

Schedule

We would be ready to install the hardware processor and drift chamber system for tuneup within one year of approval of the proposal (i.e. in spring of 1981). We would hope to develop an operating system using muons produced during tagged beam operation during this period. Following the shutdown beginning in June of 1981 and ending in the spring of 1982, we would install the remaining detector elements and expect delivery of the large analyzing magnet. This would allow us to initiate our final tuneup and begin data taking in spring or summer of 1982.

SUMMARY

In summary, we hope you will not regard our proposal as calling for just another forward spectrometer. Our spectrometer would provide unusually complete and reliable measurements of a wide range of interesting physics reactions, with flexible and precise event selection at very high interaction rates. No other forward spectrometer, at Fermilab or elsewhere, will have comparable sensitivity to high mass, rare or complex reactions. In the broad band beam, we will have access to the highest intensities and energies available anywhere, for beams of photon, neutron or K_L. We have devoted considerable effort to design studies, and we are confident that we can do as we propose.